Fabrication of nanocatalysts as nanozymes-based biosensors for the detection of glucose and ascorbic acid

A thesis submitted in fulfilment of the requirements

for the degree of

MASTER OF SCIENCE

of

RHODES UNIVERSITY

By

RIDGE CHAVALALA

ORDICD

0000-0002-1538-6087

January 2023

DEDICATIONS

Dedicated to my mother, father and siblings

ACKNOWLEDGEMENTS

I would like to thank my Lord and saviour Jesus Christ for this moment in my life. Immeasurable appreciation and my warmest thanks to my supervisor Prof. Philani Mashazi who made this work possible. Your endless advice and guidance carried me through all this scientific journey in reviewing my work progress reports, manuscripts, and this thesis. Your invaluable insights and support during my work presentations gave me hope and made me feel at home. My deepest gratitude to our nanobiosensor research group for your contributions in sharing knowledge, your cooperation, and brilliant comments, thank you.

Special thanks to my brother, sister, and my family as a whole for your support and words of encouragement. I am grateful for your love and prayers.

I would like to thank Rhodes University for Sandisa Imbewu MSc scholarship.

I wish to extend my gratitude to Rhodes University Chemistry department, staff, and my fellow postgraduate students for all the support.

ABSTRACT

Monitoring and detection of biomolecules is of great importance for prevention, identification, and treatment of various diseases. Therefore, developing convenient, highly portable, and efficient methods for the detection and monitoring of biomolecules is of importance. The development of nanozymes-based biosensors for the detection of glucose and ascorbic acid (AA) was achieved.

Noble metal or platinum group metal nanoparticles (NPs) of gold (AuNPs), palladium (PdNPs), and gold/palladium (Au/PdNPs) were fabricated on silica nanoparticles (SiO_2NPs) coated on hydroxylated indium tin oxide (ITO-OH). The formed ITO-SiO_2NPs surface acted as the absorbent for noble NPs. Prior to noble metal adsorption, ITO-SiO_2NPs was first coated with 3-mercaptoproyltrimethoxy-silane (MPTMS) to introduce a thiol functional groups for the chemisorption of AuNPs, PdNPs, and Au/PdNPs. The various surfaces were labeled as ITO-SiO_2-prS-AuNPs, ITO-SiO_2-prS-PdNPs, and ITO-SiO_2-prS-Au/PdNPs.

A simple, easily recoverable and high selectivity colorimetric assay towards glucose detection was fabricated based on the peroxidase-like activity of ITO-SiO_2-prS-PdNPs on the oxidized 3,3',5,5'-tetramethylbenzidine (TMB). A selective colorimetric assay for AA detection was fabricated based on the reduction effect of AA on the oxidized TMB using ITO-SiO_2-prS-Au/PdNPs.

The nanozymes-based bionsensors that exhibit good linear concentration range were successfully prepared and used to detect glucose and AA in (new-born calf serum, NCS), as real samples or complex matrix.

TABLE OF CONTENT

LIST OF ABBREVIATIONS

AA	Ascorbic Acid
ABTS	2,2'-Azino-bis(3-ethylbenzthiazoline-6-sulfonic acid)
Ag|AgCl	Silver|SilverChloride
ALP	Alkaline Phosphatase
a.u	Arbitrary Unit
Au/Pd	Gold/Palladium
CDs	Carbon Dots
CNTs	Carbon Nanotubes
Cty C	Cytochrome C
CV	Cyclic Voltammetry
DLS	Dynamic Light Spectroscopy
DMPO	5,5-Dimethyl-1-pyrroline N-oxide
DPBF	1,3-Diphenylisobenzofuran
EDX	Energy Dispersive X-ray spectroscopy
FAD	Flavin Adenine Dinucleotide
FT-IR	Fourier Infrared Transform Spectroscopy
GO	Graphene Oxide
GOx	Glucose Oxidase

GQDs	Quantum Dots GQDs
H_2O_2	Hydrogen Peroxide
HRP	Horse-radish Peroxidase
ITO	Indium Tin Oxide
K_m	Michaelis−Menten Constant
LoD	Limit of Detection
LoQ	Limit of Quantification
MPTMS	3-Mercaptoproyltrimethoxysilane
MOFs	Metal-Organic Frameworks
NCS	New-born Calf Serum
NPs	Nanoparticles
NTs	Nanomaterials
OPD	o-Phenylenediamine
XPS	X-ray Photoelectron Spectroscopy
XRD	X-ray Diffraction
PBS	Phosphate Buffer Solution
PDT	Photodynamic Therapy
POCT	Point-of-Care Testing
PSA	Prostate-specific Antigen
ROS	Reactive Oxygen Radical Species

RPM	Revolutions Per Minute
%RSD	Percentage Relative Standard Deviation
SOD	Superoxide Dismutase
TA	Terephthalic Acid
TEM	Transmission Electron Microscopy
TEMP	2,2,6,6-Tetramethylpiperidine
TEOS	Tetraethylorthosilicate
TMB	3,3',5,5'-Tetramethylbenzidine
TMBDI	3,3',5,5'-Tetramethylbenzidine diimine
V_{max}	Maximal Reaction Rate
UV-vis	Ultraviolet-Visible Spectroscopy

LISTS OF FIGURES

LIST OF TABLES

LIST OF SCHEMES

LIST OF PUBLICATION

Here is a list papers published or submitted for publication on this thesis and therefore will note cited further:

1. **Ridge Chavalala**, Philani Mashazi. Indium tin oxide-silica nanoparticles substrate as adsorbent for palladium nanoparticles for a reusable colorimetric sensor for glucose. **(under review).** RSC J. Mater. Science B **(2023)**.

Ridge contribution: Conceptualization, Method development, Data collection, Data curation, Analysis, Validation, Writing first draft, and Editing.

2. **Ridge Chavalala**, Philani Mashazi. Au/Pd nanocatalysts on silica nanoparticle-coated indium tin oxide for colorimetric sensing of ascorbic acid. ACS Appl. Nano Mater. **2023**, 6, 190–199.

Ridge contribution: Conceptualization, Method development, Data collection, Data curation, Analysis, Validation, Writing first draft, and Editing.

CHAPTER 1

Problem statement

Biomolecules play an important role in human body by regulating and performing very essential functions. However, their presence in higher concentrations in the body fluids such as blood, urine, saliva, and sweat possess serious dangers and also indicators of diseases. Monitoring their presence and quantities is the most crucial function. As diseases indicators their early detection is of crucial importance to diagnose, prevent, treat, and manage diseases. The methods used for the detection of biomolecules such as enzyme immunoassays involve the use of biocatalytic enzymes making these methods expensive. Recently nanomaterials have been shown to possess enzyme-like activity and properties. The use of nanomaterials is therefore a technology of the future. Noble or platinum group metal nanoparticles have been shown to possess exceptional catalytic properties and also possess enzyme-like activity. This work aims to finding methods of adsorbing noble or platinum group metal nanomaterials on the support for their reusability, simple recovery, and evaluate their enzyme-like activity for sensing applications.

1 Justification

The first ‘true’ biosensor was developed by Leland C. Clark, Jr in 1956. He used a glucose oxidase enzyme to detect glucose concentration and using sensitive oxygen or hydrogen peroxidase electrode for detection [**1**]. A biosensor is an analytical device

with fast respond and high specificity used for the detection diagnosis and monitoring of various diseases [**2**]. A typical biosensor consists of two components, the biological component and the physical component [**3**] as shown in **Figure 1.1**. The biological component consists of the bioreceptor that interacts selectivity and specifically with the biomolecule of interest [**2**]. The physical component is the physicochemical detector, the transducer, that converts the biorecognition event into a measurable signal [**2**]. The common transducers produce electrical or optical signals proportional to the concentration of analyte [**2**].

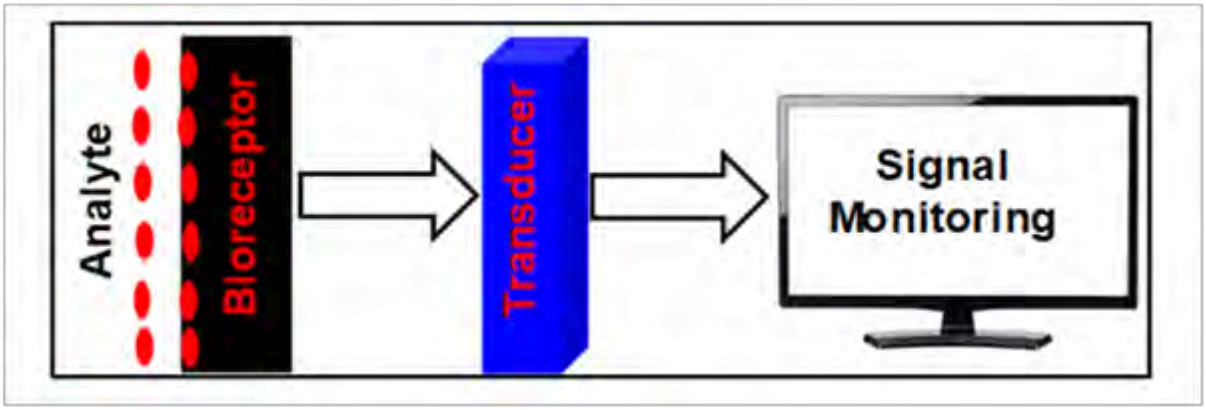

Figure 1. 1: The major component of the biosensor [**3**].

Biomolecules are building blocks of life and play an important role in many physiological and biochemical processes [**4**]. Traditional strategies used to detect biomolecules (such as ions, small molecules, nucleic acids and proteins) include colorimetric [**5**], fluorescence [**6**], chromatography [**7**], spectrometry [**8**] and electro-chemical detection [**9**]. Amongst these, colorimetric detection has received great attention due to the development of colored products based on the catalytic activity of natural enzymes. The colored products are easily observed using naked eyes and can be monitored using low-cost portable instruments. Natural enzymes play an importance role in living cells as biocatalysts [**10**]. Most natural enzymes are

composed of large, complex, well defined, and chiral organic molecules called proteins [**11**]. Natural enzymes under relatively mild conditions have unique properties including high catalytic activities and excellent substrate specificity, thus finding extensively applications in industrial, medical, and biological fields [**12**]. The commonly used natural catalytic enzymes are alkaline phosphatase (ALP) [**13**], horse-radish peroxidase (HRP) [**14**], and β-galactosidase [**15**]. The basic structure in HRP consists of (i) iron porphyrin (HEME) which acts as a metal catalytic center, (ii) imidazole groups located at both the proximal histidine and the distal histidine sides of the HEME which serve as the substrate binding sites, and (iii) arginine residue which can provide positively charged groups to stabilize the intermediate during catalysis and can facilitate the cleavage of O-O bond [**16**]. The catalytic active site of horse-radish peroxidase enzyme is the HEME shown in **Figure 1.2**.

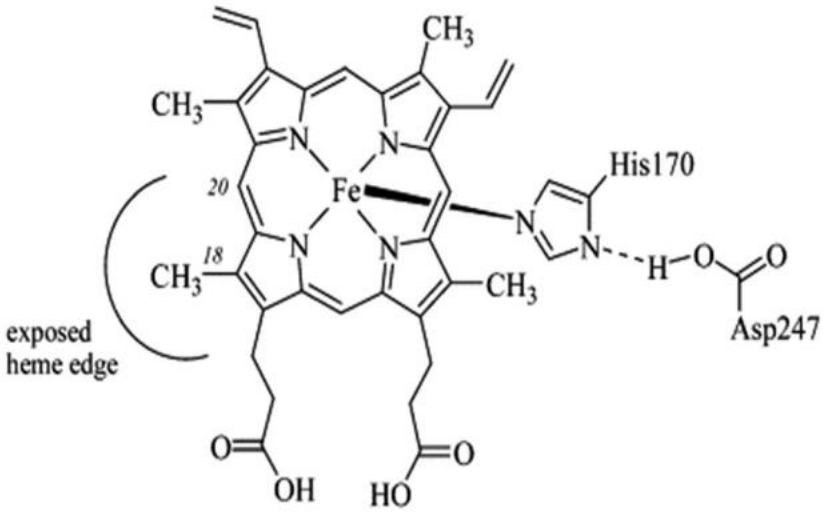

Figure 1. 2: Heme structure in horse-radish peroxidase (HRP), His170 is the proximal histidine residue and Asp247 is the carboxylate acceptor group [**14**].

Despite the advances in the natural enzymes over the past hundred years, they intrinsic limitations such as low stability in extreme environmental conditions such as

(high pH, temperature, humidity, to name a few). Natural enzymes are costly to obtain in high purity and denatures under storage and these shortcomings hinder their widespread applications [**17**]. Considering the importance of the natural enzymes in living cells and their intrinsic limitations, the emergence of artificial enzymes based on nanomaterials (named as “nanozymes”) as potential candidate to natural enzymes is of great interest in the research field. In contrast to natural enzymes, artificial enzymes have advantages such as low-cost, high environmental stability, easy modification, and possess efficient enzyme-like activity [**18**]. Nanozymes possess and can mimic enzyme-like activity of the enzymes such as peroxidase, oxidase, catalase, and superoxide dismutase [**18**,**19**]. Nanozymes that possess peroxidase-like activity were the first reported and have been extensively studied [**19**]. In 2007, Fe_3O_4 magnetic nanoparticles (NPs) were discovered to possess peroxidase-like activity [**20**] and several nanomaterials have since been explored. They are evaluated as possible substituted for biosensor applications. Nanozymes-based biosensors have been extensively explored for the sensing of important biomolecules such as glucose [**21**], ascorbic acid (AA) [**22**], uric acid [**23**], and glutathione [**24**]. Nanozymes can be produced at low-cost, are easy to prepare, and can be used for rapid colorimetric diagnostics tools in point-of-care applications.

Several research groups have investigated nanozymes that can be used as HRP mimics. Wu’s group successfully loaded hemin onto single-walled carbon nanotubes (SWCNTs) via the π-π interactions. CNs were modified with amino (SWCNT-NH_2) or carboxylic acid (SW CNT-COOH) functional groups to introduce a charge characteristics on the hemin environment [**25**]. SWCNT-NH_2@hemin exhibited the highest peroxidase-like activity compared to the hemin alone. The enhanced catalytic activity exhibited on SWCNT-NH_2@hemin was attributed to the positively charged -

NH_2 functional group which plays a significant role similar to the arginine in the HRP. Willner's group successfully synthesized Cu^{2+} modified on carbon (Cu^{2+}-C) dots [**26**]. Cu^{2+} acted as an active center, and as an HRP mimic. Yan's group preparedFe_3O_4 nanoparticles modified with histidine residues [**27**]. The interaction between the imidazole group of the histidine and H_2O_2 resulted in the formation of the hydrogen bond which increased the affinity between Fe_3O_4-histidine nanoparticles and H_2O_2. This led to the enhanced peroxidase-like activity.

In this thesis, nanoparticles of gold and palladium were prepared and used due to their low-cost synthesis, high surface area, tuneable and excellent catalytic properties. In addition, the bimetallic gold/palladium NPs were prepared and showed superior peroxidase-like activity due to the synergistic effect between the Au core and Pd shell that cannot be achieved by their monometallic nanoparticles. The use of these nanoparticles in solution showed excellent results. However, their recovery after the catalytic reaction still remains a challenge rendering their catalytic application of these nanomaterials for single use. To overcome this challenge, the use of magnetic nanoparticles with silica shell decorated with Au/PdNPs, as the method to recover the nanocatalysts magnetically was reported [**28**]. This study showed excellent results and the nanoparticles could be reused. The adsorption of metal nanoparticles on the solid support would also be beneficial for the recovery of the nanocatalysts for further use. In this thesis, we designed a method of fabricating the nanomaterials of gold, palladium, and gold/palladium as thin nanofilms on catalytically inert surfaces whilst allowing for their recovery and reuse is investigated. Indium tin oxide (ITO) glass slides will first be hydroxylated (ITO-OH) and used to attach the silica nanoparticles (SiO_2NPs) to form ITO-SiO_2NPs. The ITO-SiO_2NPs surface was used as an adsorbent for gold and palladium mono- and bi-metallic nanoparticles (Au/PdNPs) to form ITO-

SiO_2-prS-AuNPs, ITO-SiO_2-prS-PdNPs and ITO-SiO_2-prS-Au/PdNPs, respectively. Glucose is classified as monosaccharide because it cannot be broken further by hydrolysis. The chemical structure of glucose consists of six-carbons and an ether group between carbon 1 and 5 as shown in **Figure 1.3(a)**. Excessive blood glucose level is one of the main causes of diabetes [**29**]. On the other hand, AA is an antioxidant which plays an importance role in many physiological and biochemical processes. Malnutrition of AA is closely related to scurvy and can lead to psychological abnormalities [**30**]. The chemical structure of AA is shown in **Figure 1.3(b)**. Conventional glucose detection and monitoring is based on personal glucose meters (PGMs) which are easy to use and require a drop of the blood for sample analysis. However, PGMs require natural enzymes which are expensive to obtain in high purity. On the other hand, conventional detection and monitoring of AA requires expensive equipment such high- performance liquid chromatography (HPLC), fluorescence, and electrochemistry. Therefore, developing convenient, highly portable, and efficient methods for the detection of glucose and AA would be of great importance for the prevention, identification, and treatment of their related diseases for on-site/point-of-care testing (POCT).

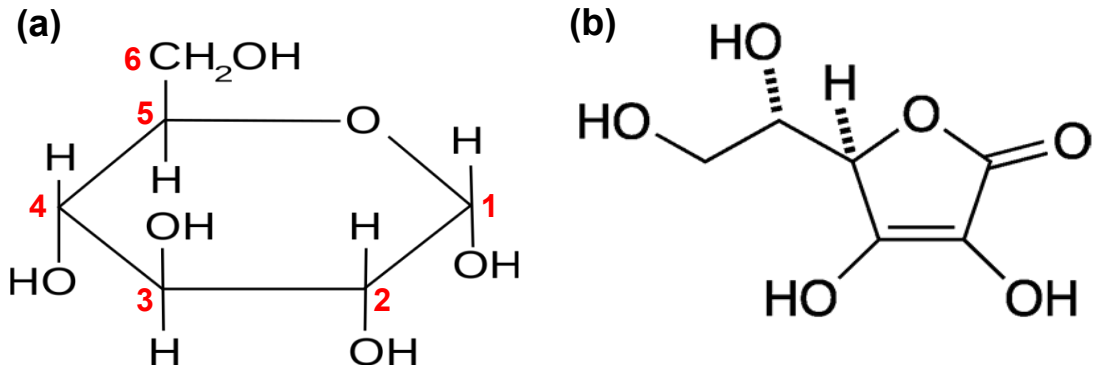

Figure 1. 3: Chemical structures of (a) glucose showing six-carbons and (b) ascorbic acid (AA).

1.1 Aim of this thesis

The aim of this thesis is to prepare nanoparticles of gold, palladium and bimetallic gold/palladium. The nanoparticles will be attached as thin nanofilms on catalytically insert surfaces to allow for their ease of recovery and reuse as colorimetric sensor for glucose and ascorbic acid (AA).

The specific objectives of the thesis were:

(i) To synthesize of silica, gold, palladium, gold/palladium nanoparticles.

(ii) To characterize the prepared nanoparticles using various analytical techniques such as UV-vis spectroscopy, Fourier Infrared Transform Spectroscopy (FT-IR), Transmission electron microscopy (TEM), Dynamic Light Spectroscopy (DLS), Energy-dispersive X-ray spectroscopy (EDX), and X-ray diffraction (XRD).

(iii) To immobilize silica nanoparticles as catalyst support onto indium tin oxide (ITO) to form ITO-SiO_2NPs as our absorbent surface.

(iv) To use ITO-SiO_2NPs to self-assembly gold (AuNPs) and palladium (PdNPs) and bi-metallic (Au/PdNPs) nanoparticles via 3-mercaptoproyltrimethoxy-silane (MPTMS), to form ITO-SiO_2-prS-AuNPs, ITO-SiO_2-prS-PdNPs and ITO-SiO_2-prS-Au/PdNPs as our catalytic nanofilms.

(v) To characterize the prepared catalytic nanofilms using surface sensitive techniques, such as X-ray photoelectron spectroscopy (XPS).

(vi) To evaluate the enzyme-like catalytic properties of our prepared catalytic nanofilms toward TMB/H_2O_2 substrate to form blue-colored products of oxidation of TMB to TMBDI.

(vii) To evaluate the catalytic performance of our prepared catalytic nanofilms for the colorimetric detection of glucose and ascorbic acid (AA) in buffer and complex serum matrix, new-born calf serum, (NCS).

1.2 References

(1) Heineman, W. R.; Jensen, W. B.; Leland C. Clark Jr. (1918–2005). *Biosens. Bioelectron.* **2026**, 21, 1403–1404. https://doi.org/10.1016/j.bios.2005.12.005

(2) Bhalla, N.; Jolly, P.; Formisano, N.; Estrela, P. Introduction to Biosensors. *Essays Biochem.* **2016**, 60, 1–8 .https://doi.org/10.1042/EBC20150001

(3) Mwanza, D.; Phal, S.; Nyokong, T.; Tesfalidet, S.; Mashazi, P. Eletcrografting of Isopthalic Acid and Covelent attachment of Antibody onto Carbon Surfaces: Construction of Capacitive Biosensor for Mtehotrexate Detection. *Electrochem. Acta* **2016**, 398, 1–9 . https://doi.org/10.1016/j.electacta.2021.139360

(4) Lee, S.; Roh, S. M.; Lee, E.; Park, Y.; Lee, B. C.; Kwon, Y.; Kim, H. J.; Kim, J. Applications of Converged Various Forces for Detection of Biomolecules and Novelty of Dielectrophoretic Force in the Applications. *Sensors* **2020**, 20, 1–18.

https://doi:org/10.3390/s20113242

(5) Liu, J.; Lu, Y. Fast Colorimetric Sensing of Adenosine and Cocaine Based on a General Sensor Design Involving Aptamers and Nanoparticles. *Angew. Chemie - Int. Ed.* **2005**, 45, 90–94. *https://*doi:org/10.1002/anie.200502589

(6) Wang, Y.; Jiang, K.; Zhu, J.; Zhang, L.; Lin, H. A FRET-Based Carbon Dot-MnO_2 Nanosheet Architecture for Glutathione Sensing in Human Whole Blood Samples. *Chem. Commun.* **2015**, 51, 12748–12751. *https://*doi.org/10.1039/c5cc04905a

(7) Nováková, L.; Solich, P.; Solichová, D. HPLC Methods for Simultaneous Determination of Ascorbic and Dehydroascorbic Acids. *TrAC - Trends Anal. Chem.* **2008**, 27, 942–958. *https://*doi.org/10.1016/j.trac.2008.08.006

(8) Miyagi, M.; Kasumov, T. Monitoring the Synthesis of Biomolecules using Mass Spectrometry. *Philos. Trans. R. Soc. A Math. Phys. Eng. Sci.* **2016**, 374, 1–7.

*https://*doi.org/10.1098/rsta.2015.0378

(9) Huang, Y.; Ren, J.; Qu, X. Nanozymes: Classification, Catalytic Mechanisms, Activity Regulation, and Applications. *Chem. Rev.* **2019**, 119, 4357–4412.

https:// doi.org/10.1021/acs.chemrev.8b00672

(10) Bornscheuer, T.; Huisman, G. W.; Kazlauskas, J.; Lutz, S.; Moore, C.; Robins, K. Engineering the Third Wave of Biocatalysis. *Nature* **2012**, 485, 185–194.

https://doi.org/10.1038/nature11117

(11) Lin, Y.; Ren, J.; Qu, X. Catalytically Active Nanomaterials: A Promising Candidate for Artificial Enzymes. *Acc. Chem. Res.* **2014**, 47, 1097–1105.

https://doi.org/10.1021/ar400250z

(12) Huang, Y.; Ren, J. Qu.; X. Nanozymes: Classification, Catalytic Mechanisms, Activity Regulation, and Applications. *Chem. Rev.* **2019**, 119, 4357–4412.

https://doi.org/10.1021/acs.chemrev.8b00672

(13) Avrameas, S.; Ternynck, T.; Guesdon, J.; L. Coupling of Enzymes to Antibodies and Antigens. *Scand. J. Immunol.* **1978**, 8, 7–23.

https://doi.org/10.1111/j.1365-3083.1978.tb03880.x

(14) Nakane, K.; Kawaoi, A. Peroxidase-Labeled a New Antibody Method of Conjugation. *J. Histochem. Cytochem.* **1974**, 22, 1084–1091

https://doi.org/10.1177/22.12.1084

(15) Craven, G. R.; Steers, E.; Anfinsen, C. B. Purification, Composition, and Molecular Weight of the β-Galactosidase of Escherichia coli K12. *J. Biol. Chem.* **1965**, 240, 2468–2477. https://doi.org/10.1016/s0021-9258(18)97348-5

(16) Veitch, N. C.; Smith, A. T. Horseradish Peroxidase. *Adv. Inorg. Chem.* **2000**, 51, 107–162. https://doi.org/10.1016/S0898-8838(00)51002-2

(17) Dray, F.; Andrieu, M.; Renaud, F. Enzyme Immunoassay of Progesterone at the Picogram Level Using β-Galactosidase as Label. *Biochimica. Biophy Acta* **1975**, 403, 131–138. https://doi.org/10.1177/22.12.1084

(18) Lin, Y.; Ren, J.; Qu, X. Catalytically Active Nanomaterials: A Promising Candidate for Artificial Enzymes. *Acc. Chem. Res.* **2014**, 47, 1097–1105.

https://doi.org/10.1021/ar400250z

(19) Liu, H.; Ding, Y.; Yang, B.; Liu, Z.; Lui, Q.; Zhang, X. Colorimetric and Ultrasensitive Detection of H_2O_2 Based on Au/Co_3O_4-CeOx Nanocomposites with Enhanced Peroxidase-Like Performance. *Sens. Act. B. Chem.* **2018**, 271, 336–345. https://doi.org/10.1016/j.snb.2018.05.108

(20) Gao, L.; Zhuang, J.; Nie, L.; Zhang, J.; Zhang, Y.; Gu, N.; Wang, T.; Feng, J.; Yang, D.; Perrett, S. Intrinsic Peroxidase-Like Activity of Ferromagnetic Nanoparticles. *Nat. Nanotechnol.* **2007**, 2, 577–583. https://doi.org/10.1038/nnano.2007.260

(21) Sun, J.; Li, C.; Qi, Y.; Guo, S.; Liang, X. Optimizing Colorimetric Assay Based on V_2O_5 Nanozymes for Sensitive Detection of H_2O_2 and Glucose. *Sensors* **2016**, 16, 584. https://doi.org/10.3390/s16040584

(22) He, S.; Balasubramanian, P.; Hu, A.; Zheng, X.; Lin, M.; Xiao, X.; Peng, H.; Deng, H.; Chen, W. One-Pot Cascade Catalysis at Neutral pH Driven by CuO Tandem Nanozyme for Ascorbic Acid and Alkaline Phosphatase Detection. *Sens. Act. B. Chem.* **2020**, 321, 128511. https://doi.org/10.1016/j.snb.2020.128511

(23) Lu, N.; Lui, Y.; Yan. X.; Xing, Y.; Song, Y.; Zhao, P., Liu, M., Gu, Y.; Zhang, Z.; Zhai, S. Bioinspired Surface Modification of Graphene-Based Hybrids as Nanozyme Sensors for Simultaneous Detection of Dopamine and Uric Acid. *ACS Appl. Nano Mater.* **2022**, 5, 11361–11370. https://doi.org/10.1021/acsanm.2c02446

(24) Mohammadpour, Z.; Malekian Jebeli, F.; Ghasemzadeh, S. Peroxidase-Mimetic Activity of FeOCl Nanosheets for the Colorimetric Determination of Glutathione and Cysteine. *Microchim. Acta* **2021**, 188, 239.

https://doi.org/10.1007/s00604-021-04903-0

(25) Fan, K.; *Wang, H.*; *Xi, J.*; *Meng, X.*; *Duan, D.*; *Gao, L.*; *Yan, X.* Optimization of Fe_3O_4 Nanozyme Activity via Single Amino Acid Modification Mimicking an Enzyme Active Site. *Chem. Commun.* **2017**, 53, 424–427.

https://doi.org/10.1039/C6CC08542C

(26) Zhang, Z.; Zhang, X.; Liu, B.; Liu, J. Molecular Imprinting on Inorganic Nanozymes for Hundred-Fold Enzyme Specificity. *J. Am. Chem. Soc.* **2017**, 139, 5412–5419. https://doi.org/10.1021/jacs.7b00601

(27) Zhang, R.; Zhou, Y.; Yan, X.; Fan, K. Advances in Chiral Nanozymes: A Review. *Microchim. Acta* **2019**, 186, 1–12. https://doi.org/10.1007/s00604-019-3922-7

(28) Adeniyi, O.; Sicwetsha, S.; Mashazi, P. Nanomagnet-Silica Nanoparticles decorated with Au@Pd for Enhanced Peroxidase-Like Activity and Colorimetric Glucose Sensing. *ACS Appl. Mater. Interf*. **2020**, 12, 1973–1987.

https://doi.org/10.1021/acsami.9b15123

(29) Cai, T.; Gao, Y.; Yan, J.; Wu, Y.; Di, J. Visual Detection of Glucose Using Triangular Silver Nanoplates and Gold Nanoparticles. *RSC Adv.* ***2017,*** 7, 29122–29128. https://doi.org/10.1039/c7ra00593h

(30) Padayatty, S.; Katz, A.; Wang, Y.; Eck, P.; Know, O.; Lee, J.; Chen, S.; Corpe, C.; Dutta, A.; Levine, M. Vitamin C as an Antioxidant: Evaluation of Its Role in Disease Prevention. *J. Am. Coll. Nutr.* ***2003****,* 22, 18–35.

https://doi.org/10.1080/07315724.2003.10719272

1.3 Thesis outline

This thesis comprises of five chapters as follows: Chapter one outlines the general introduction of the study, chapter two outlines comprehensive background and literature view of the study, chapter three discuss the study conducted for the nanomaterials thin films towards colorimetric detection of glucose, chapter four investigates gold, palladium and bimetallic of gold/palladium toward colorimetric detection of ascorbic acid, and chapter five gives the conclusions of the thesis and future perspectives.

Chapter 1: Problem statement and justification

Chapter one briefly describes the importance of biomolecules owing to the significant role they play in living cells. The use of natural enzymes in colorimetric detection of biomolecules and their limitations. Nanomaterials are described as most promising substitutes for natural enzymes and their properties are discussed. Biomolecules (glucose and ascorbic acid) deficiency and importance was also described. The use of enzyme-mimicking nanoparticles for colorimetric detection and monitoring of glucose and ascorbic acid. This chapter further outlines the aims and objectives of the study. Lastly, a brief thesis outline of the chapters is highlighted.

Chapter 2: Literature review

This chapter provides comprehensive background on nanoparticles as nanozymes. This chapter further highlights nanozymes classification, catalytic mechanism, possible strategies for tuneable catalytic activity, and their application in various fields with the emphasis on sensing.

Chapter 3: Pd nanocatalysts adsorbed onto silica nanoparticles coated indium tin oxide a reusable colorimetric sensor for glucose

Chapter three reports on the preparation and characterization of silica and palladium nanoparticles. This chapter further evaluates how nanomaterials of palladium was used as catalytic nanofilm as a peroxidase mimetic. The fabrication process of palladium nanoparticles on indium tin oxide coated with silica nanoparticles is described in detail. The palladium nanoparticles modified surface was used for the colorimetric detection of glucose using glucose oxidase (GOx).

Chapter 4: Au/Pd nanocatalysts on silica particles coated on indium tin oxide for colorimetric sensing of ascorbic acid

Chapter four reports on the preparation and characterization of silica, gold, palladium, and gold/palladium nanoparticles. The chapter also reports nanomaterials of gold and palladium as catalytic nanofilms is discussed. The fabricated catalytic nanofilms were investigated and compared for their peroxidase-like activity performance. Among them, ITO-SiO_2-prS-Au/PdNPs was further used for the colorimetric detection of AA.

Chapter 5: Conclusions and future perspectives

This chapter will report on the conclusions of this thesis and future perspectives of the study will be highlighted.

CHAPTER 2

2 Literature Review

This chapter provides comprehensive background on nanoparticles as nanozymes in contrast to the natural enzymes. This chapter further highlights nanozymes classification, catalytic mechanism, possible strategies for tuneable catalytic activity, and their application in various fields such as enhanced signal in sensing, environmental remediation, antibacterial properties, and anti-cancer properties.

2.1 Classification of nanozymes

Nanozymes, termed artificial enzymes, are nanomaterials that possess intrinsic enzyme-like activity [**1**]. Various artificial enzymes such as metal-organic frameworks (MOFs), noble metal nanoparticles, carbon nanomaterials, and transition-metal oxides have been evaluated their enzyme-like properties.

2.1.1 MOFs-based nanozymes

MOFs catalytic behaviour is based on the coordinate bonds between metal ions and organic ligands [**2**], resulting in uniform cavities with porous-like morphology [**3**]. The cavities can generate high specific surface area, tunable pore size, and high density of biomimetic catalyst centers [**4**]. Therefore, emerging MOFs are a promising novel to develop artificial nanozymes in various applications with high catalytic efficiency. MOFs that have reported possess peroxidase-like activity are MIL-53(Fe) [**5**], MIL-

101(Fe) [**6**], ZIF-8 [**7**], Fe-MIL-88NH_2 [**8**], and 2D Ni/Fe [**9**]. MOFs can mimic other enzymes such as catalase [**10**], superoxidase dismutase (SOD) [**10**], oxidase-[**11**], and lipase [**12**].

2.1.2 Carbon-based nanozymes

Carbon-based nanomaterials have received great attention to be used as nanozymes since they exhibit well-defined electronic and geometric structures by mimicking the highly evolved catalytic center of natural enzymes [**13**,**14**]. In contrast to natural enzymes, carbon nanozymes are low-cost, more stable, tunable catalytic properties [**15**,**16**]. Compared to metal-based nanozymes, carbon nanozymes can be used as alternatives for metal-free catalysts with highly exposed active sites [**16**]. Carbon-based nanomaterials that have been reported possess enzyme-like activity include fullerenes, carbon nanotubes (CNTs), graphene, graphene oxide (GO), carbon dots (CDs), graphene quantum dots (GQDs), and carbon nitride [**14**,**17**].

2.1.3 Nobel metal-based nanozymes

Metallic nanomaterials have been extensively explored as artificial enzymes due to their electronic and catalytic properties [**18,19**]. The metallic nanoparticles based on Au [**20**], Ag [**21**], Pt [**22**], Pd [**23**], Rh [**24**], Ru [**25**], and Ir [**26**] have been reported to possess multiple enzyme-like activity. Noble metal nanomaterials enzyme-mimicking behaviour are dependent on the particle size and morphology, surface modification, environmental conditions, and the nature of the active metals.

2.1.4 Transition-metal oxide-based nanozymes

Since the discovery of the peroxidase-like activity of Fe_3O_4 magnetic nanoparticles (MNPs) in 2007 [**27**], a variety of metal-oxide based nanozymes such as CeO_2 [**28**], MnO_2 [**29**], VO_x [**30**], CuO [**31**], $CeZrO_2$ [**32**], GeO_2 [**33**], MoO_3 [**34**], $MnCo_2O_4$ [**35**] have been explored and found to possess multiple enzyme-like activity. Amongst them, Fe_3O_4, CeO_2, and MnO_2 nanostructures stand out due to their unique ability to interchange between valence states [**28**,**29**,**36**].

2.1.5 Synergistic effects of bimetallic nanozymes

Bimetallic nanozymes have extensively shown to improve catalytic performance better than their monometallic analogues due to their synergistic effects [**37**]. Examples of some reported bimetallic nanozymes which exhibited superior enzyme-like are shown in **Table 2.1** and their applications. This thesis also aimed at using the bimetallic of gold/palladium NPs (Au/PdNPs) for improved peroxidase-like activity than cannot be achieved by their monometallic nanoparticles.

Table 2.1: Bimetallic nanozymes with superior enzyme-like catalytic properties.

Bimetallic Nanozymes	**Applications**
MOFs-based nanozymes	
$MnFe_2O_4$/C@Ce_6 [**38**]	Photodynamic therapy (PDT) in cancer cells
Ce/Zr-UiO-66 [**39**]	Peptide bond hydrolysis
Co/Mn [**40**]	Colorimetric detection of H_2O_2
Fe/Mn [**41**]	Glucose detection
C-Co-Cu-HNC [**42**]	Rhodamine B (RhB) degradation
Carbon-based nanozymes	
BSA-PtAu@CNS [**43**]	H_2O_2 and glucose sensing
GQD-AgNP [**44**]	Antibacterial agents
Fe_3O_4-MWCNT [**45**]	Water purification
FF@PW12@GO [**46**]	Colorimetric detection of H_2O_2
C-dots@AuNP [**47**]	Electrochemical sensing of proteins
Nobel metal-based nanozymes	
Pd-Ir [**48**]	Detection of prostate surface antigen (PSA)
Au-Ag [**49**]	CO oxidation
Au-Pt [**50**]	Antibacterial agents
Ag-Pd [**51**]	Dehydrogenation of formic acid
Ag-Pt [**52**]	H_2O_2 selectivity

2.2 Catalytic mechanism of nanozymes

Despite the advancement in nanotechnology, computer simulation, and theoretical calculation of the novel nanozymes in the recent years. The study of their catalytic mechanisms has received little attention. Understanding the catalytic mechanisms exhibited by the nanozymes is of great significance for the development of novel and highly efficient nanozymes. In this thesis, the enzymatic mechanism of the activity of nanomaterials is discussed.

2.2.1 Catalytic mechanism of peroxidase-like activity of nanozymes

The catalytic mechanism of peroxidase-like activity of nanozymes can proceed via the reduction of H_2O_2 to produce reactive oxygen species (ROS) such as hydroxyl (HO^{-}•), superoxide (O_2^{-}•), and peroxy (HO_2^{-}•) radicals or the electron-transfer mechanism [**53**].

2.2.2 Generation of reactive oxygen species (ROS)

The generation of ROS (O_2^{-}•, HO_2^{-}• and HO^{-}•) using CuO-Au nanoalloys as peroxidase mimic was achieved and evaulated by using a radical scavenger 1,3-diphenylisobenzofuran (DPBF) [**54**]. DPBF is a conjugated organic compound which absorbs at 430 nm and can be monitored using UV-vis spectroscopy. DPBF is commonly used as singlet oxygen quencher [**55**]. To confirm the generation of ROS by CuO-Au nanoalloy, the rate of degradation of DPBF was monitored against time in the presence of H_2O_2. The rate of degradation of DPBF was equivalent to the rate of ROS produced. As time was increased, a drastic decrease in the absorption peak of DPBF was observed and was attributed to the catalytic reduction of H_2O_2 to form an intermediate ROS. An analytical technique, electron paramagnetic resonance (EPR) measurements can also be used to monitor the generation of ROS produced by the nanozymes using spin trap species such as 5,5-dimethyl-1-pyrroline N-oxide (DMPO) and 2,2,6,6-tetramethylpiperidine (TEMP). TEMP was used as a spin trap to monitor the generation of ROS by sCuONRs [**56**]. The EPR signal was only observed in the reaction system of sCuONRs + TEMP + H_2O_2. The generated EPR signal was

attributed to the reaction between TEMP and ROS which produced 2,2,6,6-tetramethylpiperidinyl (TEMPO) with unique triple line pattern.

2.2.3 The nature of the reactive oxygen species (ROS)

Moreover, understanding the nature of the ROS (O_2^{-}•, HO_2^{-}• and HO^{-}•) produced by the nanozymes will be of great importance in further advancement in the nanozymology. To explore the nature of ROS generated by Ce/$ZnCO_2O_4$ as a peroxidase mimic, Yin's group used various species such as isopropanol (IPA), p-benzoquinone (PBQ) and ethylenediaminetetraacetic acid disodium salt (EDTA) corresponding to HO^{-}•, O_2^{-}•, and h^{+} radicals, respectively [**57**]. The absorbance was measured using UV-vis spectroscopy after the addition of each scavenger in the reaction system of Ce/$ZnCO_2O_4$, H_2O_2 and TMB. After the addition of PBQ, a signal response rapidly decreased. No obvious decrease in the signal was observed in the presence for IPA and EDTA. Therefore, Ce/$ZnCO_2O_4$ generated O_2^{-}• radical.

Traditionally, to confirm the production of hydroxyl (HO^{-}•) radicals generated by the nanozymes in the presence of H_2O_2, a fluorescent probe terephthalic acid (TA) is used. TA has been reported to react with HO^{-}• radicals to generate dihydroxyterephthalic acid, which can be measured and monitored using fluorescence spectrophotometer with an excitation wavelength of 315 nm [**58**]. As the concentration of the nanozyme increases, the fluorescence intensity is expected to increases as well, thus indicating the generation HO^{-}• radicals. Similarly, Xu's group used Fe_3O_4/mesoporous graphitized carbon (Fe_3O_4/m-GC) as a peroxidase mimic in the presence of a fluorescent probe TA and H_2O_2 [**59**]. The results showed that as the concentration of Fe_3O_4/m-GC increased the fluorescence intensity also increased, indicating the

generation of HO^{-}• radicals as an intermediate. The production of HO^{-}• radicals can also be verified by using an EPR with a 5,5-dimethyl-1-pyrroline N-oxide (DMPO) as a spin trap. Nanozymes such as CuO-Au nanoalloys and Fe_3O_4/m-GC in the presence of DMPO and H_2O_2 resulted in their EPR signal with the characteristic intensity showing relative intensities of 1:2:2:1. Therefore, CuO-Au nanoalloys and Fe_3O_4/m-GC were attributed to the generation of HO^{-}• radicals [**54**,**59**].

2.2.4 Electron-transfer mechanism

To determine whether the peroxidase-like activity of nanozyme originates from the electron-transfer mechanism its electrocatalytic behavior toward H_2O_2 reduction is monitored using cyclic voltammetry (CV) and amperometric measurements. The catalytic mechanism of Fe_3@SiO_2-NH_2-Au@PdNPs as peroxidase mimic was investigated [**60**]. The electrocatalytic reduction current response of Fe_3@SiO_2-NH_2-Au@PdNPs in the absent and presence of H_2O_2 was measured. The following observations were highlighted: no current response was observed in the absent of H_2O_2 whilst a dramatically increased in the current response was observed after successive addition of H_2O_2. Therefore, the catalytic mechanism of peroxidase-like activity exhibited by Fe_3@SiO_2-NH_2-Au@PdNPs was attributed to the electron-transfer mechanism. The catalytic mechanism of various peroxidase mimetics such as HRP-C [**61**], FeSe film [**62**], FePt-Au [**63**], AuNP@CDs [**64**], and MoS_2 [**65**] have been reported to proceed via electron-transfer mechanism.

Considering the great attention of nanozymes, the development of convenient, rapid, and portable instruments will be of great importance to deepen the understanding of catalytic mechanisms of nanozymes. Cytochrome C (Cyt C) is an active reactant commonly used to assess the electron accepting capability of nanocatalysts [**66**]. Sun's group used Cyt C to verify the catalytic mechanism of IrO_2/GO as peroxidase mimic [**67**]. The UV-vis spectra of Cyt C before and after the addition of IrO_2/GO was monitored. The reduced state of Cyt C alone resulted in the two characteristic peaks at 520 nm and 550 nm. In the presence of IrO_2/GO the two characteristics peaks observed in the reduced state of Cyt C disappeared. A new absorption peak was observed at 530 nm and this was attributed to the oxidized state of Cyt C. This study suggested that IrO_2/GO exhibited electron-transfer mechanism. Liu's group reported the peroxidase-like activity of Pt/CeO_2 to proceed via the electron-transfer mechanism using Cyt C [**68**]. The advantages of using Cyt C to verify the catalytic mechanism of nanozymes prove to be cost-effective and easy to study.

2.3 Tuning the catalytic activities of nanozymes

The catalytic activities of nanozymes can be tuned by many factors including nanoparticles size, morphology, composition, surface modification, addition of chiral ligands, doping some component on the surface of nanozymes, pH, temperature, activators and inhibitors. In this section, important factors that influence the catalytic activities of nanozymes are and discussed.

2.3.1 Size

The catalytic performance of nanozymes can be regulated by tuning their size. Nanozymes size plays a significant role in their properties such as optical, electrical, and biological properties [**69**]. Therefore, understanding the effects of size on the nanozymes catalytic performance will be of great importance to find a narrow and niche area of application. Chemical synthesis of gold nanoparticles (AuNPs) using various reducing agents such as sodium borohydride ($NaBH_4$), sodium citrate, ascorbic acid (AA), and tannic acid can influence the size of nanozymes. Iqbal's group investigated the effect of increasing the concentration of $NaBH_4$ as a reducing agent on the synthesized AuNPs [**70**]. As the concentration of $NaBH_4$ was increased, the increased in the AuNPs particle size was observed. In the contrary, Ghost's group observed that increasing the concentration of sodium citrate as a reducing agent resulted in a decreased in the AuNPs particle size [**71**]. Peng's group synthesized Fe_3O_4 nanoparticles with three different sizes with the average diameters of 11.0 nm, 15.0 nm, and 150.0 nm [**72**]. Fe_3O_4 nanoparticles of 11.0 nm exhibited the highest peroxidase-like activity than the other sizes of 15.0 nm and 150.0 nm. This was attributed to the larger surface-to-volume area of the nanoparticle compared to the bigger sized Fe_3O_4 nanoparticles.

2.3.2 Morphology

The catalytic performance of nanozymes can also be regulated by their morphology. Nanozymes with different morphology can exhibit different enzyme-like catalytic performance. For comparison, Yin's group synthesized palladium nanoparticles

(PdNPs) with two different morphologies [**73**]. Pd octahendrons nanoparticles showed lower surface energy and exhibited higher enzyme mimic of SOD, catalase and ROS removability compared to Pd nanocubes nanoparticles. The peroxidase-like activity of Fe_3O_4 nanoparticles with morphologies were investigated [**74**]. Fe_3O_4 truncated octahedron nanoparticles exhibited higher peroxidase-like activity compared to spherical-shaped Fe_3O_4 nanoparticles. This was attributed due to the difference in their surface energy facets.

2.3.3 Composition

The catalytic performance of nanozymes can also be regulated by changing the proportion of the components in the nanomaterials. The proportion of the copper acetate, glacial acetic acid and sodium hydroxide were changed using Sol-gel method. The obtained spherical copper oxide nanoparticles (sCuONPs) and copper oxide nanorods (CuONRs) exhibited different catalytic activity [**56**].

2.3.4 Surface modification

Surface modification including functional groups, surface charges, and surface of coating have been extensively studied their influence towards the catalytic performance of nanozymes. Liu's group reported the influence of functional groups on the surface of gold nanoclusters (AuNCs) nanozymes [**75**]. For comparison, the surface unmodified AuNCs, amino-modified gold clusters (NH_2-AuNCs) and citric-modified gold clusters (citrate-AuNCs) were investigated for their catalytic performance. The surface unmodified AuNCs exhibited the highest peroxidase-like

activity compared to NH_2-AuNCs and citrate-AuNCs when using TMB and 2,2'-Azino-bis(3-ethylbenzthiazoline-6-sulfonic acid) (ABTS) as substrates. This was attributed due to their difference in the surface charges and the functional groups introduced. Therefore, their ability to absorb the corresponding substrate was different. AuNPs modified with citrate and cysteine ligands [**76**]. The citrate-modified AuNPs exhibited glucose oxidase (GOx)-like activity whilst the cysteine-modified AuNPs exhibited peroxidase-like activity. Therefore, functional groups modification on the surface of nanomaterials can promote novel nanozymes with multiple enzyme-like properties.

Surface coating on the nanozymes surface can improve their catalytic performance. The effect of Pd-shell thickness on the peroxidase-like activity exhibited by Fe_3O_4@SiO_2-NH_2-Au@PdNPs was investigated [**60**]. Same batch of Fe_3O_4@SiO_2-NH_2-Au@PdNPs was added with different concentrations of H_2PdCl_4 from 0.10 mM to 0.50 mM and the same concentration of $NaBH_4$ as a reducing agent. When TMB was selected as the substrate, the highest absorption intensity at 652 nm was observed with the concentration of H_2PdCl_4 of 0.30 mM and decreased afterwards. The reasonable explanations to the above results were explained as follows: first, the increase in the absorption intensity at 652 nm was attributed to an increase in Pd shell thickness as the concentration of H_2PdCl_4 was increased, which would promote efficient electron-transfer between the corresponding substrate, AuNPs and Pd shell catalytic centers. Second, after the Pd shell was increased above 0.30 mM, the absorption intensity at 652 nm decreased and this was due to the inefficient electron-transfer between the corresponding substrate, AuNPs and Pd shell catalytic centers, thus leading to a decreased in the catalytic performance. Perez's group compared the oxidase-like activity exhibited by nanoceria coated with two different polymers thickness [**77**]. Nanoceria coated with a thin poly (acrylic acid) exhibited higher

oxidase-like activity than nanoceria coated with thicker dextran. This was attributed to the permeability of a thin poly (acrylic acid) coating to promote efficient electron-transfer between the corresponding substrate and the nanozyme catalytic centers compared with a thicker dextran coating.

In 2007, Zhang's group demonstrated that molecular imprinting technology could open a new strategy for improving the catalytic performance of nanozymes by forming corresponding substrate pockets [**78**]. Molecularly imprinted polymers were coated around Fe_3O_4 nanoparticles. The reaction interaction between the imprinted nanozymes and the corresponding substrate resulted in the imprinted hydrogels. The corresponding substrate pockets were formed after removing their corresponding template. The resulting cavities could selectively rebind TMB over ABTS and vice versa.

2.3.5 Chiral ligands

Chiral ligands such as amino acids, nucleic acids, and some chemical compounds modified on the surface of nanozymes have shown to open a new portal for enhancing the catalytic performance of enantioselective nanozymes [**79**]. Chiral ligands have two enantiomer structures which can be differentiated as the dextral (D)-enantiomer and levo (L)-enantiomer. This enantiomer structures have similar physical and chemical properties but have slightly different enzyme-like properties. Qu's group successfully synthesized a chiral nanozyme using a chiral zinc finger protein-like alpha-helical supramolecular complexes $[Fe_2L_3]^{4+}$ conjugated on the surface of graphene oxide (GO-COOH) to form $[Fe_2L_3]^{4+}$-GO-COOH [**80**]. For comparison, $[Fe_2L_3]^{4+}$-GO-COOH exhibited superior peroxidase-like activity than $[Fe_2L_3]^{4+}$ and GO-COOH alone, this was due to their synergistic effect. The two enantiomers of $[Fe_2L_3]^{4+}$ designed M-

$[Fe_2L_3]^{4+}$-GO-COOH and P-$[Fe_2L_3]^{4+}$-GO-COOH showed slightly difference in their peroxidase-like activity under the same conditions. The catalytic activity exhibited by P-$[Fe_2L_3]^{4+}$-GO-COOH was higher compared to M-$[Fe_2L_3]^{4+}$-GO-COOH and was attributed to its higher affinity for aromatic substrates. To achieve the specific binding ability between amino acids as chiral ligands and nanozymes, Qu's group linked various amino acids such as phenylalanine (Phe), alanine (Ala), tryptophan (Trp), histidine (His), glutamic acid (Glu), arginine (Arg), lysine (Lsy), and tyrosine (Tyr) on the surface of cerium oxide nanoparticles (CeNPs) [**81**]. CeNPs have shown to exhibit catalase-like, oxidase-like and SOD-like activities. Afterwards, a series of amino acid-coated CeNPs obtained were compared for their enzyme-like catalytic activities. Among them, Phe-modified-CeNPs exhibited superior enzyme-like catalytic activity. On the basis of that, modifying nanozymes with a specific chiral amino acid could increase their binding ability and improving specificity towards the corresponding substrates, thus leading to improving catalytic efficiency.

2.3.6 Doping

The heteroatom doping strategy has proved to be an efficient approach for improving catalytic performance of nanozymes [**72**]. Lin's group used a greener approach by introducing doped nitrogen atom onto the carbon nanozymes surface (graphene oxide, carbon dots, carbon tubes, and their derivates), via direct pyrolysis under controlled temperature without other treatments [**82**]. They motivated to use nucleobases including adenine (A), cytosine (C), guanine (G), thymine (T), and uracil (U) as nitrogen-rich biological compounds because they are cheap, abundant, and environmentally friendly. The presence of abundant graphitic N species enhanced the

peroxidase-like activity of nucleobase-derived N-doped carbon nanozymes. Amongst them, carbon nanozyme doped guanine at 900 °C (GNC900) exhibited superior peroxidase-like activity. Hu's group used N-doping strategy, by doping heteroatom N onto reduced graphene oxide (rGO) and mesoporous carbon (MC) surfaces [**83**]. The obtained N-doped rGO and N-doped-MC exhibited superior peroxidase-like activity compared with undoped nanomaterials due to the N-doping strategy. In addition, both N-doped-rGO and N-doped-MC showed high specificity for peroxidase-like activity whilst no obvious effect was obtained for oxidase-like, catalase-like, and SOD-like activities. Li's group synthesized N-doped Q-graphene (N-QG) using plasma treatment strategy [**84**]. The obtained N-QC exhibited superior peroxidase-like activity compared to pristine QC. Similar to N-doped rGO and N-doped MC aforementioned, the N-doped QC showed high specificity for peroxidase-like activity whilst no obvious effect was observed for the other enzymatic activities. Heteroatoms such as cerium (Ce) and cobalt (Co) have also been used to improve the catalytic performance of nanozymes. Yin's group used Ce doped onto $ZnCo_2O_4$ nanospheres [**57**]. The obtained Ce-doped $ZnCo_2O_4$ exhibited superior peroxidase-like activity compared to pure $ZnCo_2O_4$. Cerium was used because of its low-cost energy and high biocompatibility to form oxygen vacancies. Zhao's group used Co doped onto graphitic carbon nitride nanomaterials (g-C_3N_4) [**85**]. The obtained Co-g-C_3N_4 exhibited superior peroxidase-like activity compared to pure g-C_3N_4. The enhanced peroxidase-like activity exhibited on Co-g-C_3N_4 was highly dependent on the doping content of cobalt on the surface of g-C_3N_4 was highlighted.

2.3.7 pH and temperature

The effect of pH could influence the catalytic performance of nanozymes [**86**]. For example, under weak acidic conditions AuNPs have been demonstrated to possess peroxidase-like activity whilst under neutral or alkaline conditions AuNPs exhibited catalase-like and SOD-like activities [**87**,**88**]. Similarly, Fe_3O_4 nanoparticles under weak acidic conditions have been demonstrated to possess peroxidase-like activity whilst under neutral conditions Fe_3O_4 nanoparticles exhibited catalase-like activity [**89**]. The effect of temperature could influence the catalytic performance of nanozymes as well [**72**]. Huang's group compared the effect of temperature on the peroxidase-like activities between their synthesized BSA-$Cu_3(PO_4)_2.3H_2O$ hybrid nanoflower and free HRP under similar conditions from 15 to 65 °C [**90**]. The catalytic activity of free HRP above 37 °C was inactive whilst for BSA-$Cu_3(PO_4)_2.3H_2O$ hybrid nanoflower its catalytic activity was active even up to 65 °C. Therefore, BSA-$Cu_3(PO_4)_2.3H_2O$ hybrid exhibited good thermal stability over natural enzymes.

2.3.8 Activators and inhibitors

The catalytic performance of natural enzymes have been reported to be influenced by introducing activators and inhibitors [**91**]. The activators increase the catalytic activity whilst the inhibitors decrease the catalytic activity. Numerous studies have found great interest to regulate the catalytic performance of nanozymes using ions or molecules which can serve as modulators [**91**–**93**]. Singh's group demonstrated that the core catalytic property of CeNPs was due to the regeneration of +3 oxidation state of Ce at the surface of the nanoparticles [**92**]. CeNPs upon exposure to phosphate ions

exhibited superior catalase-like activity. The enhanced catalase-like activity was attributed to the ability of phosphate ions to keep the Ce in the +3 oxidation state. Gua's group investigated the influence of sulfide ions on the peroxidase-like activity of β-casein stabilized Pt nanoparticles (CM-PtNPs) [**93**]. When ABTS was the substrate, after the binding of sulfide ions onto the surface of CM-PtNPs its peroxidase-like activity was activated. This was attributed to the complete reduction of Pt^{2+} to Pt^{0} after sulfide ions was incorporated onto the surface of CM-PtNPs, thus leading to the formation of more active sites.

2. 4 Nanozymes applications

2.4.1 Nanozymes in sensing

Nanozymes-based biosensors have been extensively explored for the sensing of important chemicals such as metal ions, small molecules, nucleic acids, and proteins [**72**]. Nanozymes can catalyze a colored reaction to mimic a peroxidase-like activity and are used for glucose monitoring representing low-cost, easy, and rapid colorimetric diagnostics tools for point-of-care application and even for home use [**94**]. Various nanozymes have been reported to possess peroxidase-like activity and there are CuO-Au nanoalloys [**54**], CuONRs@AuPdNPs [**56**], and Fe_3O_4@SiO_2-NH_2-Au@PdNPs [**60**] could achieve the detection of glucose. These nanozymes upon addition with glucose oxidase (GOx) could selectively catalyze glucose in the presence of oxygen to produce gluconic acid and H_2O_2. The produced H_2O_2 facilitated the oxidation of TMB to its blue-colored products, TMBDI. The concentration of the blue-

colored products with absorption at 652 nm was proportional to the concentration of glucose and was used to quantify glucose.

2.4.2 Nanozymes in environmental remediation

Organic pollutions have shown harmful effects on the eco-environmental system and human health [**95**]. Organic pollutants including heavy metal ions, organic dyes, antibiotics, pesticides, and pathogens have been found to possess high resistance to degradation [**96**]. Traditionally, chemical oxidation, physical adsorption, and biological methods have been widely used to decompose organic pollutants [**97**]. However, these methods suffer from complicated process, expensive equipment and may results in secondary pullulation [**98**,**99**]. To overcome these shortcomings, researchers have used nanozyme as an ideal degradation agent. Wang's group prepared Fe_3O_4 nanoparticles as peroxidase mimics using two different methods for the oxidative removal of organic pollutants [**100**]. Fe_3O_4 nanoparticles prepared using the ultrasonic assisted method and the conventional mechanical stirring method could almost degrade 90% and less than 20% of rhodamine (RhB) in 60 min, respectively. The high thermal stability and durability exhibited by BSA-$Cu_3(PO_4)_2.3H_2O$ hybrid nanoflower to retain its peroxidase-like activity at higher temperature could catalyze the degradation of rhodamine B (RhB) with high efficiency [**90**].

Inspired by the new synergistic effects of trimetallic nanozymes to improve the enzyme catalytic activities, Wang's group used Au/Pt/Co confined in a silica scaffold to form DMSN@AuPtCo as water purifier. DMSN@AuPtCo could achieve decontaminating of organic wastewater and sewage [**101**]. After the treatment of the wastewater with DMSN@AuPtCo over 24 hours, the removal efficiency of both phenol and H_2O_2 was

over 99%. The additional advantages of DMSN@AuPtCo to overcome the challenge of secondary pollution by treating different sewage samples in one system was well-mentioned. Photocatalytic degradation under ultraviolet or visible light irradiation have shown to degrade organic pollutants. Fan's group demonstrated that titanate nanomaterials (NTs) photocatalyst modified with H_2O_2 to form HTNM under visible light exhibited enhanced photoresponse with high photocatalytic activity for the degradation of naproxen [**102**]. Fan's group further synthesized a series of MOFs structures designed ZIF-8, Ag/AgCl@ZIF-8, MOF-235, Bi_2WO_6/ML-100(Fe), and BiOBr/MOF-5 for photocatalytic inactivation of *Microcystic aeruginosa* (bacteria) for algae degradation [**103**].

Ag/AgCl@ZIF-8 exhibited superior photoresponse with high photocatalytic activity under sunlight resulting in over 90% algae removal. The enhancement in the photoresponse exhibited by Ag/AgCl@ZIF-8 was attributed to the oxidative stress due to the generation of ROS between ZIF-8 and Ag/AgC heterojunction.

2.4.3 Nanozymes in antibacteria

Over the years, multi-drug resistant bacteria and the formation of biofilms have shown to be a challenge and a problem to human health [**97**]. Traditionally, antibacterial methods include natural, organic, and inorganic antibacterial agents. These methods suffer from inherent limitations such as easy leakage of toxic ions into the environment, complicated preparation processes, expensive, poor antibacterial efficiency, heat resistance, and antibiotic resistance [**104**–**107**]. In contrast to the current antibacterial methods, nanozymes have shown to possess good biocompability and excellent antibacterial activities [**72**]. Nanozymes have shown to trigger the generation of ROS

which can attack bacteria and biofilms due to their high oxidation capability. Zinc-based zeolitic-imidazolate-framework (ZIF-8)-derived Zn-N-C single-atom nanozyme (SAzyme) with improved peroxidase-like activity was investigated [**108**]. This was attributed to the coordinately unsaturated Zn-N_4 active sites, and the decomposition of H_2O_2 to generate high oxidative HO^{-}• radicals. The generated HO^{-}• radicals could trigger the oxidation of cellular components, thus resulting in inhibiting the growth of the bacteria (*Pseudomons aeruginosa*) by up to 99.9% and significantly promoting wound healing with low toxicity. The concentration of H_2O_2 plays an important role for bacterial inactivation and wound disinfection [**109**]. The higher concentration of H_2O_2 has inherent bactericidal effect which could results in potential toxicity to healthy tissues and even delay wound healing. Wang's group successfully integrated AuNPs with ultrathin graphitic carbon nitride (g-C_3N_4) to form g-C_3N_4@AuNPs (CNA) hybrid [**109**]. The obtained CNA activated biologically relevant concentrations of H_2O_2 to combat bacterial infections. A remarkably excellent peroxidase-like activity exhibited by CNA catalyzed the decomposition H_2O_2 to HO^{-}• radicals and was much more efficient, resulting in excellent bacterial efficiencies against both Gram-negative and Gram-positive. Also, made it possible to destroy biofilms and prevented formation of new biofilms. Besides, a CNA-based band aid with ultralow concentrations of H_2O_2 of 10 μM could significantly prohibit bacterial infections and accelerated wound healing. More importantly, with the excellent peroxidase-like activity of CNA, they successfully constructed an acute lung infection model and reported that CNA could alleviated the inflammation caused by *Methicillin-resistant Straphylococcus aureus* (MRSA).

2.4.4 Nanozymes in cancer therapy

Nanozymes have received great attention in biomedical application for improving diagnostic and therapeutic efficacies of different diseases such as cancer [**97**]. The treating of cancer using nanozymes can be summarized into two conditions: (i) normoxic conditions and (ii) hypoxic conditions. Under normoxic conditions, the nanozyme is mainly based on the oxygen supply and the external stimuli such as magnetic field, light, ultrasound, and heat for the generation of ROS, which can cause the apoptosis of tumor cells [**97**]. Li's group reported PtFe@Fe_3O_4 exhibited photothermal effect with photo-enhanced catalase-like activity (i.e. catalyzes H_2O_2 to generate oxygen) and peroxidase-like activity (i.e. generates toxic ROS under tumor environment) [**110**]. Due to the ROS induced apoptosis, the nanozyme-based PtFe@Fe_3O_4 could serve as a promising strategy for the treatment of malignant tumor. However, under hypoxic conditions, oxygen supply is reduced which might affect the generation of ROS, thus leading to limited therapeutic efficacy. Qu's group rationally designed and synthesized a biomimetic nanoflower through the self-assembly of PtCo and MnO_2 to form MnO_2@PtCo nanoflower based-nanozyme. PtCo and MnO_2 exhibited peroxidase-like activity and catalase-like activity, respectively [**111**]. Therefore, MnO_2@PtCo nanoflower could achieve a remarkable therapeutic efficacy for hypoxic tumors. The major role that H_2O_2 plays in the applications of nanozymes is crucial for the generation of ROS or oxygen depending on the mechanism of action. This work will explore the possible ROS generation and electron-transfer mechanism. Noble metal nanozymes show enhanced activity and hence their mono and bimetallic nanoparticles applications would be studied. Of importance is the recovery of the noble

metal catalysts due to cost. The study looks at designing a method of attaching noble metal nanoparticles (by absorption) that allow their continued use and reuse.

2.5 References

(1) Yang, W.; Li, J.; Wang, M.; Sun, X.; Liu, Y.; Yang, J.; Ng, D. A Colorimetric Strategy for Ascorbic Acid Sensing Based on the Peroxidase-Like Activity of Core-Shell Fe_3O_4/CoFe-LDH hybrid. *Coll. Surf. B. Biointerf.* **2020**, 188, 110742.

https://doi.org/10.1016/j.colsurfb.2019.110742

(2) Zhou, H.; Long. J. R.; Yaghi, O. M. Introduction to Metal−Organic Frameworks. *Chem. Rev*. **2012**, 112, 673–674. https://doi.org/10.1021/cr300014x

(3) Younis, S. A.; Bhardwaj, N.; Bhardwaj, S. K.; Kim, K. H.; Deep, A. Rare Earth Metal–Organic Frameworks (RE-MOFs): Synthesis, Properties, and Biomedical Applications. *Coord. Chem. Rev.* **2012**, 429, 213620.

https://doi.org/10.1016/j.ccr.2020.213620

(4) Wong, E. L. S.; Vuong, K. Q.; Chow, E. Nanozymes for Enivromental Pollutant Monitoring Remediation. *Sensors* **2021**, 21, 408. https://doi.org/10.3390/ s21020408

(5) Dong, W.; Liu, X.; Shi, W.; Huang, Y. Metal-Organic Framework MIL-53(Fe): Facile Microwave-Assisted Synthesis and use as a Highly Active Peroxidase Mimetic for Glucose Biosensing. *RSC Adv.* **2015**, 5, 17451–17457.

https://doi.org/10.1039/c4ra15840g

(6) Guo, J.; Wu, S.; Wang, Y.; Zhao, M. A Label-Free Fluorescence Biosensor Based on a Bifunctional MIL-101(Fe) Nanozyme for Sensitive Detection of Choline and Acetylcholine at NanomolarLevel. *Sens. Act. B. Chem.* **2020**, 312, 128021. https://doi.org/10.1016/j.snb.2020.128021

(7) Bagheri, N.; Khataee, A.; Hassanzadeh, J.; Habibi, B. Sensitive Biosensing of Organophosphate Pesticides Using Enzyme Mimics of Magnetic ZIF-8. *Spectrochim. Acta - Part A Mol. Biomol. Spectrosc.* **2019**, 209, 118–125.

https://doi.org/10.1016/j.saa.2018.10.039

(8) Liu, Y. L.; Zhao, X. J.; Yang, X. X.; Li, Y. F. A Nanosized Metal-Organic Framework of Fe-MIL-88NH_2 as a Novel Peroxidase Mimic Used for Colorimetric Detection of Glucose. *Analyst* **2013**, 138, 4526–4531. https://doi.org/10.1039/c3an00560g

(9) Li, Q.; Wang, Q.; Li, Y.; Zhang, X.; Huang, Y. 2D Bimetallic Ni/Fe MOF Nanosheet Composites as a Peroxidase-Like Nanozyme for Colorimetric Assay of Multiple Targets. *Anal. Methods* **2021**, 13, 2066–2074. https://doi.org/10.1039/d1ay00281c

(10) Navyatha, B.; Singh, S.; Nara, S. Au Peroxidase Nanozymes: Promises and Applications in Biosensing. *Biosens. Bioelectron.* **2021**, 175, 112882.

https://doi.org/10.1016/j.bios.2020.112882

(11) Luo, L.; Hunag, L.; Liu, X.; Zhang, W.; Yao, X.; Dou, L.; Zhang, X.; Nian, Y.; Sun, J.; Wang, J. Mixed-Valence Ce-BPyDC Metal-Organic Framework with Dual Enzyme-Like Activities for Colorimetric Biosensing. *Inorg. Chem.* **2019**, 58, 11382–11388.

https://doi.org/10.1021/acs.inorgchem.9b00661

(12) Liu, X.; Qi, W.; Wang, Y.; Su, R.; He, Z. Exploration of Intrinsic Lipase-Like Activity of Zirconium-Based Metal-Organic Frameworks. *Eur. J. Inorg. Chem.* **2018**, 4579–4585 (2018). https://doi.org/ 10.1002/ejic.201800898

(13) Patel, K. D.; Singh, R. K.; Kim, H. W. Carbon-Based Nanomaterials as an Emerging Platform for Theranostics. *Mater. Horizons.* **2019**, 6, 434–469.

https://doi.org/10.1039/c8mh00966j

(14) Ding, H.; Hu, B.; Zhang, B.; Zhang, H.; Yan, X.; Nie, G.; Liamg, M. Carbon-Based Nanozymes for Biomedical Applications. *Nano Res.* **2021**, 14, 570–583.

https://doi.org/10.1007/s12274-020-3053-9

(15) Sun, H.; Zhou, Y.; Ren, J.; Qu, X. Carbon Nanozymes: Enzymatic Properties, Catalytic Mechanism, and Applications. *Angew. Chemie - Int. Ed.* **2018**, 57, 9224–9237. https://doi.org/10.1002/anie.201712469

(16) Lv, Y.; Ma, M.; Huang, Y.; Xia, Y. Carbon Dot Nanozymes: How to Be Close to Natural Enzymes. *Chem. - A Eur. J.* **2019**, 25, 954–960.

https://doi.org/10.1002/chem.201804419

(17) Nasir, M.; Nawaz, M.; Latif, U.; Yaqub, M.; Hayat, A.; Rahim, A. An Overview on Enzyme-Mimicking Nanomaterials for use in Electrochemical and Optical Assays. *Microchim. Acta* **2017**, 184, 323–342. https://doi.org/10.1007/s00604-016-2036-8

(18) Wei, H.; Wang, E. Nanomaterials with Enzyme-Like Characteristics (Nanozymes): Next-Generation Artificial Enzymes. *Chem. Soc. Rev.* **2013**, 42, 6060–6093.

https://doi.org/10.1039/c3cs35486e

(19) Chen, W.; Li, S.; Wang, J.; Sun, K.; Si, Y. Metal and Metal-Oxide Nanozymes: Bioenzymatic, Characteristics, Catalytic Mechanism, and Eco-Environmental Applications. *Nanoscale* **2019**, 11, 15783–15793. https://doi.org/10.1039/c9nr04771a

(20) Logan, N.; McVey, C.; Elliott, C.; Cao, C. Amalgamated Gold-Nanoalloys with Enhanced Catalytic Activity for the Detection of Mercury Ions (Hg^{2+}) in Seawater Samples. *Nano Res.* **2020**, 13, 989–998. https://doi.org/10.1007/s12274-020-2731-y

(21) Landry, M. J.; Gellé, A.; Meng, B. Y.; Barrett, C. J.; Moores, A. Surface-Plasmon-Mediated Hydrogenation of Carbonyls Catalyzed by Silver Nanocubes under Visible Light. *ACS Catal.* **2017**, 7, 6128–6133. https://doi.org/10.1021/acscatal.7b02128

(22) Chen, J.; Lim, B.; Lee, E. P.; Xia, Y. Shape-Controlled Synthesis of Platinum Nanocrystals for Catalytic and Electrocatalytic Applications. *Nano Today* **2009**, 4, 81–95. https://doi.org/10.1016/j.nantod.2008.09.002

(23) Xi, Z.; Cheng, X.; Gao, Z.; Wang, M.; Cai, T.; Muzzio, M.; Davidson, E.; Chen, O.; Jung, Y.; Sun, S.; Xu, Y.; Xia, X. Strain Effect in Palladium Nanostructures as Nanozymes. *Nano Lett.* **2020**, 20, 272–277.

https://doi.org/10.1021/acs.nanolett.9b03782

(24) Tan, L. L.; Wei, M.; Shang, L.; Yang, Y. W. Cucurbiturils-Mediated Noble Metal Nanoparticles for Applications in Sensing, SERS, Theranostics, and Catalysis. *Adv. Funct. Mater.* **2021**, 31, 1–26. https://doi.org/10.1002/adfm.202007277

(25) Ye, H.; Mohar, J.; Wang, Q.; Catalano, M.; Kim, M.; Xia, X. Peroxidase-Like Properties of Ruthenium Nanoframes. *Sci. Bull.* **2016**, 61, 1739–1745.

https://doi.org/10.1007/s11434-016-1193-9

(26) Chen, J.; Ma, Q.; Li, M.; Chao, D.; Huang, L.; Wu, W.; Fang, Y.; Dong, S. Glucose-Oxidase-Like Catalytic Mechanism of Noble Metal Nanozymes. *Nat. Commun.* **2021**, 12, 1–9. https://doi.org/10.1038/s41467-021-23737-1

(27) Gao, L.; Zhuang, J.; Nie, L.; Zhang, J.; Zhang, Y.; Gu, N.; Wang, T.; Feng, J.; Yang, D.; Perret, S.; Yan, X. Intrinsic Peroxidase-Like Activity of Ferromagnetic Nanoparticles. *Nat. Nanotechnol*. **2007**, 2, 577−583.

https://doi.org/10.1038/nnano.2007.260

(28) Zhu, M.; Wen, Y.; Song, S.; Zheng, A.; Li, J.; Sun, W.; Dai, Y.; Yin, K.; Sun, L. Synergistic Effects Between Polyvinylpyrrolidone and Oxygen Vacancies on Improving the Oxidase-Mimetic Activity of Flower-Like CeO_2 Nanozymes *Nanoscale* **2020**, 12, 19104–19111. https://doi.org/10.1039/d0nr04177g

(29) Li, H.; Li, F.; Wu, J.; Yang, Q.; Li, Q. Two-Dimensional MnO_2 Nanozyme-Mediated Homogeneous Electrochemical Detection of Organophosphate Pesticides without the Interference of H_2O_2 and Color. *Anal. Chem.* **2021**, 93, 4084–4091.

https://doi.org/10.1021/acs.analchem.0c05257

(30) Zeb, A.; Xie, X.; Yousaf, A.; Imran, M.; Wen, T.; Wang, Z.; Guo, H.; Jiang, Y.; Qazi, I.; Xu, A. Highly Efficient Fenton and Enzyme-Mimetic Activities of Mixed-Phase VOx Nanoflakes. *ACS Appl. Mater. Interf.* **2016**, 8, 30126–30132.

https://doi.org/10.1021/acsami.6b09557

(31) Feng, Y.; Hong, L.; Liu, A.; Chen, W.; Li, G.; Chen, W.; Xia, X. High-Efficiency Catalytic Degradation of PhenolBased on the Peroxidase-Like Activity of Cupric Oxide Nanoparticles. *Int. J. Environ. Sci. Technol.* **2015**, 12, 653–660.

https://doi.org/10.1007/s13762-013-0442-6

(32) Li, X.; Liu, B.; Hu, Z.; Liu, P.; Ye, K.; Pan, J.; Niu, X. Smartphone-Assisted off–on Photometric Determination of Phosphate Ion Based on Target-Promoted Peroxidase-Mimetic Activity of Porous CexZr1-xO_2 (x≥0.5) Nanocomposites. *Environ. Res.* **2020**, 189, 109921. https://doi.org/10.1016/j.envres.2020.109921

(33) Liang, X.; Han, L. White Peroxidase-Mimicking Nanozymes: Colorimetric Pesticide Assay without Interferences of O_2 and Color. *Adv. Funct. Mater.* **2020**, 30, 1–10. https://doi.org/10.1002/adfm.202001933

(34) Yang, C.; Xie, Z.; Zhang, H.; Li, H.; Cai, Y.; Wang, J.; Du, J.; Yu, H. Molybdenum Oxide Nanosheet-Supported Ferrous Ion Artificial Peroxidase for Visual Colorimetric Detection of Triacetone Triperoxide. *ACS Sustain. Chem. Eng.* **2019**, 7, 18985–18991. https://doi.org/10.1021/acssuschemeng.9b04462

(35) Wen, S.; Ma, X.; Liu, H.; Chen, G.; Deng, G.; Zhang, Y.; Song, W.; Zhao, B.; Ozaki, Y. Accurate Monitoring Platform for the Surface Catalysis of Nanozyme Validated by Surface-Enhanced Raman-Kinetics Model. *Anal. Chem.* **2020**, 92, 11763–11770. https://doi.org/10.1021/acs.analchem.0c01886

(36) Xiao, M.; Li, N.; Lv, S. Iron Oxide Magnetic Nanoparticles Exhibiting Zymolyase-Like lytic Activity. *Chem. Eng. J.* **2020**, 394, 1–6.

https://doi.org/10.1016/j.cej.2020.125000

(37) Liu, C.; Yan, Y.; Zhang, X.; Mao, Y.; Ren, X.; Hu, C.; He, W.; Yin, J. Regulating the Pro- and Anti-oxidant Capabilities of Bimetallic Nanozymes for the Detection of Fe^{2+} and Protection of: Monascus Pigments. *Nanoscale* **2020**, 12, 3068–3075.

https://doi.org/10.1039/c9nr10135g

(38) Han, X.; Lin, Y.; Zhou, Y.; Song, Z.; Deng, Y.; Qin, J.; Jiang, Z. Metal-Organic Frameworks-Derived Bimetallic Nanozyme Platform Enhances Cytotoxic Effect of Photodynamic Therapy in Hypoxic Cancerc Cells. *Mater. Des.* **2021**, 204, 1–9. https://doi.org/10.1016/j.matdes.2021.109646

(39) Loosen, A.; Simms, C.; Smolders, S.; De Vos, D. E.; Parac-Vogt, T. N. Bimetallic Ce/Zr UiO-66 Metal-Organic Framework Nanostructures as Peptidase and Oxidase Nanozymes. *ACS Appl. Nano Mater.* **2021**, 4, 5748–5757.

https://doi.org/10.1021/acsanm.1c00546

(40) Qi, X.; Tian, H.; Dang, X.; Fan, Y.; Zhang, Y.; Zhao, H. A Bimetallic Co/Mn Metal-Organic-Framework with a Synergistic Catalytic Effect as Peroxidase for the Colorimetric Detection of H_2O_2. *Anal. Methods* **2019**, 11, 1111–1124.

https://doi.org/10.1039/c8ay02514b

(41) Dang, X.; Zhao, H. Bimetallic Fe/Mn Metal-Organic-Frameworks and Au Nanoparticles Anchored Carbon Nanotubes as a Peroxidase-Like Detection Platform with Increased Active Sites and Enhanced Electron Transfer. *Talanta* **2020**, 210, 1–9. https://doi.org/10.1016/j.talanta.2019.120678

(42) Li, S.; Hou, Y.; Chen, Q.; Zhang, X.; Cao, H.; Huang, Y. Promoting Active Sites in MOF-Derived Homobimetallic Hollow Nanocages as a High-Performance Multifunctional Nanozyme Catalyst for Biosensing and Organic Pollutant Degradation. *ACS Appl. Mater. Interf.* **2020**, 12, 2581–2590.

https://doi.org/10.1021/acsami.9b20275

(43) Mou, J.; Xu, X.; Zhang, F.; Xia, J.; Wang, Z. Promoting Nanozyme Cascade Bioplatform by ZIF-Derived N-Doped Porous Carbon Nanosheet-Based Protein/Bimetallic Nanoparticles for Tandem Catalysis. *ACS Appl. Bio Mater.* **2020**, 3, 664–672. https://doi.org/10.1021/acsabm.9b01012

(44) Chen, S.; Quan, Y.; Yu, Y.; L.; Wang, J. H. Graphene Quantum Dot/Silver Nanoparticle Hybrids with Oxidase Activities for Antibacterial Application. *ACS Biomater. Sci. Eng.* **2017**, 3, 313–321.

https://doi.org/10.1021/acsbiomaterials.6b00644

(45) Wang, H.; Jiang, H.; Wang, S.; Shi, W.; He, J.; Liu, H.; Huang, Y. Fe_3O_4-MWCNT Magnetic Nanocomposites as Efficient Peroxidase Mimic Catalysts in a Fenton-Like Reaction for Water Purification without pH Limitation. *RSC Adv.* **2014**, 4, 45809–45815. https://doi.org/10.1039/c4ra07327d

(46) Ma, Z.; Qiu, Y.; Yang, H.; Huang, Y.; Lui, J.; Lu, Y.; Zhang, C.; Hu, P. Effective Synergistic Effect of Dipeptide-Polyoxometalate-Graphene Oxide Ternary Hybrid Materials on Peroxidase-Like Mimics with Enhanced Performance. *ACS Appl. Mater. Interf.* **2015**, 7, 22036–22045.https://doi.org/10.1021/acsami.5b07046

(47) Qin, X.; Dong, Y.; Wang, M.; Zhu, Z.; Li, M.; Chen, X.; Yang, S.; Shao, Y. C-Dots Assisted Synthesis of Gold Nanoparticles as Labels to Catalyze Copper Deposition for Ultrasensitive Electrochemical Sensing of Proteins. *Sci. China Chem.* **2018**, 61, 476–482. https://doi.org/10.1007/s11426-017-9204-8

(48) Xia, X.; Zhang, J.; Lu, N.; Kim, M. J.; Ghale, K.; Xu, Y.; McKenzie, E.; Lui, J.; Ye, H. Pd-Ir Core-Shell Nanocubes: A Type of Highly Efficient and Versatile Peroxidase Mimic. *ACS Nano* **2015**, 9, 9994–10004.

https://doi.org/10.1021/acsnano.5b03525

(49) Liu, J. H.; Wang, A. Q.; Chi, Y. S.; Lin, H. P.; Mou, C. Y. Synergistic Effect in an Au-Ag Alloy Nanocatalyst: CO Oxidation. *J. Phys. Chem. B*. **2005**, 109, 40–43. https://doi.org/10.1021/jp044938g

(50) Zhao, Y.; Ye, C.; Liu, W.; Chen, R.; Jiang, X. Tuning the Composition of AuPt Bimetallic Nanoparticles for Antibacterial Application. *Angew. Chemie - Int. Ed.* **2014**, 53, 8127–8131. https://doi.org/10.1002/anie.201401035

(51) Zhang, S.; Metin, Ö.; Su, D.; Sun, S. Monodisperse AgPd Alloy Nanoparticles and theirSuperior Catalysis for the Dehydrogenation of Formic Acid. *Angew. Chemie - Int. Ed.* **2013**, 52, 3681–3684. https://doi.org/10.1002/anie.201300276

(52) Wilson, N. M.; Pan, Y. T.; Shao, Y. T.; Zuo, J. M.; Yang, H.; Flaherty, D. W. Direct Synthesis of H_2O_2 on AgPt Octahedra: The Importance of Ag-Pt Coordination for High H_2O_2 Selectivity. *ACS Catal.* **2018**, 8, 2880–2889.

https://doi.org/10.1021/acscatal.7b04186

(53) Chen, C.; Zhao, D.; Jiang, Y.; Ni, P.; Zhang, C.; Wang, B.; Yang, F.; Lu, Y.; Sun, J. Logically Regulating Peroxidase-Like Activity of Gold Nanoclusters for Sensing Phosphate-Containing Metabolites and Alkaline Phosphatase Activity. *Anal. Chem.* **2019**, 91, 15017–15024. https://doi.org/10.1021/acs.analchem.9b03629

(54) Mvango, S.; Mashazi, P. Materials Science and Engineering C Synthesis, Characterization of Copper Oxide-Gold Nanoalloys and Their Peroxidase-Like Activity Towards Colorimetric Detection of Hydrogen Peroxide and gGucose. *Mater. Sci. Eng. C*. **2019**, 96, 814–823. https://doi.org/10.1016/j.msec.2018.12.010

(55) Tada, D. B.; Baptista, M. S. Photosensitizing Nanoparticles and the Modulation of ROS Generation. *Front. Chem.* **2015**, 3, 1–14.

https://doi.org/10.3389/fchem.2015.00033

(56) Sicwetsha, S.; Mvango, S.; Nyokong, T.; Mashazi, P. Effective ROS Generation and Morphological Effect of Copper Oxide Nanoparticles as Catalysts. *J. Nanoparticle Res.* **2021**, 23, 1–19. https://doi.org/10.1007/s11051-021-05334-x

(57) Yin, D.; *Yang, H.*; *Wang, S.*; *Yang, Z.*; *Lui, Q.*; *Zhang, X.* Ce-doped $ZnCo_2O_4$ Nanospheres: Synthesis, Double Enzyme-Like Performances, Catalytic Mechanism and Fast Colorimetric Determination for Glutathione. *Coll. Surf. A Physicochem. Eng. Asp.* ***2020,*** 607,1–10.

https://doi.org/10.1016/j.colsurfa.2020.125466

(58) Tao, Y.; Ju, E.; Ren, J.; Qu, X. Bifunctionalized Mesoporous Silica-Supported Gold Nanoparticles: Intrinsic Oxidase and Peroxidase Catalytic Activities for Antibacterial Applications. *Adv. Mater.* ***2015,*** 27, 1097–1104.

https://doi.org/10.1002/adma.201405105

(59) Xu, Z.; Li, L.; Chen, L.; Tu, J.; Chen, W.; Zhu, H.; Cheng, H. Peroxidase-Mimetic Activity of a Nanozyme with Uniformly Dispersed Fe_3O_4 NPs Supported by Mesoporous Graphitized Carbon for Determination of Glucose. *Microchim. Acta* **188**, (2021). https://doi.org/10.1007/s00604-021-05035-1

(60) Adeniyi, O.; Sicwetsha, S.; Mashazi, P. Nanomagnet-Silica Nanoparticles Decorated with Au@Pd for Enhanced Peroxidase-Like Activity and Colorimetric Glucose Sensing. *ACS Appl. Mater. Interf.* **2020**,12, 1973–1987.

https://doi.org/10.1021/acsami.9b15123

(61) Mu, J.; Wang, Y.; Zhao, M.; Zhang, L. Intrinsic Peroxidase-Like Activity and Catalase-Like Activity of Co_3O_4 Nanoparticles. *Chem. Commun.* ***2012***, 48, 2540–2542. https://doi.org/10.1039/C2CC17013B

(62) Kumar, A.; Maji, K.; Mondal, A.; Karmakar, B.; Biswas, P.; Adhikary, B. Iron Selenide Thin Film Peroxidase-Like Behavior, Glucose Detection and Amperometric Sensing of Hydrogen Peroxide. *Sens. Act. B. Chem.* **2012**, 173, 724–731.

https://doi.org/10.1016/j.snb.2012.07.070

(63) Ding, Y.; Yang, B.; Liu, H.; Lui, Z.; Zhang, X.; Zheng, X.; Lui, Q. FePt-Au Ternary Metallic Nanoparticles with the Enhanced Peroxidase-Like Activity for Ultrafast Colorimetric Detection of H_2O_2. *Sens. Act. B. Chem.* **2018**, 259, 775–783.

https://doi.org/10.1016/j.snb.2017.12.115

(64) Zheng, C.; Ke, W.; Yin, T.; An, X. Intrinsic Peroxidase-Like Activity and the Catalytic Mechanism of Gold@Carbon Dots Nanocomposites. *RSC Adv.* ***2016***, 6, 35280–35286. https://doi.org/10.1039/C6RA01917J

(65) Han, L.; Shi, J.; Liu, A.; Liu, A. Novel Biotemplated MnO_2 1D Nanozyme with Controllable Peroxidase-Like Activity and Unique Catalytic Mechanism and its Application for Glucose Sensing. *Sens. Act. B. Chem.* ***2017***, 252, 919–926.

https://doi.org/10.1016/j.snb.2017.06.096

(66) Sun, H.; *Lui, X.*; *Wang, X.*; *Han, Q.*; *Qi, C.*; *Li, Y.*; *Wang, C.*; *Chen, Y.*; *Yang, R.* Colorimetric Determination of Ascorbic Acid using a Polyallylamine-Stabilized IrO_2/Graphene Oxide Nanozyme as a Peroxidase Mimic. *Microchim. Acta* ***2020****,* 187, 1–9. https://doi.org/10.1007/s00604-019-3897-4

(67) Su, H.; Lui, D.; Zhao, M.; Hu, L.; Xue, S.; Cao, Q.; Le, Y. Dual-Enzyme Characteristics of Polyvinylpyrrolidone-Capped Iridium Nanoparticles and Their Cellular Protective Effect against H_2O_2-Induced Oxidative Damage. *ACS Appl. Mater. Interf.* ***2015****,* 7, 8233–8242. https://doi.org/10.1021/acsami.5b01271

(68) Liu, X.; Wang, X.; Qi, C.; Han, Q.; Xiao, W.; Cai, S.; Wang, C.; Yang, Y. Sensitive Colorimetric Detection of Ascorbic Acid using Pt/CeO_2 Nanocomposites as Peroxidase Mimics. *Appl. Surf. Sci.* **2019**, 479, 532–539.

https://doi.org/10.1016/j.apsusc.2019.02.135

(69) Schmid, G.; Corain, B. Nanoparticulated Gold Syntheses, Structures, Electronics, and Reactivities. *Eur. J. Inorg. Chem.* ***2003****, 17,* 3081–3098.

https://doi.org/10.1002/ejic.200300187

(70) Iqbal, M.; Usanase, G.; Oulmi, K.; Aberkane, F.; Bendaikha, T.; Fessi, H.; Zine, N.; Agusti, G.; Errachid, S.; Elaissari, A. Preparation of Gold Nanoparticles and Determination of Their Particles Size via Different Methods. *Mater. Res. Bull.* **2016**, 79, 97–104. https://doi.org/10.1016/j.materresbull.2015.12.026

(71) Ghosh, S. K.; Pal, A.; Kundu, S.; Nath, S.; Pal, T. Fluorescence Quenching of 1-Methylaminopyrene Near Gold Nanoparticles: Size Regime Dependence of the Small Metallic Particles. *Chem. Phys. Lett.* **2004**, 395, 366–372.

https://doi.org/10.1016/j.cplett.2004.08.016

(72) Peng, F.; Zhang, Y.; Gu, N. Size-Dependent Peroxidase-Like Catalytic Activity of Fe3O4 nanoparticles. *Chine. Chem. Lett.* **2008**, 19, 730–733.

https://doi.org/10.1016/j.cclet.2008.03.021

(73) Ge, C.; Fang, G.; Shen, X.; Chong, Y.; Warmer, G.; Gao, X.; Chai, Z.; Chen, C.; Yin, J. Facet Energy Versus Enzyme-like Activities: The Unexpected Protection of Palladium Nanocrystals against Oxidative Damage. *ACS Nano* **2016**, 10, 10436–10445. https://doi.org/10.1021/acsnano.6b06297

(74) Puvvada, N.; Panigrahi, P. K.; Mandal, D.; Pathak, A. Shape Dependent Peroxidase Mimetic Activity Towards Oxidation of Pyrogallol by H_2O_2. *RSC Adv.* ***2012,*** **2**, 3270–3273. https://doi.org/10.1039/C2RA01081J

(75) Zhang, Y.; Li, S.; Liu, H.; Long, W.; Zhang, X. D. Enzyme-Like Properties of Gold Clusters for Biomedical Application. *Front. Chem.* **2020**, 8, 1–13.

https://doi.org/10.3389/fchem.2020.00219

(76) Lin, Y.; Li, Z.; Chen, Z.; Ren, J.; Qu, X. Mesoporous Silica-Encapsulated Gold Nanoparticles as Artificial Enzymes for Self-Activated Cascade Catalysis. *Biom.* **2013**, 34, 2600–2610.

https://doi.org/10.1016/j.biomaterials.2013.01.007

(77) Asati, A.; Santra, S.; Kaittanis, C.; Nath, S.; Perez, J. M. Oxidase-Like Activity of Polymer-Coated Cerium Oxide Nanoparticles. *Angew. Chemie*. **2009**, 121, 2344–2348. https://doi.org/10.1002/ange.200805279

(78) Veitch, N. C.; Smith, A. T. Horseradish Peroxidase. *Adv. Inorg. Chem.* **2000**, 51, 107–162. https://doi.org/10.1016/S0898-8838(00)51002-2

(79) Wu, W.; Wang, Q.; Chen, J.; Huang, L.; Zhang, H.; Rong, K.; Dong, S. Biomimetic Design for Enhancing the Peroxidase Mimicking Activity of Hemin. *Nanoscale* **2019**, 11, 12603–12609. https://doi.org/10.1039/C9NR03506K

(80) González, M.; Liao, C.; Cazelles, R.; Wang, S.; Yu, X.; Gutkin, V.; Wilner, I. Mimicking Horseradish Peroxidase Functions Using Cu^{2+}-Modified Carbon Nitride Nanoparticles or Cu^{2+}-Modified Carbon Dots as Heterogeneous Catalysts. *ACS Nano* **2017**, 11, 3247–3253. https://doi.org/10.1021/acsnano.7b00352

(81) Fan, K.; *Wang, H.*; *Xi, J.*; *Meng, X.*; *Duan, D.*; *Gao, L.*; *Yan, X.* Optimization of Fe_3O_4 Nanozyme Activity via Single Amino Acid Modification Mimicking an Enzyme Active Site. *Chem. Commun.* **2017**, 53, 424–427.

https://doi.org/10.1039/C6CC08542C

(82) Zhang, Z.; Zhang, X.; Liu, B.; Liu, J. Molecular Imprinting on Inorganic Nanozymes for Hundred-fold Enzyme Specificity. *J. Am. Chem. Soc.* **2017**, 139, 5412–5419. https://doi.org/10.1021/jacs.7b00601

(83) Zhang, R.; Zhou, Y.; Yan, X.; Fan, K. Advances in Chiral Nanozymes: A Review. *Microchim. Acta* **2019**, 186, 1–12. https://doi.org/10.1007/s00604-019-3922-7

(84) Xu, C.; Zhao, C.; Li, M.; Ren, J.; Qu, X. Artificial Evolution of Graphene Oxide Chemzyme with Enantioselectivity and near-Infrared Photothermal Effect for Cascade Biocatalysis Reactions. *Small* **2014**,10, 1841–1847.

https://doi.org/10.1002/smll.201302750

(85) Sun, Y.; Zhao, C.; Gao, N.; Ren, J.; Qu, X. Stereoselective Nanozyme Based on Ceria Nanoparticles Engineered with Amino Acids. *Chem. - A Eur. J.* **2017**, 23, 18146–18150. https://doi.org/10.1002/chem.201704579

(86) Cheng, H.; Lin, S.; Muhammad, F.; Lin, Y. W.; Wei, H. Rationally Modulate the Oxidase-Like Activity of Nanoceria for Self-Regulated Bioassays. *ACS Sens.* ***2016,*** 1, 1336–1343. https://doi.org/10.1021/acssensors.6b00500

(87) Lin, Y.; Ren, J.; Qu, X. Nano-Gold as Artificial Enzymes: Hidden Talents. *Adv. Mater.* **2014**, 26, 4200–4217. https://doi.org/10.1002/adma.201400238

(88) Shen, X.; Liu, W.; Gao, X.; Lu, Z.; Wu, X.; Gao, X. Mechanisms of Oxidase and Superoxide Dismutation-like Activities of Gold, Silver, Platinum, and Palladium, and Their Alloys: A General Way to the Activation of Molecular Oxygen. *J. Am. Chem. Soc.* **2015**, 137, 15882–15891. https://doi.org/10.1021/jacs.5b10346

(89) Chen, Z.; Yin, J.; Zhou, T.; Zhang, Y.; Song, L.; Song, M.; Hu, S.; Gu, N. Dual Enzyme-Like Activities of Iron Oxide Nanoparticles and Their Implication for Diminishing Cytotoxicity. *ACS Nano* **2012**, 6, 4001–4012.

https://doi.org/10.1021/nn300291r

(90) Huang, Y.; Ran, X.; Lin, Y.; Ren, J.; Qu, X. Self-Assembly of an Organic-Inorganic Hybrid Nanoflower as an Efficient Biomimetic Catalyst for Self-Activated Tandem Reactions. *Chem. Commun.* **2015**, 51, 4386–4389.

https://doi.org/10.1039/C5CC00040H

(91) Arsalan, A.; Younus, H. Enzymes and Nanoparticles: Modulation of Enzymatic Activity via Nanoparticles. *Int. Biol. Macromol.* **2018**, 118, 1833–1847.

https://doi.org/10.1016/j.ijbiomac.2018.07.030

(92) Singh, S.; Dosani, T.; Karakoti, S.; Kumar, A.; Seal, S.; William, T. A Phosphate-Dependent Shift in Redox State of Cerium Oxide Nanoparticles and its Effects on Catalytic Properties. *Biom.* **2011**, 2, 6745–6753.

https://doi.org/10.1016/j.biomaterials.2011.05.073

(93) Liu, Y.; Zheng, Y.; Ding, D.; Guo, R. Switching Peroxidase-Mimic Activity of Protein Stabilized Platinum Nanozymes by Sulfide Ions: Substrate Dependence, Mechanism, and Detection. *Langmuir*. **2017**, 33, 13811–13820.

https://doi.org/10.1021/acs.langmuir.7b03430

(94) Larossi, M.; Schiattarella, C.; Rea, I.; Stefano, D.; Fittipaldi, R.; Vecchione, A.; Velotta, R.; Ventura, D. Colorimetric Immunosensor by Aggregation of Photo-chemically Functionalized Gold Nanoparticles. *ACS Omega* **2018**, 3, 3805–3812. https://doi.org/10.1021/acsomega.8b00265

(95) Hu, L.; Zhang, C.; Zeng, G.; Chen, G.; Wan, J.; Guo, Z.; Wu, H.; Yu, Z.; Lui, J. Metal-Based Quantum Dots: Synthesis, Surface Modification, Transport and Fate in Aquatic Environments and Toxicity to Microorganisms. *RSC Adv.* ***2016,*** 6, 78595–78610. https://doi.org/10.1039/C6RA13016J

(96) Rathi, B. S.; Kumar, P. S.; Show, P. L. A Review on Effective Removal of Emerging Contaminants from Aquatic Systems: Current Trends and Scope for Further Research. *J. Hazard. Mater.* **2021**, 409, 1–20.

https://doi.org/10.1016/j.jhazmat.2020.124413

(97) Hou, L.; Jiang, G.; Sun. Y.; Zhang, X.; Huang, J.; Lui, S.; Lin, T.; Ye, F.; Zhao, S. Progress and Trend on the Regulation Mtheods for Nanozyme Activity and its Application. *Catalysts* **2019**, 9, 1–17. https://doi.org/10.3390/catal9121057

(98) Zhou, C.; Lai, C.; Xu, P.; Zeng, G.; Huang, D.; Zhnag, C.; Cheng, M.; Hu, L.; Wan, J.; Lui, Y.; Xiong, W.; Deng, Y.; Wen, W. In Situ Grown AgI/$Bi_{12}O_{17}Cl_2$ Heterojunction Photocatalysts for Visible Light Degradation of Sulfamethazine: Efficiency, Pathway, and Mechanism. *ACS Sustain. Chem. Eng.* **2018**, 6, 4174–4184.

https://doi.org/10.1021/acssuschemeng.7b04584

(99) Jiang, J.; He, C.; Wang, S.; Jiang, H.; Li, J.; Li, L. Recyclable Ferromagnetic Chitosan Nanozyme for Decomposing Phenol. *Carbohydr. Polym.* ***2018,*** 198, 348–353. https://doi.org/10.1016/j.carbpol.2018.06.068

(100) Wang, N.; Zhu, L.; Wang, D.; Wang, M.; Lin, Z.; Tang, H. Sono-Assisted Preparation of Highly-Efficient Peroxidase-Like Fe_3O_4 Magnetic Nanoparticles for Catalytic Removal of Organic Pollutants with H_2O_2. *Ultrason. Sonochem.* **2010**, 17, 526–533. https://doi.org/10.1016/j.ultsonch.2009.11.001

(101) Wang, F.; Zhang, Y.; Liu, Z.; Ren, J.; Qu, X. A Mesoporous Encapsulated Nanozyme for Decontaminating two kinds of Wastewater and Avoiding Secondary Pollution. *Nanoscale* **2020**, 12, 14465–14471. https://doi.org/10.1039/D0NR03217D

(102) Fan, G.; Zhan, J.; Luo, J.; Zhang, J.; Chen, Z.; You, Y. Photocatalytic Degradation of Naproxen by a H_2O_2-Modified Titanate Nanomaterial under Visible Light Irradiation. *Catal. Sci. Technol.* ***2019,*** 9, 4614–4628.

https://doi.org/10.1039/C9CY00965E

(103) Fan, G.; Zhou, J.; Zheng, X.; Luo, J.; Hong, L.; Qu, F. Fast Photocatalytic Inactivation of *Microcystis aeruginosa* by Metal-Organic Frameworks under Visible Light. *Chemosphere* **2020**, 239, 1–11.

https://doi.org/10.1016/j.chemosphere.2019.124721

(104) Chopra, I.; Hodgson, J.; Metcalf, B.; Poste, G. The Search for Antimicrobial Agents Effective against Bacteria Resistant to Multiple Antibiotics. *Antimicrob. Agents Chemother.* ***1997,*** 41, 497–503. https://doi.org/10.1128/AAC.41.3.497

(105) Krasucka, P.; Pan, B.; Yong, S.; Mohan, D.; Sarkar, B.; Oleszczuk, P. Enginneered Biochar- A Sustaionble solution for the Removal of Antibiotivs from Water. *Chem. Eng. J*. **2021**, 405, 1-27.https://doi.org/10.1016/j.cej.2020.126926

(106) Chernousova, S.; Epple, M. Silver as Antibacterial Agent: Ion, Nanoparticle, and Metal. *Angew. Chemie.* **2013**, 52, 1636–1653.

https://doi.org/10.1002/anie.201205923

(107) Stewart, P. S.; Costerton, J. W. Antibiotic Resistance of Bacteria in Biofilms. *Lancet* **2001**, 358, 135–138. https://doi.org/10.1016/S0140-6736(01)05321-1

(108) Xu, B.; Wang, H.; Wang, W.; Gao, L.; Li, S.; Pan, X.; Wang, H.; Yang, H.; Meng, X.; Wu, Q.; Zheng, L.; Chen, S.; Shi, X.; Fan, K.; Yan, X.; Liu, H. A Single-Atom Nanozyme for Wound Disinfection Applications. *Angew. Chemie.* **2019**, 58, 4911–4916. https://doi.org/10.1002/ange.201813994

(109) Wang, Z.; Dong, K.; Lui, Z.; Zhang, Y.; Chen, Z.; Sun, H.; Ren, J.; Qu, X. Activation of Biologically Relevant Levels of Reactive Oxygen Species by Au/g-C_3N_4 Hybrid Nanozyme for Bacteria Killing and Wound Disinfection *Biom*. **2017**, 113, 145–157. https://doi.org/10.1016/j.biomaterials.2016.10.041

(110) Li, S.; *Shang, L.*; *Xu, B.*; *Wang, B.*; *Wang, S.*; *Gu, K.*; *Wu, Q.*; *Sun, Y.*; *Zhang, Q.*; *Yang, H.*; *Zhang, F.*; *Gu, L.*; *Zhang, T.*; *Lui, H.* A Nanozyme with Photo-Enhanced Dual Enzyme-Like Activities for Deep Pancreatic Cancer Therapy. *Angew. Chemie*. **2019**, 131, 12754–12761. https://doi.org/10.1002/ange.201904751

(111) Wang, Z.; Zhang, Y.; Ju, E.; Lui, Z.; Cao, F.; Chen, Z.; Ren, J.; Qu, X. Biomimetic Nanoflowers by Self-Assembly of Nanozymes to Induce Intracellular Oxidative Damage against Hypoxic Tumors. *Nat. Commun.* **2018**, 9,1–14.

https://doi.org/10.1038/s41467-018-05798-x

CHAPTER 3

3 Pd nanocatalysts adsorbed onto silica nanoparticles coated indium tin oxide a reusable colorimetric sensor for glucose

Abstract

Nanozymes are nanomaterials that possess enzyme-like activity upon exposure to substrate solution. The use of noble or platinum group metals has been shown to give enhanced enzyme-like catalysis. However, noble metals are obtained at a high cost, therefore their recovery after use is of high importance. Herein, we report the fabrication of indium tin oxide-silica nanoparticles decorated with palladium nanoparticles (ITO-SiO_2-prS-PdNPs). The ITO-SiO_2-prS-PdNPs were evaluate for peroxidase-like activity toward the oxidation of 3,3',5,5'-tetramethylbenzidine (TMB) in the presence of H_2O_2. A colour change from clear or colourless TMB to blue colour (oxidized TMB products) was observed confirming the peroxidase-like activity. A typical Michaelis−Menten enzyme-like behaviour with K_m values for H_2O_2 (0.68 mM) and TMB (0.47 mM) is better than the reported values for horse-radish peroxidase (HRP) for the same substrate. The peroxidase-like activity of ITO-SiO_2-prS-PdNPs was found to proceed via the electron-transfer mechanism. The ITO-SiO_2-prS-PdNPs were renewed by rinsing with water and ethanol solution thus making the surface simple, easy to recover. A reusable and highly selective colorimetric assay for glucose detection based on the peroxidase-like activity of ITO-SiO_2-prS-PdNPs gave excellent results. ITO-SiO_2-prS-PdNPs exhibited good linear range of 5.0–30 μM, a low limit of

detection (LoD) of 1.84 µM and a limit of quantification (LoQ) of 6.14 µM. Finally, the nanozyme ITO-SiO_2-prS-PdNPs was successfully used to detect glucose in a complex new-born calf serum (NCS), representing a real sample.

3.1 Introduction

Glucose plays an important role in living cells as a metabolic intermediate and source of energy [**1**,**2**]. It has been reported that normal level of glucose enhance communication between cells, increase memory and stimulate calcium absorption [**3**]. However, excessive glucose level is one of the main causes of diabetes [**4**]. The International Diabetes Federation (IDF) estimated that over 420 million people suffer from diabetes at this moment [**5**,**6**]. The global threats imposed by diabetes and its complications was a motivation behind this study.

The conventional detection and monitoring of glucose is based on personal glucose meters (PGMs) and recently colorimetric sensors using chromogenic agents [**7**]. PGMs utilize glucose oxidase (GOx) enzyme to detect glucose. Glucose is oxidized by GOx enzyme to produce D-gluconolactone which undergoes spontaneous hydrolysis to form gluconic acid. During glucose oxidation, GOx enzyme cofactor (FAD) is reduced to GOx-$FADH_2$ which is an unnatural state. The enzyme GOx ($FADH_2$) in the presence of oxygen is oxidized to GOx(FAD). Simultaneously, hydrogen peroxide (H_2O_2) is produced as an enzymatic reaction by-product. Colorimetric sensors have received research attention due to their simplistic operation and the results are visible to the naked eye as blue coloured products. In colorimetric sensing, H_2O_2 is reduced to reactive oxygen radical species (ROS) by nanomaterials

[**8**]. ROS oxidizes a chromogen (TMB) to blue-coloured products. Other chromogenic species can also be used for as long as they produce coloured products observable using naked eyes and can also be monitored using UV-vis spectroscopy [**9**]. Horse-radish peroxidase (HRP) enzyme can be used to monitor the colorimetric oxidation of TMB to coloured products. However, this will be an expensive bi-enzyme system. Natural enzymes have numerous limitations such as low stability in extreme conditions. The loss of stability for natural enzymes is expected at high pH, temperature, and humidity conditions. Natural enzymes are costly to obtain in high purity. Natural enzymes and known t denature under storage, and thus hindering their widespread applications [**10**].

Nanomaterials are emerging as the most promising substituents for natural enzymes for biosensor fabrication and applications. They have been shown to possess enzyme-like activity and excellent environmental stability [**11**]. The enzyme-like activity of nanomaterials have been shown to mimic peroxidase, catalase, and also superoxide dismutase-like activity [**12**]. The differences in the enzyme that nanomaterials mimic is influenced by the mechanism of action and the products they produce. Some nanomaterials have the ability to catalytically reduce hydrogen peroxide to reactive oxygen species (ROS). A series of noble metal nanoparticles (NPs) such as gold [**13**], palladium [**14**], platinum [**15**], and silver [**16**], have been investigated for their direct electrocatalytic oxidation of glucose. Enhanced catalytic activity was observed when small gold nanoparticles were introduced in the aerobic oxidation of glucose [**17**]. Combining two monometallic nanoparticles of AuNPs and AgNPs produced bimetallic (AuNPs-AgNPs) nanoparticles with improved catalytic activity and excellent optical properties for colorimetric detection of glucose [**17**]. The use of nanoparticles in

solution showed excellent results, however their recover and reuse still remain a world-wide research challenge.

We recently reported the use of magnetic nanoparticles with silica shell decorated with Au@PdNPs, as the method to recover the nanocatalysts magnetically [**18**]. This study showed excellent results and the nanoparticles could be reused. The adsorption of metal nanoparticles on the solid support would also be beneficial for the recovery of the nanocatalysts for further use. An easier method for nanocatalysts is the attachment onto solid support. Indium thin oxide (ITO) functionalized with silica nanoparticles has been reported to yield excellent nanocatalsy attachment [**18**]. ITO is good conductor. Upon coating with silica nanoparticle ITO becomes inert and thus an excellent catalyst support. Herein, we report the fabrication of indium thin oxide substrates first to form hydroxylated ITO (ITO-OH) for the attachment of inert silica nanoparticles (SiO_2NPs), thus forming ITO-SiO_2NPs. On ITO-SiO_2-prS-PdNPs, palladium nanoparticles (PdNPs) were dispersed via 3-mercaptoproyltrimethoxysilane (MPTMS) to form ITO-SiO_2-prS-PdNPs. ITO-SiO_2-prS-PdNPs surface was evaluated its properties as a potential nanozyme (peroxidase mimic) towards the oxidation of TMB in the presence of H_2O_2. A feasible approach with high selectivity and specificity towards colorimetric detection of glucose was also investigated.

Aims of this chapter

(i) To synthesize and characterize silica (SiO_2NPs) and palladium (PdNPs).

(ii) To immobilize SiO_2NPs as a noble metal NP catalyst support onto the indium tin oxide (ITO) to form ITO-SiO_2NPs as the absorbent.

(iii) To introduce thiol functional groups from MPTMS on the ITO-SiO_2NPs surfaces.

(iv) To adsorb and disperse PdNPs onto ITO-SiO_2NPs surfaces to form ITO-SiO_2-prS-PdNPs.

(v) To evaluate the enzyme-like catalytic properties of the fabricated ITO-SiO_2-prS-PdNPs toward TMB/H_2O_2 substrate to form blue-colored products of oxidation of TMB, oxTMB.

(vi) To use the enzyme-like activity of ITO-SiO_2-prS-PdNPs to detect glucose as a biomolecule using glucose oxidase enzyme in buffer and in complex serum solutions.

3.2 Experimental

3.2.1 Materials and reagents

Palladium chloride ($PdCl_2$), tetraethylorthosilicate (TEOS), sodium borohydride ($NaBH_4$), glacial acetic acid (CH_3COOH), 3,3',5,5'-tetramethylbenzidine (TMB), 3-mercaptoproyltrimethoxysilane (MPTMS), D-glucose (Glu) powder, glucose oxidase (GOx, EC 1.1.3.4. from Aspergillus, Type VII), fructose (Fru), sucrose (Suc), lactose (Lac), 1,3-phenyllisobenzefuran (DPBF), terephthalic acid (TA) and Indium Tin Oxide (ITO) substrates were purchased from Sigma Aldrich. Hydrochloric acid (32% HCl), ammonia hydroxide (NH_4OH), ethanol (EtOH), and methanol (MeOH) were purchased from B&M Scientific. Disodium hydrogen orthophosphate (Na_2HPO_4) and sodium dihydrogen orthophosphate (NaH_2PO_4) were purchased from Associated Chemical Enterprises (ACE Chemicals). All the reagents were of analytical grade. All aqueous solutions were prepared using ultrapure water with a resistivity of 18.2 ΩM.cm obtained from a MilliQ system (Millipore, Corp, Bedford, MA, USA).

3.2.2 Apparatus

The UV-vis measurements were carried out on a Thermo-Scientific, Multiskan Sky w Cuvette and Touch Screen, 100-240 V, Belgium. Fourier Transform Infrared Spectroscopy (FTIR) measurements were carried out on a Perkin Elmer Spectrum 100 FTIR. The hydrodynamic and Zeta potential were carried out on a Malvern Zetasizer Nano-ZS90 series equipped with a 633 nm He/Ne laser. A disposable folded capillary cell (DTS 1060) was used for data collection for Zeta potential measurements. Transmission electron microscopy (TEM) micrographs were obtained using a Zeiss Libra 120 TEM operating at 80 kV. The nanoparticles were dissolved in water and dropped onto a carbon-coated copper grid, and allowed to dry overnight at room temperature before measurement. Scanning electron microscopy (SEM) and Energy dispersive X-ray spectroscopy (SEM-EDX) images and elemental composition were obtained from INCA PENTA FET coupled with VGA TASCAM at 20 kV acceleration voltage. X-ray diffraction (XRD) patterns were recorded on a Bruker D8 Discover equipped with a Lynx Eye detector, using Cu-Ka radiation (1.5405 Å, nickel filter). The samples were placed on a silicon wafer slide. The data was collected in the range from 2θ = 10° to 100°. X-ray photoelectron spectroscopy (XPS) measurements were conducted using XPS Kratos - DLD Ultra, UK. Vision processing 2 software was used for elemental composition and fitting of the high-resolution spectra. Electrochemical measurements were performed using Autolab Galvanostat/Potentialstat 302N workstation controlled by Proline computer running on NOVA 1.10 software.

3.2.3 Preparation of silica nanoparticles (SiO_2NPs)

The preparation of silica NPs (SiO_2NPs) was achieved using Stöber method [**19**]. Briefly, 15 mL NH_4OH was added into 250 mL EtOH and the mixture was heated at 40°C with stirring at 200 rpm for 30 min. TEOS (2.5 mL) was added and the mixture was left for 12 hours with constant stirring at 40°C. Additional 1.25 mL of TEOS was added at an interval of one hour for 12 hours to grow a silica shell. The translucent milky solution was obtained indicating the formation of silica nanoparticles (SiO_2NPs). The solution was centrifuged, washed several times with ethanol and deionized water.

3.2.4 Preparation of palladium nanoparticles (PdNPs)

The preparation of palladium NPs (PdNPs) was achieved using sodium borohydride ($NaBH_4$) reduction of H_2PdCl_4 a method reported in literature with slight cnages [**20**]. Briefly, palladium (II) hydrogen chloride precursor (H_2PdCl_4) was obtained by dissolving $PdCl_2$ (1 mM) with hydrochloric acid (32%, 10 mL) in 100 mL of deionized water under stirring for 3 hours. The obtained H_2PdCl_4 solution was yellowish in colour. An ice-cold 0.50 mL of $NaBH_4$ (0.026 M, 1.0 mg) was added into H_2PdCl_4 solution dropwise over 30 min under stirring. As the $NaBH_4$ was added, the yellow solution of H_2PdCl_4 turned black. The colour changes signify the formation of palladium nanoparticles (PdNPs). The solution was centrifuged, washed several times with deionized water and the obtained precipitates were air-dried at room temperature.

3.2.5 Fabrication of ITO-SiO_2-prS-PdNPs, Scheme 3.1

The preparation of ITO-SiO_2-prS-PdNPs was achieved following the method in **Scheme 3.1**. Properly cleaned bare ITO substrate (transparent conducting oxides) was hydroxylated in the mixture of NH_4OH:H_2O_2:H_2O in the ratio 1:1:5 at 60 °C for 30 min in an oven to form hydroxy ITO-OH surface. SiO_2NPs (2.0 mg, mL^{-1}) in ethanol were coated onto ITO-OH for 24 hours to form ITO-SiO_2NPs. Covalent bonds between ITO-OH substrate and silanol (Si-OH) of SiO_2NPs groups resulting in the formation of siloxane (Si-O-Si) functional groups and loss of H_2O. Attachment of SiO_2NPs resulted in an increase in the surface area of the flat ITO to form ITO-SiO_2NPs. MPTMS (40 mM) in methanol was used to modify the ITO-SiO_2NPs to form thiol-functionalized ITO-SiO_2-prSH and this reaction took 3 hours. The terminal −SH functional groups on ITO-SiO_2-prSH served as an anchor for the chemisorption of the noble metal NPs. Aqueous solution PdNPs (2.0 $mg.mL^{-1}$) was dispersed using ultrasonication. The ITO-SiO_2-prSH was immersed into the dispersed PdNPs solution to form ITO-SiO_2-prS-PdNPs in 24 hours. ITO-SiO_2-prS-PdNPs were rinsed with water to remove physically adsorbed PdNPs and dried with N_2 gas. The color of the ITO-SiO_2-prS-PdNPs was blackish, confirming successful deposition of PdNPs.

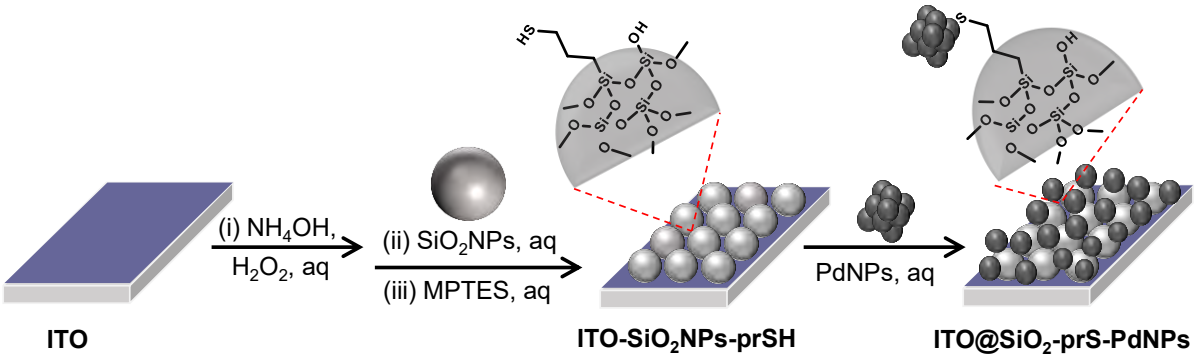

Scheme 3.1: Step-by-step schematic representation of fabrication of ITO-SiO_2-prS-PdNPs as described in Section 3.2.5.

3.2.6 Peroxidase-like activity of ITO-SiO_2-prS-PdNPs

The catalytic oxidation of TMB in the presence of H_2O_2 was investigated at room temperature (25 °C). Briefly, the reaction of ITO-SiO_2-prS-PdNPs (0.50 cm x 1.0 cm), H_2O_2 (0.20 M, 200 µL), TMB (4.2 mM, 200 µL) and acetate buffer (pH 4.0, 0.20 M) were incubated together for 15 min. A blue colour was observed, monitored using UV-vis spectrophotometer and measured wavelength was between 300 and 800 nm.

3.2.7 Glucose detection using ITO-SiO_2-prS-PdNPs

Glucose detection was performed by following these steps: (a) 100 µL of GOx (4 $mg.mL^{-1}$) and 200 µL of glucose with different concentrations in 0.010 M PBS (pH 7.0) were incubated at 37 °C. The reaction was allowed to take for 45 min. (b) In this solution of 100 µL of 2.0 mM TMB, and ITO-SiO_2-prS-PdNPs in 0.20 M acetate buffer (pH 4.0) were incubated at 37 °C for 15 min. An increase in the absorption band at 652 nm was observed and monitored using UV-vis spectrophotometer. Each

concentration of glucose was measured triplicates (n=3) and an average absorption was recorded. The percentage relative standard deviation (%RSD) was also calculated for the measurements.

3.2.8 Monitoring ROS generation using a radical scavenger

The two studies were conducted:

(i) 1,3-Diphenylisobenzofuran (DPBF) has an absorption at 420 nm. Upon reacting with reactive oxygen radical species (ROS) the absorption decreases and this can be monitored using UV–vis spectrophotometer. Experimentally, ITO-SiO_2-prS-PdNPs was immersed into 1 mL acetate buffer (pH 4.0) solution of H_2O_2 (5.0 mM) followed by addition of 200 µL of 0.25 mM DPBF (also in acetate buffer pH 4.0). The UV-vis spectra were measured for 10 minutes at 1 min interval. The initial solution of 200 µL of 0.25 mM DPBF was diluted into 1 mL acetate buffer and measured fresh after preparation. Also we allowed the reaction to stand for 10 min and measured.

(ii) Terephthalic acid, TA (a fluorescent hydroxyl radical quencher) was used in the presence of ITO-SiO_2-prS-PdNPs and H_2O_2. The reaction of 1.0 mM TA in ethanol (1 mL) with acetate buffer (pH 4.0, 4 mL) was mixed with ITOSiO_2-prS-PdNPs in the presence of 3.0 mM H_2O_2 and incubated for 10 min. Fluorescence emission spectra excited at 320 nm were measured.

3.2.9 Electrochemical measurements

All electrochemical experiments were studied using a three-electrode system with ITO-SiO_2-prS-PdNPs as the working electrode, coiled platinum wire as counter electrode and Ag|AgCI as pseudo-reference electrode in acetate buffer pH 4.0 at room temperature. The electrocatalytic oxidation of ITO-SiO_2-prS-PdNPs toward H_2O_2 was performed using amperometric technique and +0.50 V applied potential.

3.3 Results and discussion

3.3.1 Characterization of SiO_2NPs

Figure 3.1 shows (a) TEM image, (b) size distribution histogram, (c) FT-IR spectra, (d) EDX and (e) DLS measurements for silica nanoparticles (SiO_2NPs). The TEM image of SiO_2NPs in **Figure 3.1(a)** shows spherical monodispersed nanoparticles. The particle size distribution in **Figure 3.1(b)** of SiO_2NPs was 77.0 ± 11.0 nm. The FT-IR spectra in **Figure 3.1(c)** shows the characteristic peaks of silica at 793, 952, and 1063 cm^{-1} assigned to siloxane (Si-O-Si) symmetric stretching, silanol (Si-OH) stretching, and Si-O-Si asymmetric stretching vibrations, respectively. The peak at 3235 cm^{-1} was assigned to the O-H stretching of the silanol group. The EDX analysis in **Figure 3.1(d)** shows the elemental composition of SiO_2NPs which showed the presence of Si K, O K, and C K with 40.3%, 57.2% and 2.5% in the particles, respectively. The DLS was used to measure the particle size and was found to be 78.8 nm in **Figure 3.1(e)** and was similar to the TEM particle size.

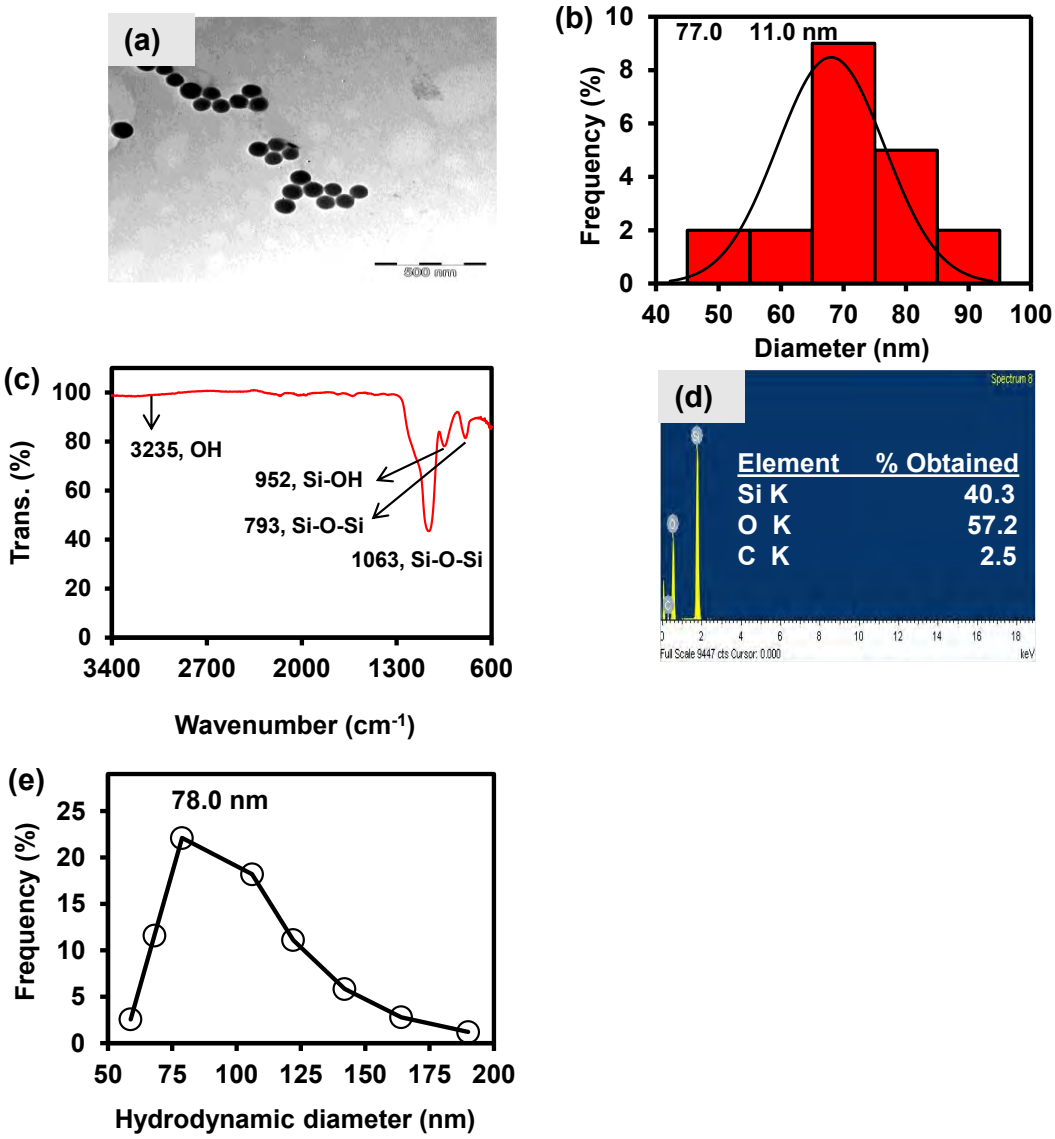

Figure 3.1: (a) TEM image, (b) size distribution histogram, (c) FT-IR spectrum, (d) EDX and (e) DLS of silica nanoparticles (SiO_2NPs).

3.3.2 Characterization of PdNPs

Figure 3.2 shows (a) TEM image, (b) size distribution histogram, (c) EDX, (d) DLS and (e) XRD measurements for palladium nanoparticles (PdNPs). The TEM image in **Figure 3.2(a)** exhibited some agglomeration of the particles and this is due to the oxide species on the surface leading to particle-particle interaction. The particle size distribution in **Figure 3.2(b)** showed that the palladium nanoparticles had 7.9 ± 1.2 nm. The EDX spectrum in **Figure 3.2(c)** shows the elemental composition of PdNPs which showed the presence of Pd M, O K and C K with 97.8%, 1.7% and 0.5%, respectively. The presence of O and C were attributed to the residual compounds of the $NaBH_4$ acting as a reducing agent on the surfaces of the PdNPs. The DLS in **Figure 3.2(d)** showed particles with a diameter of 15.7 nm. The particle size diameter was higher than the TEM image and this was due to the agglomeration as observed in the TEM image. The formation of PdNPs was also confirmed using XRD. The XRD pattern of PdNPs in **Figure 3.2(e)** showed five characteristic diffraction peaks at the following 2θ (degree) values with their Miller Indices in brackets 38.8º (111), 44.9º (200), 64.8º (202), 78.3º (311) and 81.4º (222), matching with a Pd JCPDS (05-0681). The Miller Indices confirmed the presence of metallic Pd with face-centered cubic (FCC) structure. The PdNPs average crystallite size (~ 5.0 nm) was calculated using the Debye-Scherrer equation [**21**] and was close to the TEM particle size.

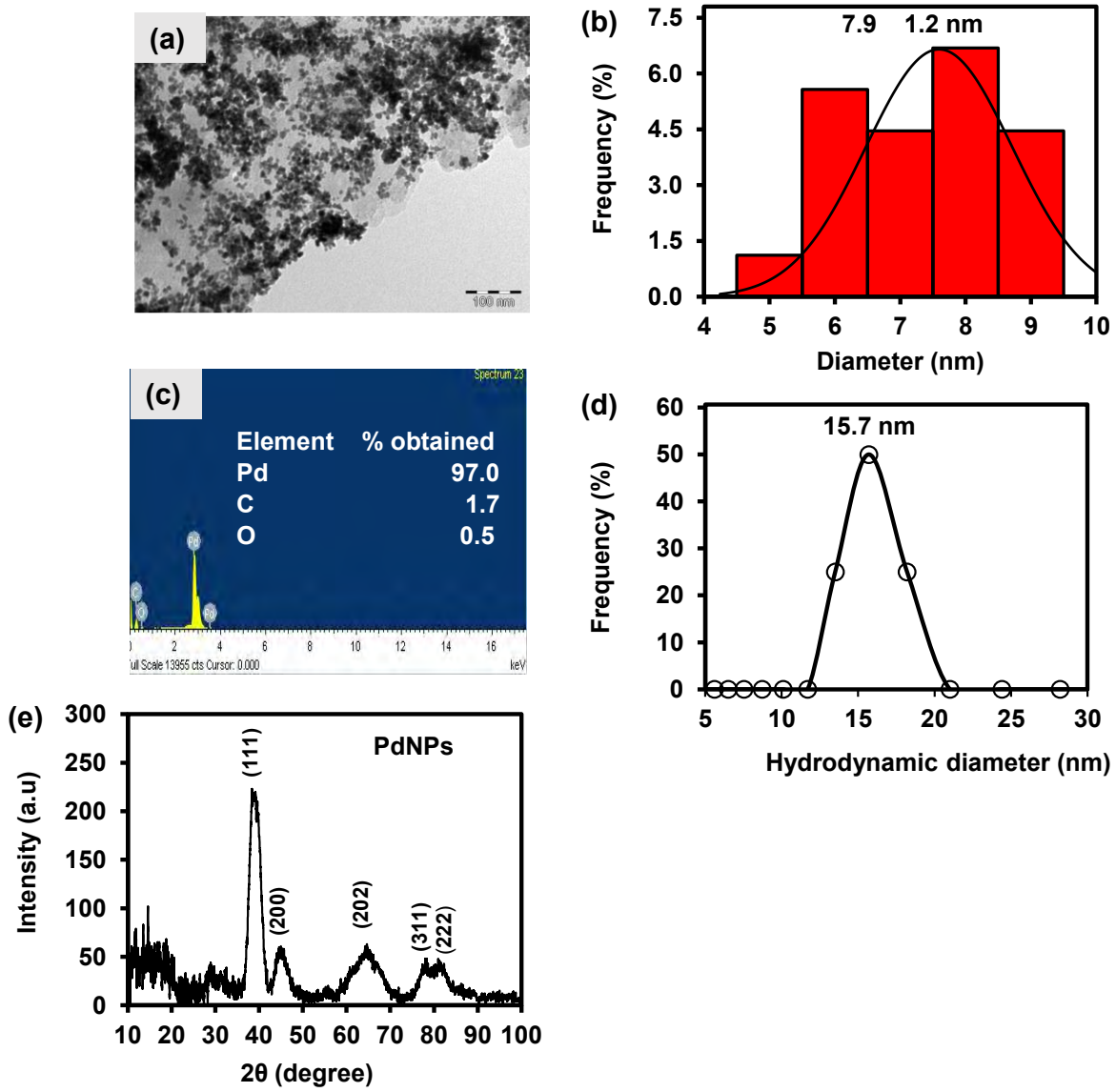

Figure 3.2: (a) TEM image, (b) size distribution histogram, (c) EDX, (d) DLS and (e) XRD of palladium nanoparticles (PdNPs).

3.3.3 Characterization of ITO-SiO_2-prS-PdNPs

The elemental composition of ITO-SiO_2-prS-PdNPs was investigated using EDX. **Figure 3.3** shows the EDX of **(a)** bare ITO and **(b)** ITO-SiO_2-prS-PdNPs. The components composition are displayed as inset. The EDX spectrum of ITO shows the composition of a glass slide (substrate) with silicone (Si K), oxygen (O K) and metal ions (Mg K, Ca K, Al K, and Na K) that form part of the glass. In addition, the glass substrate showed the presence of In M and Sn M due to the thin conducting layer. The EDX spectrum of ITO-SiO_2-prS-PdNPs confirmed the presence of Pd M (24.5%), due to successful deposition of PdNPs onto ITO-SiO_2-prSH together with other elements from ITO substrate.

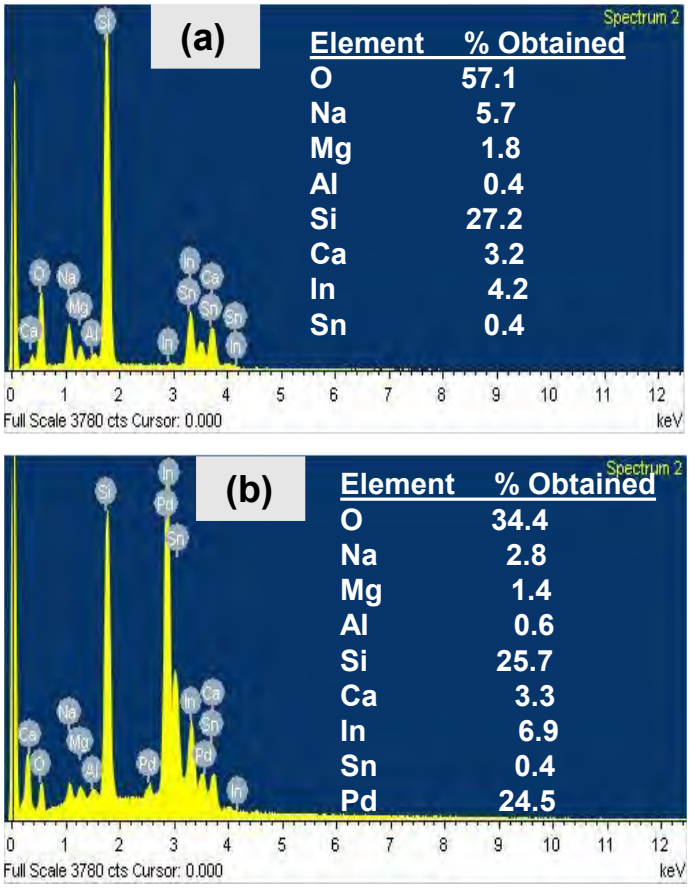

Figure 3.3: EDX of the (a) bare ITO and (b) the ITO-SiO_2-prS-PdNPs.

In addition, the XPS was used as a reliable quantitative technique to investigate the composition and oxidation states of Pd on the ITO-SiO_2-prS-PdNPs surface. The survey spectrum in **Figure 3.4(a)** confirmed the presence of Pd 3d (0.7%), Si 2p (15.8%), O 1s (24.7%), and C 1s (54.9%) as the elements of interest. Furthermore, ITO-SiO_2-prS-PdNPs showed the presence of In 3d (3.4%) and Sn 3d (0.5%) which were attributed to the underlying ITO surface. The difference in quantitative results between the XPS and EDX is due to the fact that XPS has a low-depth resolution in nm compared to µm for EDX. In **Figure 3.4(b)** shows high-resolution spectrum of Pd 3d with Pd^0 at 337.7 eV (21.6%) and Pd^{2+} oxidation states at 335.2 eV (32.9%), 340.5 eV (26.8%) and at 342.9 eV (18.7%). The spin-orbit coupling of 5.26 eV was observed for Pd components at higher binding energies. Other high-resolution spectra for Si 2p in **Figure 3.4(c)**, O 1s in **Figure 3.4(d)** and C 1s in **Figure 3.4(e)** are from the SiO_2NPs which was used as adsorbent for PdNPs. The component assignments and composition are displayed as an inset in the figure.

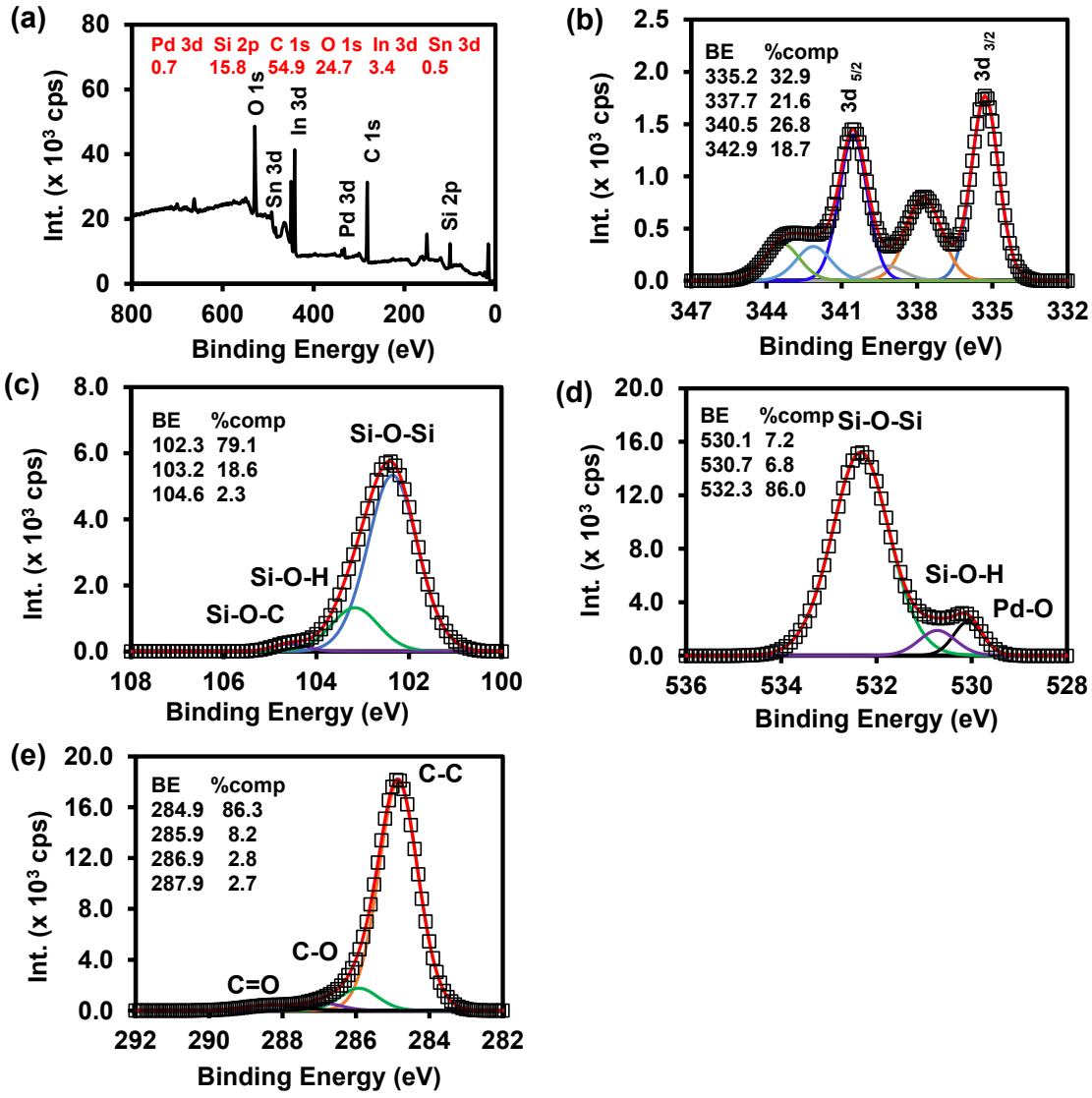

Figure 3.4: (a) Survey spectrum, and high-resolution spectra of (b) Pd 3d, (c) Si 2p, (d) O 1s, and (e) C 1s of ITO-SiO_2-prS-PdNPs.

3.3.4 Peroxidase-like activity of ITO-SiO_2-prS-PdNPs

The peroxidase-like activity of ITO-SiO_2-prS-PdNPs was investigated by the oxidation of TMB with H_2O_2. In **Figure 3.5**, the reaction between (i) H_2O_2 + ITO-SiO_2-prS-PdNPs and (ii) TMB + ITO-SiO_2-prS-PdNPs showed clear solutions. The UV-vis spectrum of TMB + ITO-SiO_2-prS-PdNPs showed a small absorption peak at 652 nm and this was due to oxidation of TMB as is light sensitive compound. **Figure 3.5(iii)** shows ITO-SiO_2-prS-PdNPs in the presence of H_2O_2 and TMB. The solution turned blue in colour and this was accompanied with an increase in the absorption peaks at 370 nm and 652 nm. This confirm that ITO-SiO_2-prS-PdNPs possess peroxidase-like activity. The ITO and ITO-SiO_2NPs did not show peroxidase-like activity. Therefore, peroxidase-like activity was dependent on the presence of PdNPs adsorbed onto ITO-SiO_2-prSH as nanocatalysts [**22**]. The results further confirmed that both TMB and H_2O_2 are both necessary in evaluating the peroxidase-like activity of ITO-SiO_2-prS-PdNPs. This behaviour is similar to that observed for the commonly used enzyme, (HRP) for the oxidation of TMB in the presence of H_2O_2 [**23**].

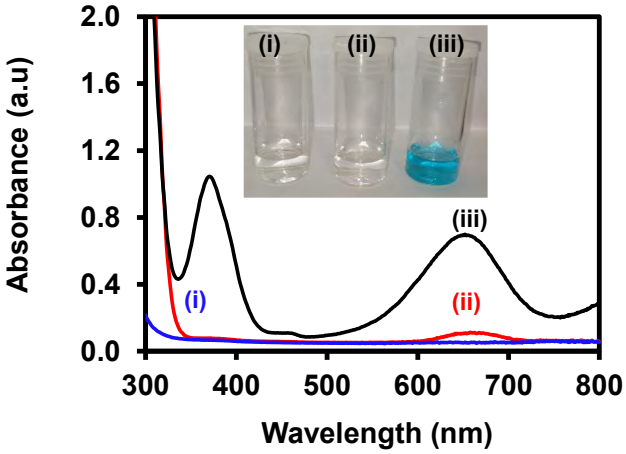

Figure 3.5: UV-vis absorption spectra of (i) H_2O_2 + ITO-SiO_2-prS-PdNPs, (ii) TMB + ITO-SiO_2-prS-PdNPs and (iii) H_2O_2 + TMB + ITO-SiO_2-prS-PdNPs. (Insert photograph for the corresponding colour change of different reaction systems).

3.3.5 Effect of conditions on peroxidase-like activity of ITO-SiO_2-prS-PdNPs

The peroxidase-like activity of ITO-SiO_2-prS-PdNPs was investigated in different environmental conditions, such as pH, reaction time, concentrations of H_2O_2 and TMB, and temperature. **Figure 3.6** shows the effect of (a) pH (2–6), (b) time (5–50 min) (c) [H_2O_2] (1–6 mM), (d) [TMB] (0.1–0.7 mM), and temperature (25–90 °C) on ITO-SiO_2-prS-PdNPs. **Figure 3.6(a)** (red) shows that pH 4.0 gave the highest absorbance band at 652. This was due to the acidity of SiO_2NPs as a catalyst support thus allowing for PdNPs to be retained on the thiolated surface and the SiO_2NPs staying intact [**18**]. The absorption intensity at 652 nm increased from pH 2.0 to pH 4.0. The intensity decreased after pH 4.0. In acidic condition, H_2O_2 remains stable thus allowing for catalytic reduction. PdNPs on ITO-SiO_2-prS-PdNPs participates in the catalytic reduction of H_2O_2 to form radicals (O_2^{-}•, HO_2^{-}• and HO^{-}•), which can oxidize TMB [**24**]. The optimum pH for peroxidase-like activity of pure PdNPs not coated onto the ITO in **Figure 3.6(a)** (black) was 5. **Figure 3.6(b)** shows that the blue colour intensity increased as the time continued and due to 3,3',5,5'-tetramethylbenzidine diamine (TMBDI) products by ITO-SiO_2-prS-PdNPs and H_2O_2. Oxidized TMB formed a strong blue colour and the intensity of the reaction increased from 5 to 50 min. The regression equation for the reaction time was Abs_{652} = 0.0326x + 0.187 with R^2 of 0.99. The catalytic process of 15 min was selected for further investigations**.** An increase in absorption at 652 nm was observed as the concentration of H_2O_2 increased, **Figure 3.6(c)** and also as the concentration of TMB increase, **Figure 3.6(d)**. At higher concentration of H_2O_2 (> 5.0 mM), a drastic decrease in absorption was observed and for TMB at (> 0.50 mM) a plateau was observed. The plateau and a decrease in intensity were attributed to the saturation of catalytic sites on the ITO-SiO_2-prS-PdNPs

resulting in the decreased on the catalytic activity. Similar phenomenon was observed for HRP and some other nanozymes with peroxidase-like activity at high concentration for H_2O_2 and TMB [**25**,**26**]. In **Figure 3.6(e)**, the effect of increasing the temperature from 25–90 °C on the peroxidase-like activity was investigated. The relative activity measured at 652 nm was stable and above 90% up to 70 °C as shown in **Figure 3.6(e)**. At high temperature above 70 °C, the activity drastically decreased due to the composition of H_2O_2 at high temperature. The stability of the peroxidase-like activity of ITO-SiO_2-prS-PdNPs was high compared to natural enzymes which has a narrow window of activity.

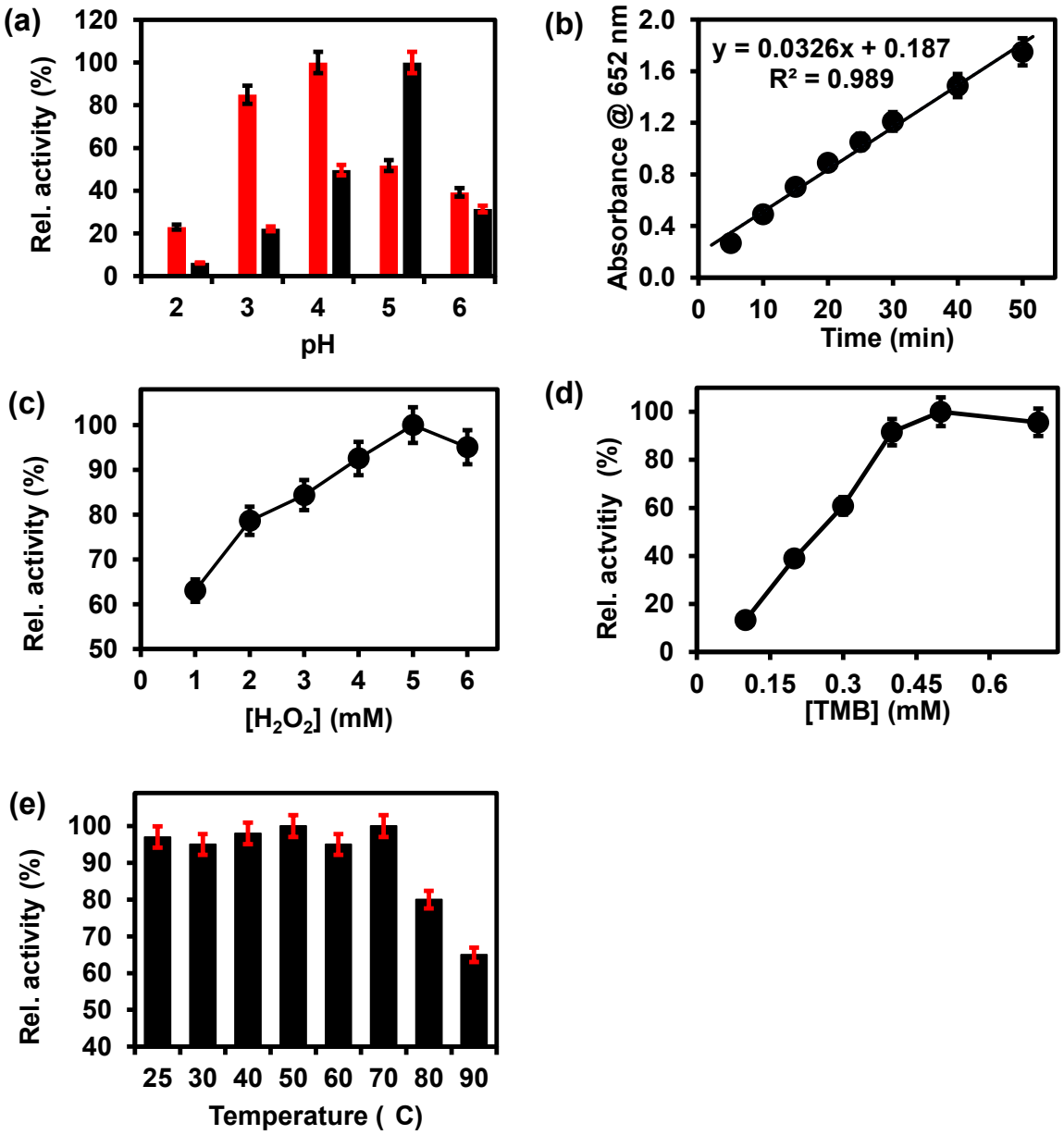

Figure 3.6: Effect of (a) pH (red), (b) reaction time, concentrations of (c) H_2O_2 and (d) TMB, and (e) temperature on the peroxidase-like activity of ITO-SiO_2-prS-PdNPs. (Effect of pH (a) (black) on the peroxidase-like activity of PdNPs)

3.3.6 Confirmation of mechanism for enzyme-like properties

The mechanism of peroxidase-like nanozymes can proceed either via the generation of reactive oxygen radical species such as $O_2^{-}\bullet$, $HO_2^{-}\bullet$, and $HO^{-}\bullet$ or the electron-transfer mechanism [**24**]. First, we investigated the generation of ROS using the oxygen radical ($O_2\bullet-$) and singlet oxygen ($^1O_2$) quencher, DPBF. The absorption of DPBF at 420 nm in **Figure 3.7(a)** is expected to decrease due to ROS generated. There was no change in the intensity of DPBF for up to 10 min in **Figure 3.7(b)**, confirming that no ROS was generated. A similar study was investigated using TA as a hydroxyl radical trap. No fluorescence signal was observed and therefore no hydroxyl radical was generated. In order to verify whether ITO-SiO_2-prS-PdNPs peroxidase-like activity originates from the electron-transfer mechanism its electrocatalytic behavior towards H_2O_2 was investigated using chronoamperometric measurements. **Figure 3.7(c)** shows the chronoamperomogram of ITO-SiO_2-prS-PdNPs upon successive addition of 100 µL of 0.10 mM H_2O_2 (indicated by arrows) with stirring and a working potential of +0.50 V (vs. Ag|AgCl) in acetate buffer (0.10 M, pH 4.0). The current response increases steadily due to the electrocatalytic oxidation. The oxidation of H_2O_2 results in the reduction of PdNPs which then oxidize TMB to blue-coloured products as shown in **Scheme 3.2**. Therefore, the peroxidase-like activity of ITO-SiO_2-prS-PdNPs was attributed to the electron-transfer mechanism and similar to the natural horse-radish peroxidase enzyme.

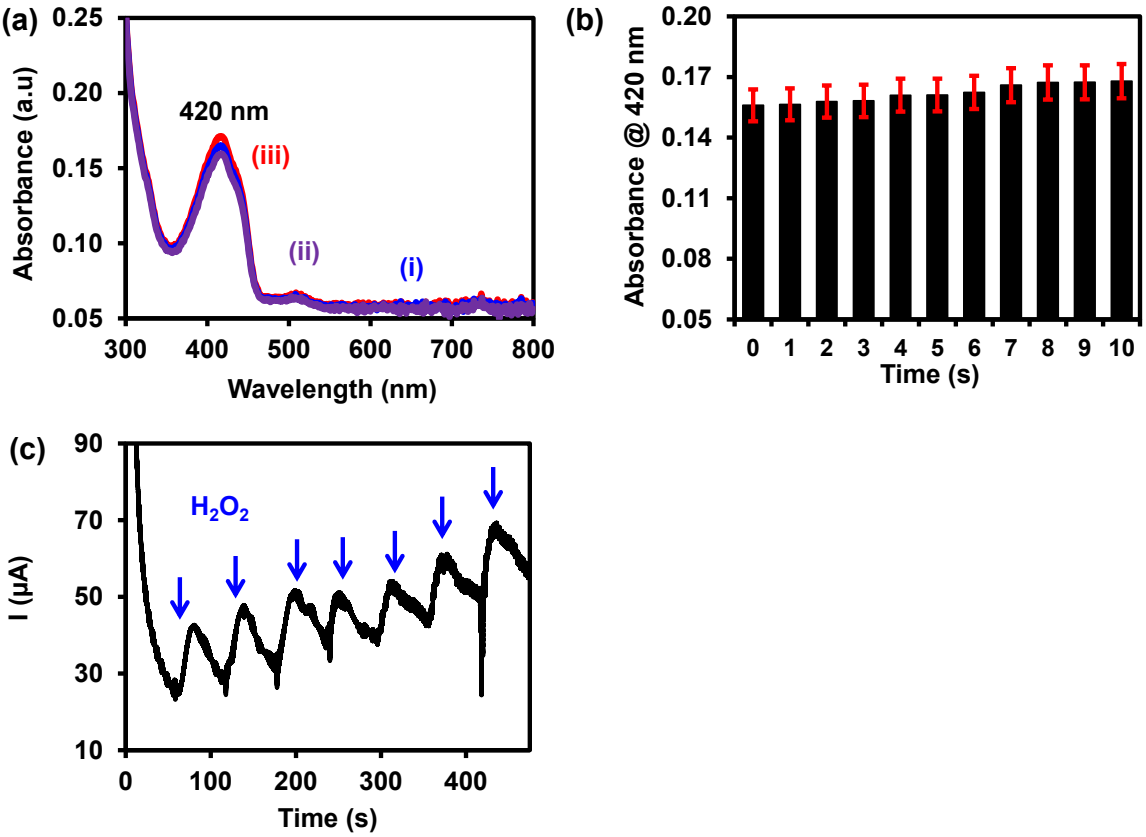

Figure 3.7: UV-vis absorption spectra of (a)(i) DPBF alone (blue), (ii) DPBF + H_2O_2 (purple), (iii) DPBF + H_2O_2 + ITO-SiO_2-prS-PdNPs (red). (b) Absorption of DPBF at 420 nm in the presence of H_2O_2 and ITO-SiO_2-prS-PdNPs at the predetermined time interval of 1 minute up to 10 minutes. (c) Chronoamperomogram of the modified ITO-SiO2-prS-PdNPs with addition of 10 μL H_2O_2 (1.0 mM) into 10 mL pH 4.0 acetate buffer.

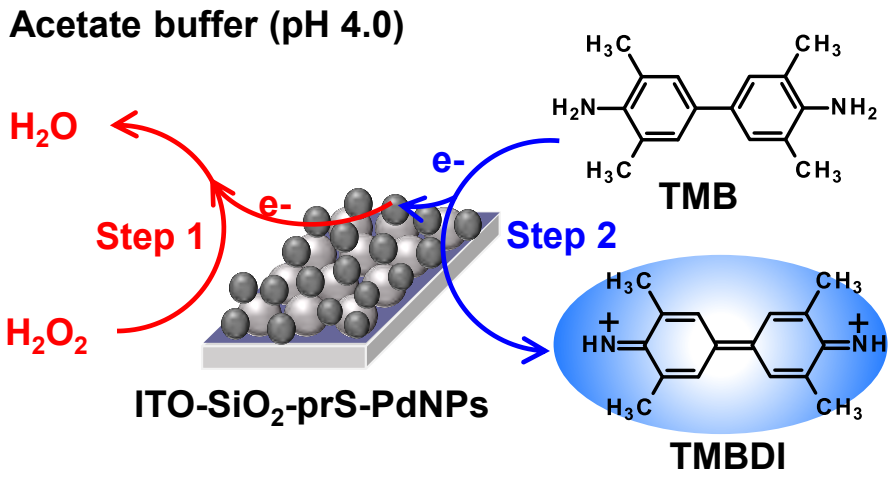

Scheme 3.2: ITO-SiO_2-prS-PdNPs electron-transfer mechanism for TMB oxidation in 10 mM acetate buffer (pH 4.0).

3.3.7 Steady-state kinetic analysis of ITO-SiO_2-prS-PdNPs

The steady-state kinetics were investigated on H_2O_2 and TMB substrates. The peroxidase-like activity of ITO-SiO_2-prS-PdNPs was further investigated by varying the concentration of H_2O_2 at constant TMB and vice versa. A series of initial rates (V_0) for TMB oxidation were obtained from the time-dependent absorption value at 652 nm. The absorbance value were converted to concentration using the molar absorption coefficient (ε) of oxidized TMB at 652 nm using **Equation (3.1):**

$$[\text{oxidized TMB}] = A/\varepsilon \times L \qquad \textbf{(3.1)}$$

where A is the absorbance at 652 nm, ε is the molar absorption of oxidized TMB at 652 nm (39 000 M^{-1} cm^{-1}), and L is the path length (1 cm) [**27**]. In **Figure 3.8(a)**, the plot of initial rates (V_0) against the concentrations of substrate H_2O_2 and TMB (in **Figure 3.8(b)**) were evaluated. The graphs showed an increase in V_0 with increasing

concentration of [H_2O_2] in **Figure 3.8(a)** and [TMB] in **Figure 3.8(b)**. The graphs reached a plateau at high concentrations, 5.0 mM for H_2O_2 and 0.50 mM for TMB. This confirmed a typical Michaelis−Menten enzyme-like behaviour for the ITO-SiO_2-prS-PdNPs. The double reciprocal plots in **Figure 3.8(c)** for H_2O_2 and (**d**) for TMB were plot and used to calculate the K_m from the slope and V_{max} from the y-intercept using **Equation (3.2):**

$$\frac{1}{V_0} = \frac{K_m}{V_{max}} \frac{1}{[S]} + \frac{1}{V_{max}} \qquad \textbf{(3.2)}$$

where V_0 is the initial rate, V_{max} is the maximal reaction rate, [S] is the concentration of the substrate (H_2O_2 or TMB), and K_m is the Michaelis−Menten constant. The affinity between the enzyme and the substrate is defined by K_m. The high K_m value indicates weak affinity, whereas the low K_m value suggests a strong affinity. The calculated kinetic parameters of ITO-SiO_2-prS-PdNPs and the comparison with HRP and other nanozymes are summarized in **Table 3.1**. The K_m value for ITO-SiO_2-prS-PdNPs with H_2O_2 as the substrate was (0.68 mM) and is lower than that of HRP (3.70 mM) [**20**]. Most nanozymes such as CuONRs@Pd_6NPs (2.94 mM) [**28**], and CuO-Au nanoalloys (4.08 mM) [**9**], had K_m values higher than ITO-SiO_2-prS-PdNPs. Comparable K_m values were observed for MnSe-g-C_3N_4 (0.62 mM) [**29**], indicating that ITO-SiO_2-prS-PdNPs has greater affinity for H_2O_2. On the other hand, the K_m value for the ITO-SiO_2-prS-PdNPs with TMB as the substrate was 0.47 mM and comparable to that of HRP (0.43 mM) [**20**], but significantly lower than of other nanozymes such as CuO-Au nanoalloys (3.54 mM) [**9**], and Zn-CuO (10 mM) [**30**], suggesting that ITO-SiO_2-prS-PdNPs has a high affinity for TMB. The excellent affinity of ITO-SiO_2-prS-PdNPs to HRP and other

reported nanozymes are due to the use of PdNPs and their homogeneous distribution on the SiO_2NPs surface.

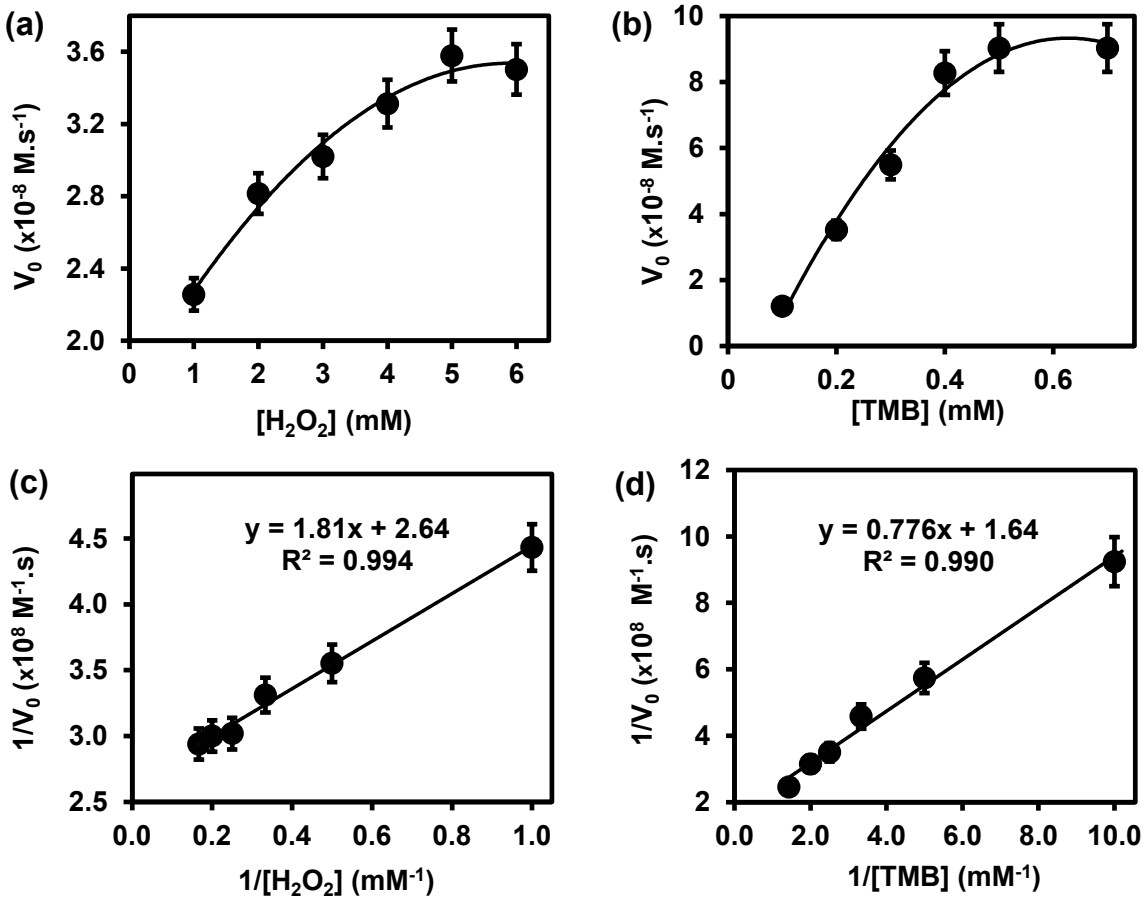

Figure 3.8: The steady-state kinetic plots for the ITO-SiO_2-prS-PdNPs by (a) varying [H_2O_2] at a fixed [TMB], (b) varying [TMB] at a fixed [H_2O_2] and their corresponding double reciprocal plots (c) [H_2O_2] at a fixed [TMB], and (d) [TMB] at a fixed [H_2O_2].

Table 3.1: Comparison of the kinetic parameters (K_m and V_{max}) for the peroxidase-like activity of ITO-SiO_2-prS-PdNPs with HRP and other previously reported nanozymes.

Nanozymes	**K_m (mM)**		**V_{max} (x 10^{-8} M.s^{-1})**	
	H_2O_2	TMB	H_2O_2	TMB
ITO-SiO_2-prS-PdNPs^{TW}	0.68	0.47	3.79	6.10
CuO-Au nanoallaoys [**9**]	4.08	3.54	0.0105	0.0111
HRP [**24**]	3.7	0.43	8.71	10.0
CuONRs@Pd_6NPs [**29**]	2.94	3.74	1.23	1.65
MnSe-g-C_3N_4 [**30**]	0.62	0.137	2.85	2.40
Zn/CuO [**31**]	71.0	10.0	0.30	2.87

TW-This Work

3.3.8 Colorimetric detection of glucose using ITO-SiO_2-prS-PdNPs

The peroxidase-like activity exhibited by ITO-SiO_2-prS-PdNPs as nanozyme was used for the potential application of glucose detection. (a) Glucose was oxidized GOx to form gluconic acid and H_2O_2 is produced as an enzyme reaction by-product. (b) The produced enzymatic H_2O_2, in the presence of ITO-SiO_2-prS-PdNPs oxidize TMB to its blue-coloured products, oxTMB, as illustrated in **Scheme 3.3**.

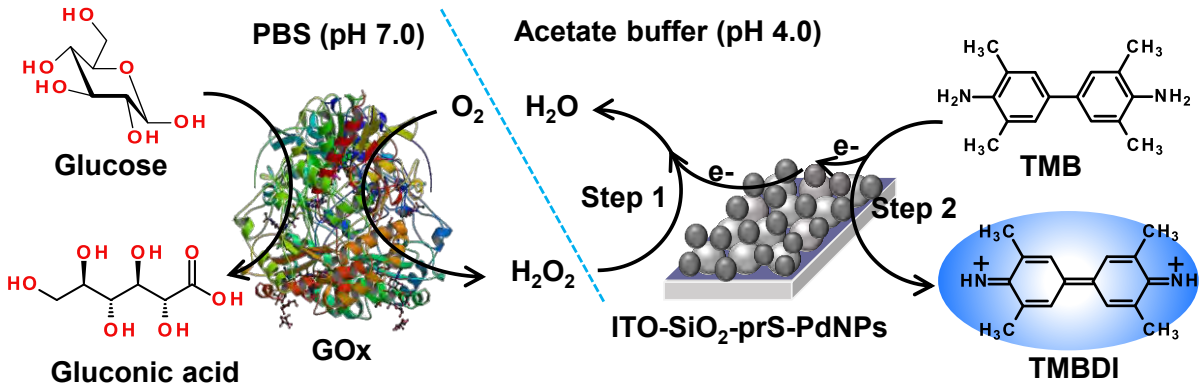

Scheme 3.3: Schematic illustration for the colorimetric determination of glucose using ITO-SiO_2-prS-PdNPs.

The intensity of the blue-coloured products at 652 nm was proportional to the concentration of glucose. **Figure 3.9(a)** shows an increase in the UV-vis absorption spectra at 652 nm as the concentration of glucose increased and the calibration curve is shown in **Figure 3.9(b)**. The response was linear up to 30 μM. At higher concentration of glucose, the catalytic activity of ITO-SiO_2-prS-PdNPs formed a plateau due to saturation of catalytic sites on our ITO-SiO_2-prS-PdNPs, thus similar absorption intensity. The LoD and the LoQ were calculated to be 1.84 μM and 6.14 μM, respectively, using $3S_b$/slope for LoD, and $10S_b$/slope for LoQ, S_b is the standard deviation [**32**] of the blank samples (n = 10) and the slope was from **Figure 3.9(b)**. Compared with other nanozyme for glucose sensing our proposed colorimetric method using ITO-SiO_2-prS-PdNPs showed better or comparable detection of limit and linear range as summarized in **Table 3.2**.

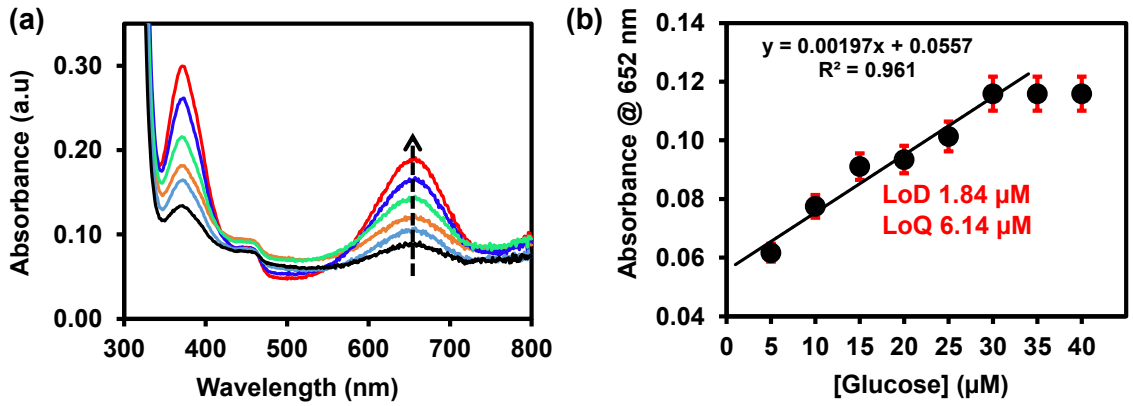

Figure 3.9: (a) UV-vis absorption spectra and (b) the corresponding linear calibration curve of glucose detection using ITO-SiO_2-prS-PdNPs.

Table 3.2: Comparison of ITO-SiO_2-prS-PdNPs for colorimetric detection of glucose with other nanozyme-based glucose biosensors.

Nanozymes	**Linear range (µM)**	**LoD (µM)**	**LoQ (µM)**
ITO-SiO_2-pr-PdNPs^{TW}	5-30	1.84	6.14
CuO-Au nanoalloys [**9**]	0-30	6.80	-
CuONRs@Pd_6NPs [**29**]	0-70	8.87	39.9
GO-COOH [**32**]	1-20	1.00	-
Cu-Ag/rGO [**33**]	1-30	3.80	-

TW-This Work

3.3.9 Selectivity studies

The selectivity analysis for ITO-SiO_2-prS-PdNPs for glucose detection was investigated using glucose analogues in place of glucose (0.50 mM). The glucose analogues (fructose, lactose and sucrose) were dissolved in phosphate buffer and kept at the

concentration of 5 mM. As shown in **Figure 3.10(a)**, a blue colour was observed only in the presence of glucose, but not observed for fructose, lactose and sucrose even though the concentration of these glucose analogues were 10-fold more than glucose. The results showed that our proposed ITO-SiO_2-prS-PdNPs as glucose sensor has high selectivity towards glucose. The high selectivity was attributed to the high affinity and specificity of GOx for glucose.

3.3.10 Reusability of ITO-SiO_2-prS-PdNPs for glucose detection

The reusability of ITO-SiO_2-prS-PdNPs for glucose detection was investigated by repeating the detection of 15.0 µM glucose for 5 successful cycles. After each measurement, the ITO-SiO_2-prS-PdNPs was removed from the detection solution and washed several times with ethanol, methanol, and Milli-Q water. The recovered ITO-SiO_2-prS-PdNPs was reused for glucose detection in the next cycle. **Figure 3.10(b)** shows that about 95.2% of the peroxidase-like activity of glucose detection by ITO-SiO_2-prS-PdNPs after 5 successive cycle was retained with the percentage relative standard deviation (%RSD) value of 1.90%, which indicates the feasibility of ITO-SiO_2-prS-PdNPs for glucose detection for practical applications.

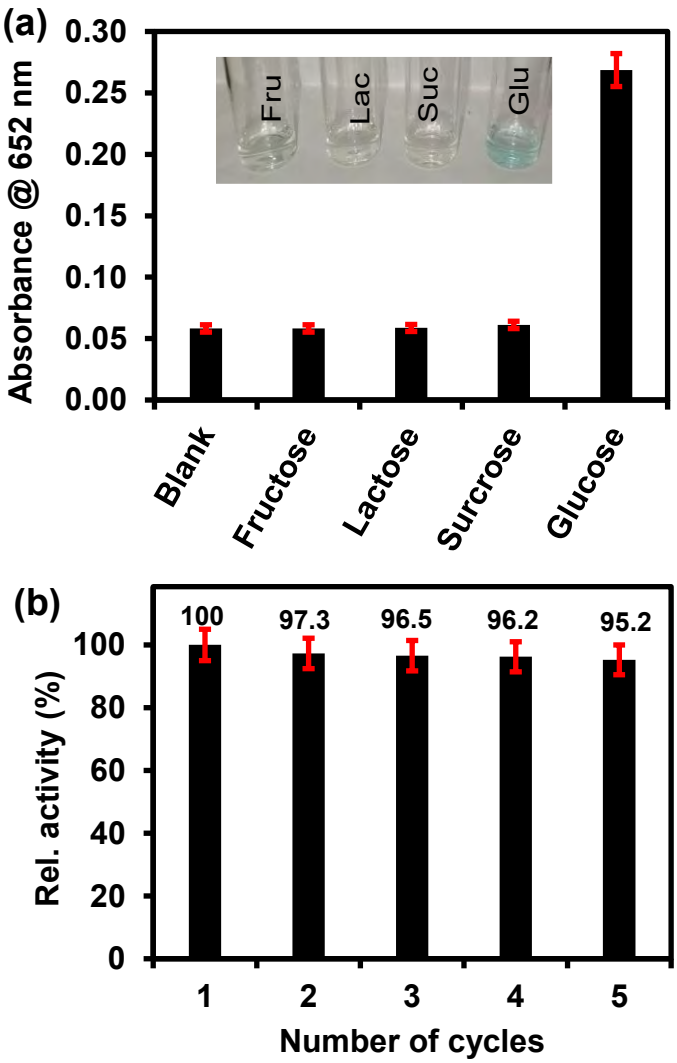

Figure 3.10: (a) Selectivity of colorimetric assay for glucose detection and other interfering substances for ITO-SiO_2-prS-PdNPs (inset: the corresponding images of the reaction solutions) and (b) reusability of ITO-SiO_2-prS-PdNPs towards detection of glucose.

3.3.11 Colorimetric detection of glucose in new-born calf serum (NCS) samples

To investigate the feasibility of our proposed colorimetric sensor (ITO-SiO_2-prS-PdNPs) for glucose was used for detection in real samples, that is 10% new-born calf serum (NCS). 10% NCS is representative of real samples was spiked with known concentrations of glucose. As listed in **Table 3.3**, the % recovery of glucose in 10%

NCS was between 92.5 and 105.3%. The percentage relative standard deviation (%RSD) values were between 2.12 and 3.04%. The results showed feasibility and reliability of the proposed ITO-SiO_2-prS-PdNPs as glucose sensor for detecting glucose in real10% NCS.

Table 3.3: Detection of glucose in 10% NCS (n=3) using recovery method and linear curve in **Figure 3.9(b)**.

Sample	Added [Glucose] µM	Added [Glucose] µM	Recovery (%)	RSD (%)
10% NCS + 4.0 µM glucose	4.0	3.7	92.5	3.04
10% NCS + 10.0 µM glucose	10.0	9.7	97.0	2.12
10% NCS + 15.0 µM glucose	15.0	15.8	105.3	3.17

3.4 Conclusions

The preparation of SiO_2NPs and PdNPs was successful. The fabricated nanomaterials (SiO_2NPs and PdNPs) were used to fabricate ITO-SiO_2-prS-PdNPs which exhibited intrinsic peroxidase-like activity. The optimum environmental conditions for peroxidase-like activity of ITO-SiO_2-prS-PdNPs were obtained at 652 nm at pH 4 and <70 °C. A typical Michaelis−Menten enzyme behaviour was observed for the ITO-SiO_2-prS-PdNPs using steady-state kinetic analysis. The ITO-SiO_2-prS-PdNPs showed good affinity for both H_2O_2 (K_m 0.68 mM) and TMB (K_m 0.47 mM) compared to HRP and other reported peroxidase-mimetics. The mechanism of the peroxidase-like activity of ITO-SiO_2-prS-PdNPs was confirmed to be via an electron-transfer

mechanism between H_2O_2 and TMB. ITO-SiO_2-prS-PdNPs was used as glucose sensor and showed good specificity and selectivity towards glucose with a linear concentration range between (5.0–30 μM), LoD (1.84 μM) and LoQ (6.14 μM). Our proposed colorimetric glucose sensor based on ITO-SiO_2-prS-PdNPs was simple and easy to recover for glucose detection. Real sample analysis using 10% NCS samples confirmed the reliability for glucose detection in practical applications.

3.5 References

(1) Wang, J. Electrochemical Glucose Biosensors. *Electrochem. Sensors, Biosens. their Biomed. Appl.* **2008**, 108, 814–825. https://doi.org/10.1021/cr068123a

(2) Dutt, A. K.; Maji, S. K.; Mondal, A.; Karmakar, B.; Biswas, P.; Adhikary, B. Chemical Iron Selenide Thin Film Peroxidase-like Behavior, Glucose Detection and Amperometric Sensing of Hydrogen Peroxide. *Sens. Act. B. Chem.* ***2012,*** 173*,* 724-731. https://doi.org/10.1016/j.snb.2012.07.070

(3) Wu, Q.; Wang, L.; Yu, H.; Wang, J.; Chen, Z. Organization of Glucose-Responsive Systems and Their Properties. *Chem. Rev.* **2011**,111, 7855–7875.

https://doi.org/10.1021/cr200027j

(4) Cai, T.; Gao, Y.; Yan, J.; Wu, Y.; Di, J. Nanoplates and Gold Nanoparticles. *RSC Adv.* **2017**, 7, 29122–29128. https://doi.org/10.1039/C7RA00593H

(5) Cash, K. J.; Clark, H. A.Nanosensors and Nanomaterials for Monitoring Glucose in Diabetes. *Trends Mol. Med*. **2010**, 16, 584–593.

https://doi.org/10.1016/j.molmed.2010.08.002

(6) Alam, U.; Asghar, O.; Azmi, S.; Malik, R. General Aspects of Diabetes Mellitus. *Handb. Clin. Neurol. Elsevier* **2014**, 126, 211–222.

https://doi.org/10.1016/B978-0-444-53480-4.00015-1

(7) Tromans, A.; Samanta, K.; Chapman, A.; Davis, A. Selective Glucose Sensing in Complex Media using Biomimetci Receptor. *Chem. Sci*. **2020**, 11,3223–3227.

https://doi:org/10.1039/c9sc05406e

(8) Ferri, S.; Kojima, K.; Sode, K. Review of Glucose Oxidases (GOx) and Glucose Dehydrogenases. *Diabetes Sci Technol*. **2011**, 5, 1068-1076.

https://doi.org/10.1177%2F193229681100500507

(9) Mvango, S.; Mashazi, P. Synthesis , Characterization of Copper Oxide-Gold Nanoalloys and Their Peroxidase-Like Activity Towards Colorimetric Detection of Hydrogen Peroxide and Glucose. *Mater. Sci. Eng. C*. **2019**, 96, 814–823.

https://doi.org/10.1016/j.msec.2018.12.010

(10) Harris, J. M.; Reyes, C.; Lopez, G. P. Common Causes of Glucose Oxidase Instability. *Diabetes Sci Technol*. **2013**, 7, 1030–1038.

https://doi.org/10.1177%2F193229681300700428

(11) Bao, S. J.; Li, M. C.; Zang, J. F.; Cui, X. Q.; Qiao, Y.; Guo, F. New Nanostructured TiO_2 for Direct Electrochemistry and Glucose Sensor Applications. *Adv. Fun. Mat*. **2008**, 18, 591–599. https://doi:org/10.1002/adfm.200700728

(12) Yang, W.; Li, J., Wang, M.; Sun, X.; Liu, Yong.; L, Yang, J.; Ng, D. H. A Colorimetric Strategy for Ascorbic Acid Sensing Based on the Peroxidase- Like Activity of Core-Shell Fe_3O_4/ CoFe-LDH hybrid. *Coll. Surf. B Bioint*. **2020**,188, 110742. https://doi.org/10.1016/j.colsurfb.2019.110742

(13) Bai, Y.; Yang, W.; Sun, Y.; Sun, C. Chemical Enzyme-free Glucose Sensor Based on a Three-dimensional Gold Film Electrode. *Sens. Act. B. Chem*. **2008**, 134, 471–476. https://doi.org/10.1016/j.snb.2008.05.028

(14) Meng, L.; Jin, J.; Yang, G.; Lu, T.; Zhang, H.; Cai, C. Nonenzymatic Electrochemical Detection of Glucose Based on Palladium-Single-Walled Carbon Nanotube Hybrid Nanostructures. *J. Phys. Chem. C*. **2009**, 81, 7271–7280.

https://doi.org/10.1021/ac901005p

(15) Tang, H.; Chen, J.; Yao, S.; Nie, L.; Deng, G. Amperometric Glucose Biosensor Based on Adsorption of Glucose Oxidase at Platinum Nanoparticle-Modified Carbon Nanotube Electrode. *Anal. Biochem.* **2004**, 331, 89–97.

https://doi.org/10.1016/j.ab.2004.05.005

(16) Zhang.; Cobley, C. M.; Zeng, J.; Wen, L.; Chen, J.; Xia, X. Dissolving Ag from Au-Ag Alloy Nanoboxes with H_2O_2: A Method for Both Tailoring the Optical Properties and Measuring the H_2O_2 Concentration. J*. Phys. Chem. C.* **2010**, 114, 6396-6400.

https://doi.org/10.1021/jp100354z

(17) He, H.; Xu, X.; Wu, H.; Jin, Y. Enzymatic Plasmonic Engineering of Ag/Au Bimetallic Nanoshells and Their Use for Sensitive Optical Glucose Sensing. *Adv. Mat. J*. **2012**, 24, 1736–1740. https://doi:org/10.1002/adma.201104678

(18) Adeniyi, O.; Sicwetsha, S.; Mashazi, P. Nanomagnet-Silica Nanoparticles decorated with Au@Pd for Enhanced Peroxidase-Like Activity and Colorimetric Glucose Sensing. *ACS Appl. Mater. Interf*. **2020**, 12, 1973-1987.

https://doi.org/10.1021/acsami.9b15123

(19) Ran, Z.; Yang, W. Silica/CdTe/silica Fluorescent Composite Nanoparticles via Electronic Assembly as a pH Ratiometer. *RSC Adv.* **2014**, 40, 37921–37927.

https://doi.org/10.1039/C4RA05897F

(20) Wang, Q.; Cui, X.; Chen, J.; Zheng, X.; Liu, C.; Xue, T.; Jin, Z.; Qiao, L.; Zheng, W. Well-Dispersed Palladium Nanoparticles on Graphene Oxide as a Non-Enzymatic Gucose Sensor. *RSC Adv.* **2012**, 2, 6245–6249..

https://doi.org/10.1039/C2RA20425H

(21) Holzwarth, U.; Gibson, N. The Scherre Equation Versus the 'Debye-Scherre Equation'. *Nanotech.* **2012**, 6, 21027. https://doi.org/10.1038/nnano.2011.145

(22) Wu, J.; Wang, X.; Wang, Q.; Lou, Z.; Li, S.; Zhu, Y.; Qin, L.; Wei, H. Nanomaterials with Enzyme-Like Characteristics (Nanozymes): Next-Generation Artificial Enzymes (II). *Chem. Soc. Rev.* **2019**, 48, 1004–1076. https://doi.org/10.1039/C8CS00457A

(23) Gao, L.; Zhuang, J.; Nie, L.; Zhang, J.; Zhang, Y.; Gu, N.; Wang, T.; Feng, J.; Yang, D.; Perret, S.; Yan, X. Intrinsic Peroxidase-Like Activity of Ferromagnetic Nanoparticles. *Nat. Nanotechnol.* **2007**, 2, 577–583.

https://doi.org/10.1038/nnano.2007.260

(24) Chen, L.; Li, X.; Zhang, J.; Fang, J.; Huang, Y.; Wang, P.; Ma, J. Production of Hydroxyl Radical via the Activation of Hydrogen Peroxide by Hydroxylamine. *Environ. Sci. Technol.* **2015**, 49, 10373–10379. https://doi.org/10.1021/acs.est.5b00483

(25) Yang, Y.; Shen, D.; Long, Y.; Xie, Z.; Zheng, H. Intrinsic Peroxidase-Like Activity of Ficin. *Sci. Rep.* **2017**, 7, 1-8. https://doi.org/10.1038/srep43141

(26) Nicell, J. A.; Wright, H. A Model of Peroxidase Activity with Inhibition by Hydrogen Peroxide. *Enzyme Microb. Technol.* **1997**, 21, 302–310.

https://doi.org/10.1016/S0141-0229(97)00001-X

(27) Liu, Y.; Zhu, G.; Yang, J.; Yuan, A.; Shen, X. Peroxidase-Lke Catalytic Activity of Ag_3PO_4 nanocrystals prepared by a colloidal route. *PLoS One*. **2014**, 9, 3–9.

https://doi.org/10.1371/journal.pone.0109158

(28) Sicwetsha, S.; Adeniyi, O.; Mashazi, P. Bimetallic Gold and Palladium Nanoparticles Supported on Copper Oxide Nanorods for Enhanced H_2O_2 Catalytic Reduction and Sensing. *RSC Adv.* **2021**, 11, 28818–28828.

https://doi.org/10.1039/D1RA05247K

(29) Su, L.; Feng, J.; Zhou, X.; Ren, C.; Li, H.; Chen, X. Colorimetric Detection of Urine Glucose Based $ZnFe_2O_4$ Magnetic Nanoparticles. *Anal. Chem.* **2012**, 84, 5753–5758. https://doi.org/10.1021/ac300939z

(30) Nagvenkar, A. P.; Gedanken, A. $Cu_{0.89}Zn_{0.11}O$, A New Peroxidase-Mimicking Nanozyme with High Sensitivity for Glucose and Antioxidant Detection. *ACS Appl. Mater. Interf*. **2016**, 8, 22301–22308. https://doi.org/10.1021/acsami.6b05354

(31) Awual, M. R.; Khraisheh, M.; Alharthi, N. H.; Luqman, M.; Islam, A.; Karim, M. R.; Rahman, M. M.; Khaleque, M. A. Efficient Detection and Adsorption of Cadmium(II) Ions using Innovative Nano-Composite Materials. *Chem. Eng. J.* **2018**, 343, 118–127. https://doi.org/10.1016/j.cej.2018.02.116

(32) Song, Y.; Qu, K.; Zhao, C.; Ren, J.; Qu, X. Graphene Oxide: Intrinsic Peroxidase Catalytic Activity and its Application to Glucose Detection. *Adv. Mater.* **2010**, 22, 2206–2210. https://doi.org/10.1002/adma.200903783

(33) Darabdhara, G.; Sharma, B.; Das, M. R.; Boukherroub, R.; Szunerits, S. Cu-Ag Bimetallic Nanoparticles on Reduced Graphene Oxide Nanosheets as Peroxidase Mimic for Glucose and Ascorbic Acid Detection. *Sens, Act. B. Chem.* **2017**, 238**,** 842–851. https://doi.org/10.1021/cr068123a

CHAPTER 4

4 Au/Pd nanocatalysts on silica nanoparticle-coated indium tin oxide for colorimetric sensing of ascorbic acid

Abstract

Nanomaterials of gold and palladium have received research attention due to their excellent catalytic properties. Their recovery after the catalytic reaction still remains a challenge rendering the catalytic application of these nanomaterials for single use. In this study, a method of fabricating nanomaterials as thin nanoparticle films on catalytically inert surfaces whilst allowing for their recovery and reuse was investigated. Indium tin oxide (ITO) glass slides were first hydroxylated (ITO-OH) and used to attach the silica nanoparticles (SiO_2NPs) to form ITO-SiO_2NPs. The ITO-SiO_2NPs surface was used as an adsorbent for gold and palladium mono- and bi-metallic nanoparticles (Au/PdNPs) to form ITO-SiO_2-prS-Au/PdNPs, which was evaluated for the enzyme-like catalytic activity. The fabricated film with bimetallic nanoparticles, ITO-SiO_2-prS-Au/PdNPs, exhibited excellent peroxidase-like activity for the oxidation of 3,3',5,5'-tetramethylbenzidine (TMB) with H_2O_2 when compared with monometallic thin nanoparticle films, ITO-SiO_2-prS-AuNPs and ITO-SiO_2-prS-PdNPs. A typical Michaelis−Menten enzyme-like behavior of the bimetallic nanoparticle film, ITO-SiO_2-prS-Au/PdNPs, was observed for H_2O_2 and TMB with Michaelis-Menten constants (K_m) of 0.33 mM and 3.46 mM, respectively. A simple, sensitive, and selective colorimetric assay for ascorbic acid (AA) detection was fabricated based on the reduction effect of AA on the oxidized TMB. The fabricated AA colorimetric sensor

exhibited a good linear range from 0.50 to 30.0 μM, with the limit of detection of 0.50 μM and the limit of quantification of 1.65 μM. Finally, our proposed colorimetric sensor, ITO-SiO_2-prS-Au/PdNPs successfully detected AA in new-born calf serum (NCS) samples, as a real sample representative.

4.1 Introduction

Ascorbic acid (AA), commonly known as vitamin C, plays an importance role in many physiological and biochemical processes [**1**]. The biosynthesis of AA requires gulonolactone oxidase enzyme. Primates including humans lack gulonolactone oxidase enzyme thus they cannot synthesize their own AA during metabolism [**2**]. Therefore, AA administration for humans is via food intake and supplementation. The recommended AA daily intake is between 100–200 mg [**3**]. The serum of healthy human naturally has approximately 40–120 μM AA concentration [**4**]. The malnutrition of AA is closely related to scurvy [**5**], and can lead to psychological abnormalities [**6**]. Therefore, it is of great importance to develop a convenient, sensitive, selective, and rapid method for the determination of AA in physiological and clinical samples. Over the years, the conventional detection of AA has been accomplished using a variety of methods that included high-performance liquid chromatography (HPLC) [**7**], fluorescence [**8**], chemiluminescence [**9**], and electrochemistry [**10**]. These conventional methods give good selectivity and low detection of limits (LoD). However, they suffer from inherent issues such as cost of their production and applications, bulky equipment requirement and are time-consuming. To overcome these challenges, nanomaterials that possess enzyme-like activity have been investigated for their potential applications in colorimetric sensing. They offer several advantages, the most

important of which are excellent stability and low cost over natural enzymes [**11**]. Since the discovery of the peroxidase-like activity of Fe_3O_4 magnetic nanoparticles (NPs) reported in 2007 [**12**], a variety of nanomaterials that possess enzyme-like catalytic activity have been widely explored as nanomaterial-based enzymes (nanozymes) or artificial enzymes. Nanozymes that have been investigated are noble metal NPs [**13**], transition-metal oxides [**14**], carbon nanomaterials [**15**], and metal-organic frameworks [**16**]. These have been found to possess intrinsic peroxidase-like activity and have been applied in colorimetric detection of biomolecules.

The nanozymes catalyze the oxidation of various substrates such as 3,3',5,5'-tetramethylbenzidine (TMB), 2,2'-azino-bis(3-ethylbenzthiazoline-6-sulfonic acid) (ABTS) and o-phenylenediamine (OPD) to develop blue-, green- and orange- colored products, respectively. In the presence of AA and due to its antioxidant properties, the peroxidase-like activity exhibited by the nanozymes can reduce the blue-colored oxidized TMB (oxTMB) back to TMB. Nanozymes that exhibited intrinsic peroxidase-like activity were reported for AA detection with high selectivity and sensitivity [**17**]. Monometallic noble metal NPs such as silver (AgNPs) [**18**], gold (AuNPs) [**19**], platinum (PtNPs) [**20**], and palladium (PdNPs) [**21**] exhibit enzyme-like activity. They possessed intrinsic peroxidase-like [**22**], oxidase-like [**23**], catalase-like [**24**], and superoxide dismutase-like [**25**] activities. As an alternative to monometallic noble metal NPs, bimetallic noble metal NPs have drawn much attention in preparation of NPs due to their synergistic catalytic properties. Bimetallic noble NPs such as Au/PdNPs [**26**] and Au-AgNPs [**27**] have been shown to exhibit superior enzyme-like activity that cannot be achieved by their monometallic nanoparticles. Despite the preparation of noble metal NPs in solution showing excellent enzyme-like activity, their recovery after

catalytic reaction still remains a major challenge. Adsorption of noble metal NPs on the solid support would be beneficial for the recovery of the catalysts for further use.

The nature of the catalytic metal determines the redox properties of bimetallic nanostructures. On the basis of that, Lin and Kurouski investigated the redox reactivity and selectivity of Au@PdNPs and Au@PtNPs using plasmon-derived reactions of 4-mercaptophenyl methanl (MPM) to 4-mercaptobenzoic acid (MBA) and vice versa [**28**]. The plasmon-derived reduction of MBA to MPM was evident for Au@PdNPs, while the plasmon-derived oxidation Au@PtNPs of MPM to MBA was observed. These results inspired the research into exploiting the reduction properties of Au@PdNPs over Au@PtNPs for the detection of AA as a reducing agent. Bimetallic nanozymes such as Ce-MOF [**29**], Fe-Mn [**30**], Cu-Pt [**31**], and IrO_2-GO [**32**] have been reported for AA detection.

In this study, the hydroxylated indium tin oxide (ITO) substrates were first coated with inert silica NPs to form ITO-SiO_2NPs as a noble metal catalyst support and to increase the surface area of bare ITO. ITO-SiO_2NPs was used to absorb and disperse gold (AuNPs), palladium (PdNPs), and gold/palladium (Au/PdNPs) NPs. Prior to noble metal adsorption, ITO-SiO_2NPs was first coated with 3-mercaptoproyltrimethoxysilane (MPTMS) to introduce a thiol functional groups for the chemisorption of AuNPs, PdNPs and Au/PdNPs. The various surfaces were labeled as ITO-SiO_2-prS-AuNPs, ITO-SiO_2-prS-PdNPs and ITO-SiO_2-prS-Au/PdNPs. These were evaluated for their enzyme-like catalytic properties toward TMB/H_2O_2 to form blue-colored oxidation products of TMB, ox TMB. The NP-modified surfaces were renewable by successive refreshing in ethanol and distilled water and used to detect of AA colorimetrically. The ITO-SiO_2-prS-Au/PdNPs surfaces were evaluated for enzyme-like activity of the modified surface and according to our knowledge are reported here for the first time.

In addition, the NP-modified surfaces are reusable after rinsing, thus affording a low-cost fabrication of the novel ITO-SiO_2-prS-Au/PdNPs.

Aims of this chapter

(i) To synthesize and characterize silica NPs (SiO_2NPs), gold NPs (AuNPs), palladium NPs (PdNPs), and gold/palladium NPs (Au/PdNPs).

(ii) To immobilize SiO_2NPs as a noble metal NP catalyst support onto the indium tin oxide (ITO) to form ITO-SiO_2NPs as the absorbent.

(iii) To introduce thiol functional groups from MPTMS on the ITO-SiO_2NPs surfaces.

(iv) To adsorb and disperse AuNPs, PdNPs, and Au/PdNPs onto ITO-SiO_2NPs surfaces to form ITO-SiO_2-prS-AuNPs, ITO-SiO_2-prS-PdNPs, and ITO-SiO_2-prS-Au/PdNPs, respectively.

(v) To evaluate the enzyme-like catalytic properties of our fabricated ITO-SiO_2-prS-AuNPS|PdNPs|Au/PdNPs surfaces toward TMB/H_2O_2 substrate to form blue-colored products of oxidation of TMB, oxTMB.

(vi) To investigate ITO-SiO_2-prS-Au/PdNPs for the detection of AA in buffer and new-born calf serum (real and complex matrix)

4.2 Experimental

4.2.1 Materials and reagents

Hydrogen tetrachloroaurate trihydrate ($HAuCl_4 \cdot 3H_2O$), palladium chloride ($PdCl_2$), sodium borohydride ($NaBH_4$), tetraethylorthosilicate (TEOS), sodium chloride (NaCl), potassium chloride (KCl), calcium chloride ($CaCl_2$), acetic acid (CH_3COOH), 3,3',5,5'-tetramethylbenzidine (TMB), ascorbic acid (AA), 3-mercaptoproyltrimethoxysilane

(MPTMS), D-glucose, sucrose, urea, glycine, guanine, cytosine, adenine, and Indium Tin Oxide (ITO) substrates were purchased from Sigma-Aldrich. 32% Hydrochloric acid (HCl), dimethyl sulfoxide (DMSO), ethanol (EtOH), ammonia hydroxide (NH_4OH), and methanol (MeOH) were purchased from B&M Scientific. Magnesium sulphate ($MgSO_4$) was purchased from Associated Chemical Enterprises (ACE Chemicals). All the reagents were of analytical grade. All aqueous solutions were prepared using ultrapure water with a resistivity of 18.2 ΩM.cm obtained from a MilliQ system (Millipore, Corp, Bedford, MA, USA).

4.2.2 Apparatus

The UV-vis measurements were carried out on a Thermo-Scientific, Multiskan Sky w Cuvette and Touch Screen, 100-240 V, Belgium. Fourier Transform Infrared Spectroscopy (FTIR) measurements were carried out on a Perkin Elmer Spectrum 100 FTIR. The hydrodynamic and Zeta potential were carried out on a Malvern Zetasizer Nano-ZS90 series equipped with a 633 nm He/Ne laser. A disposable folded capillary cell (DTS 1060) was used for data collection for Zeta potential measurements. Transmission electron microscopy (TEM) micrographs were obtained using a Zeiss Libra 120 TEM operating at 80 kV. The nanoparticles were dissolved in water and dropped onto a carbon-coated copper grid, and allowed to dry overnight at room temperature before measurement. Scanning electron microscopy (SEM) and Energy dispersive X-ray spectroscopy (SEM-EDX) images and elemental composition were obtained from INCA PENTA FET coupled with VGA TASCAM at 20 kV acceleration voltage. X-ray diffraction (XRD) patterns were recorded on a Bruker D8 Discover equipped with a Lynx Eye detector, using Cu-Ka radiation (1.5405 Å, nickel filter). The samples were placed on a silicon wafer slide. The data was collected in the range from

2θ = 10° to 100°. X-ray photoelectron spectroscopy (XPS) measurements were conducted using XPS Kratos - DLD Ultra, UK. Vision processing 2 software was used for elemental composition and fitting of the high-resolution spectra. Electrochemical measurements were performed using Autolab Galvanostat/Potentialstat 302N workstation controlled by Proline computer running on NOVA 1.10 software.

4.2.3. Preparation of gold nanoparticles (AuNPs)

The preparation of SiO_2NPs and PdNPs were prepared and discussed as in *Section 3.2.3 and 3.2.4*. The preparation of gold nanoparticles (AuNPs) was prepared using reduction of gold chloride ($HAuCl_4 \cdot 3H_2O$) using sodium borohydride ($NaBH_4$) as described in literature [33]. Briefly, $HAuCl_4 \cdot 3H_2O$ (0.25 mM, 10.0 mg) was dissolved in deionized water (100 mL) under vigorous stirring. An ice-cold 0.50 mL of $NaBH_4$ (0.026 M, 1.0 mg) was added into gold solution dropwise over 30 min. As the $NaBH_4$ was added, the solution of gold turned from yellowish colour to ruby-red. The colour changes signify the formation of gold nanoparticles.

4.2.4. Preparation of gold/palladium nanoparticles (Au/PdNPs)

The as-prepared AuNPs (0.23 μM, 25 mL) acted as a site for nucleation for PdNPs deposition, thus forming a shell or an alloy on AuNPs. Palladium shell was deposited *in situ* by reducing H_2PdCl_4 using an ice-cold 0.50 mL of $NaBH_4$ (0.026 M, 1.0 mg). After palladium deposition to form Au/PdNPs, the color of the substrate changed from reddish to blackish, confirming the deposition of a palladium shell on the AuNPs.

4.2.5 Hydrolysis of ITO glass substrate

The bare ITO substrates were cleaned in an ultrasonic bath of acetone, methanol, ethanol and deionized water for 15 min each before being dried with N_2 gas. The substrates were hydroxylated in the mixture of H_2O_2:NH_4OH:H_2O in the ratio1:1:5 at 60 °C. The hydroxyl ITO surface (ITO-OH) was formed after 30 min and rinsed with deionized water. The substrates were then dried with N_2 gas.

4.2.6 Fabrication of AuNPs, PdNPs, and Au/PdNPs onto ITO-SiO_2-prSH, Scheme 4.1

Scheme 4.1 shows the representaion of ITO fabrication and attachment of noble mono- and bimetallic nanoparticles. The preparation of ITO-SiO_2-prS-AuNPs, ITO-SiO_2-prS-PdNPs, or ITO-SiO_2-prS-Au/PdNPs was achieved using cleaned ITO substrate, which was first hydroxylated to form hydroxyl active ITO surface (ITO-OH). SiO_2NPs (2.0 mg.mL^{-1}) in ethanol were coated via covalent bonds onto the ITO-OH substrate to act as a support for catalyst adsorption and increase the surface area to form IT$OSiO_2$NPs for 24 hours. MPTMS (40 mM) in methanol was used to modify the ITO-SiO_2NPs to form thiol-functionalized ITO-SiO_2-prSH for 3 hours. The terminal −SH functional group on ITO-SiO_2-prSH served as an anchor for the chemisorption of the noble metal NPs. Gold NPs (AuNPs, 0.23 μM, 5.0 mL) synthesized using $NaBH_4$ reduction of $HAuCl_4 \cdot 3H_2O$ method were dispersed onto the surface of IT$OSiO_2$-prSH to form ITO-SiO_2-prS-AuNPs for 24 hours. The color of the IT$OSiO_2$-prS-AuNPs was reddish, confirming successful deposition of AuNPs and rinsed with water to remove physically adsorbed AuNPs and dried with N_2 gas. The detailed procedure and amounts of reagents used for the fabrication of ITO-SiO_2-prS-PdNPs are as described

in *Section 3.2.5*. For the bimetallic NPs, ITO-SiO_2-prS-AuNPs acted as a site for nucleation for PdNPs deposition, thus forming a shell or an alloy on AuNPs. Palladium shell was deposited *in situ* by reducing H_2PdCl_4 using an ice-cold 0.50 mL of $NaBH_4$ (0.026 M, 1.0 mg). After palladium deposition to form ITO-SiO_2-prS-Au/PdNPs, the color of the substrate changed from reddish to blackish, confirming the deposition of a palladium shell on the AuNPs. The ITO-SiO_2-prS-Au/PdNPs surface was rinsed with water to remove excess H_2PdCl_4 and physically adsorbed PdNPs and dried with N_2 gas.

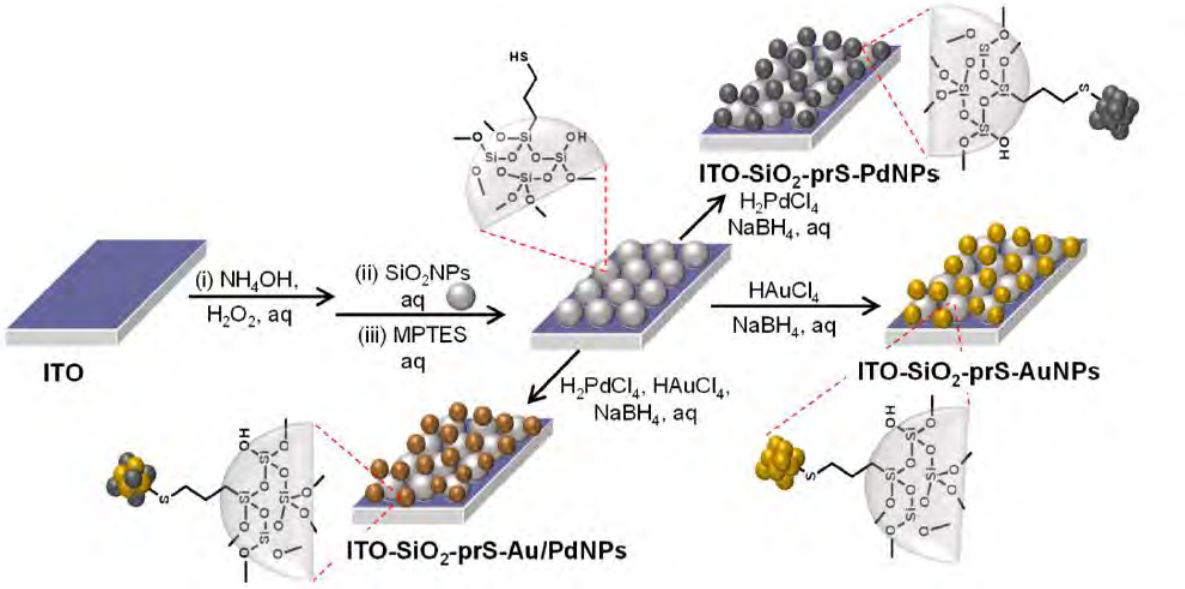

Scheme 4.1: Fabrication of AuNPs, PdNPs and bimetallic Au/PdNPs on ITO-SiO_2-prSH to form ITO-SiO_2-prS-AuNPs|PdNPs|Au/PdNPs as described in Section 4.2.6.

4.2.7 Monitoring ROS generation using a radical scavenger

The two studies were conducted:

(i) 1,3-Diphenylisobenzofuran (DPBF) has an absorption at 420 nm. Upon reacting with reactive oxygen radical species (ROS) the absorption decreases and this can be monitored using UV–vis spectrophotometer. Experimentally, ITO-SiO_2-prS-Au/PdNPs was immersed into 1 mL acetate buffer (pH 4.0) solution of H_2O_2 (6.0 mM) followed by addition of 200 µL of 0.25 mM DPBF (also in acetate buffer pH 4.0). The UV-vis spectra were measured for 10 minutes at 1 min interval. The initial solution of 200 µL of 0.25 mM DPBF was diluted into 1 mL acetate buffer and measured fresh after preparation. Also we allowed the reaction to stand for 10 min and measured.

(ii) Terephthalic acid, TA (a fluorescent hydroxyl radical quencher) was used in the presence of ITO-SiO_2-prS-Au/PdNPs and H_2O_2. The reaction of 1.0 mM TA in ethanol (1 mL) with acetate buffer (pH 4.0, 4 mL) was mixed with ITOSiO_2-prS-Au/PdNPs in the presence of 3.0 mM H_2O_2 and incubated for 10 min. Fluorescence emission spectra excited at 320 nm were measured.

4.2.8 Electrochemical measurements

All electrochemical experiments were studied using a three-electrode system with ITO-SiO_2-prS-Au/PdNPs as the working electrode, coiled platinum wire as counter electrode and Ag|AgCI as pseudo-reference electrode in acetate buffer pH 4.0 at room temperature. The electrocatalytic oxidation of ITO-SiO_2-prS-Au/PdNPs toward H_2O_2 was performed using amperometric technique.

4.3 Results and discussion

4.3.1 Characterization of AuNPs

The nanoparticles of SiO_2NPs and PdNPs were successfully synthesized and characterized as described in *Section 3.3.1 and 3.3.2*, respectively. The gold nanoparticles TEM in **Figure 4.1(a)** was spherical and monodispersed**.** The corresponding size distribution curve in **Figure 4.1(b)** was obtained using ImageJ and an average particle size was 7.1 ± 1.8 nm. The number of AuNPs seeds was calculated using **Equation 4.1** [**34**], a spherical shape nanoparticles and assuming a reaction yield of 100%. The number of Au seeds was estimated to be 1.36 $x10^{16}$ particles per millilitre which were converted to 0.23 µM.

$$\mathbf{N_{seed} = \frac{[Au]\ X\ M\ X\ 6\ X\ 10^{21}}{\rho \pi D^3}} \qquad \mathbf{(4.1)}$$

where ρ is the density of Au (19.3 $g.cm^{-3}$), D is the diameter (7.1 ± 1.8 nm), [Au] is the initial concentration of the $HAuCl_4 \cdot 3H_2O$ and M is the atomic weight of Au (197.0 $g.mol^{-1}$). The UV-vis spectrum was measured in **Figure 4.1(c)** with the Surface Plasmon Resonance (SPR) peak at 522 nm. The EDX in **Figure 4.1(d)** showed the presence of Au M, O K and C K. The C K and O K elements were due to the organic capping agent on the surface of gold nanoparticles. The DLS was used to measure the particle size and was found to be 7.0 nm in **Figure 4.1(e)** and was similar to the TEM particle size.

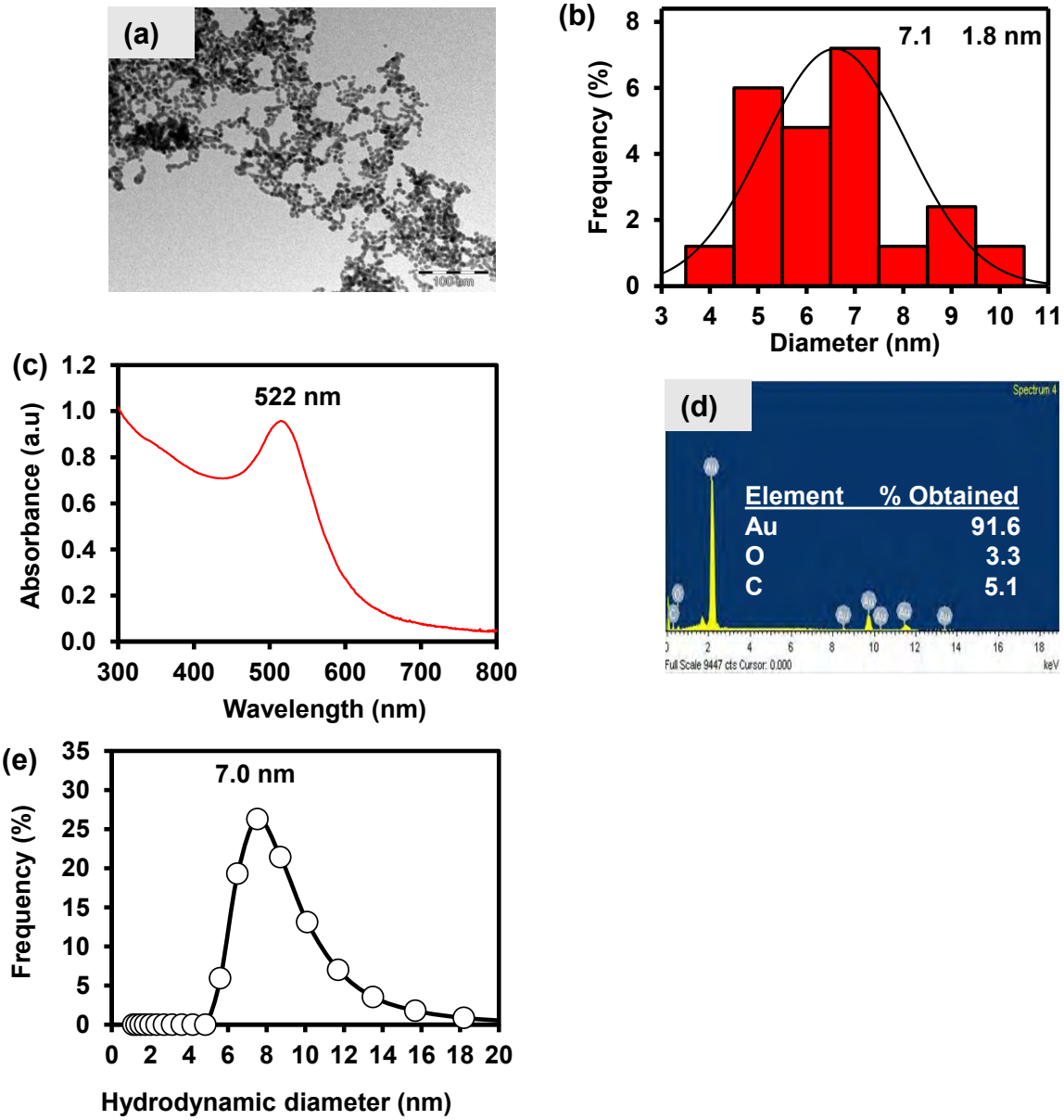

Figure 4.1: (a) TEM image, (b) size distribution histogram, (c) UV-vis absorption spectrum, (d) EDX, and (e) DLS of gold nanoparticles (AuNPs).

4.3.2 Characterization of Au/PdNPs

To confirm the formation of the Pd shell on gold nanoparticles, i.e. Au/PdNPs, the *ex situ* experiment was conducted. The AuNPs as synthesized in **Figure 4.1** with the particle size diameter of 7.1 ± 1.8 nm were used as seed and nucleation sites for Pd shell to form. H_2PdCl_4 was reduced onto AuNPs using $NaBH_4$. The TEM image in **Figure 4.2(a)** showed agglomerated Au/PdNPs with the particle size distribution in **Figure 4.2(b)** showing an increase in the diameter from 7.1 ± 1.8 for AuNPs to 23.5 ± 3.3 nm as the palladium formed a shell. AuNPs acted as nucleation sites for Pd deposition. The same concentration solution for the pure PdNPs used gave the diameter of 7.9 ± 1.2 nm. Therefore, an increase in particle size diameter to 23.5 ± 3.3 nm was due to the shell forming on the AuNPs seed. The UV-vis spectrum of the Au/PdNPs showed a broad SPR peak at 544 nm in **Figure 4.2(c)** and this shifted from 522 nm for AuNPs. The EDX spectrum in **Figure 4.2(d)** showed that the composition contained both Pd M, Au M, O K and C K. O K and C K elements were from the MPTMS. The Pd shell showed high intensity and was 68.9% compared to gold 28.4% and this is due to the Pd forming a shell on AuNPs. The DLS particle size in **Figure 4.2(e)** also showed an increase in diameter for Au/PdNPs to 32.9 nm and much bigger than the AuNPs (7.1 ± 1.8 nm) in **Figure 4.1** and PdNPs (7.9 ± 1.2 nm) in **Figure 3.2**.

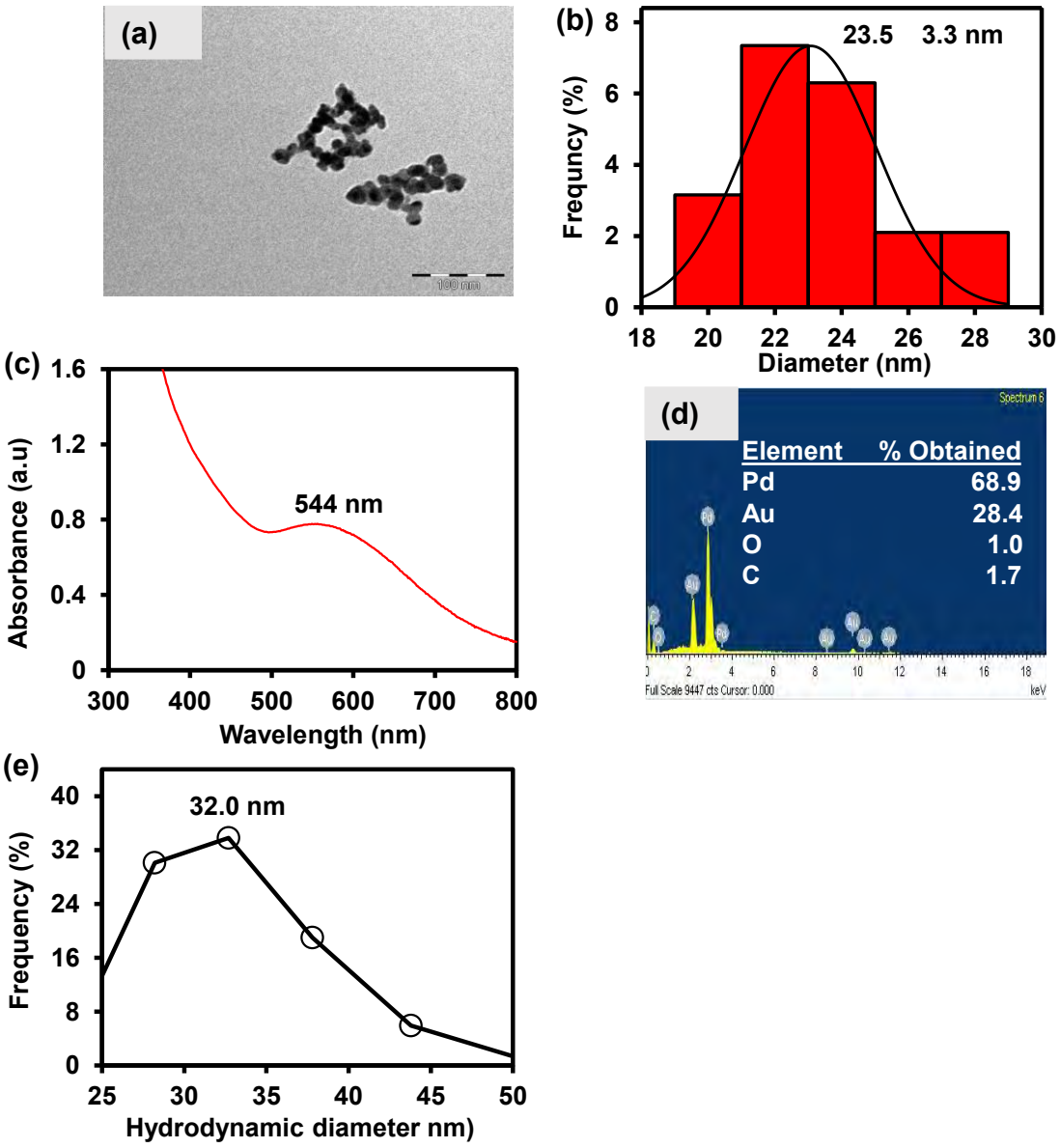

Figure 4.2: (a) TEM image, (b) size distribution histogram, (c) UV-vis absorption spectrum (d) EDX, and (e) DLS of gold/palladium (Au/PdNPs).

To further confirm the formation of the Pd shell, the XRD of powder PdNPs and Au/PdNPS were measured and are shown in **Figure 4.3(a)** and (**b**), respectively. The XRD pattern of PdNPs showed broad peaks at the following 2θ (degree) values with their Miller Indices in brackets at 38.8º (111), 44.9º (200), 64.8º (202), 78.3º (311) and 81.4º (222). The Miller Indices confirmed the formation of a face-centred cubic (FCC) structure. When the palladium shell formed on AuNPs (Au/PdNPs) the XRD peaks

were narrower (crystalline) in **Figure 4.2(b)** and at the following 2θ (degree) values with their Miller Indices in brackets at 39.9º (111), 46.1º (200), 67.8º (202), 81.8º (311) and 85.6º (222) further confirming the formation of FCC. The XRD pattern for the Au/PdNPs was similar to the PdNPs with slight shift in 2θ values to higher values confirming further the formation of a Pd shell. For Miller Indices identification, a Pd JCPDS (05-0681) was used. Pure AuNPs will have the 2θ values lower.

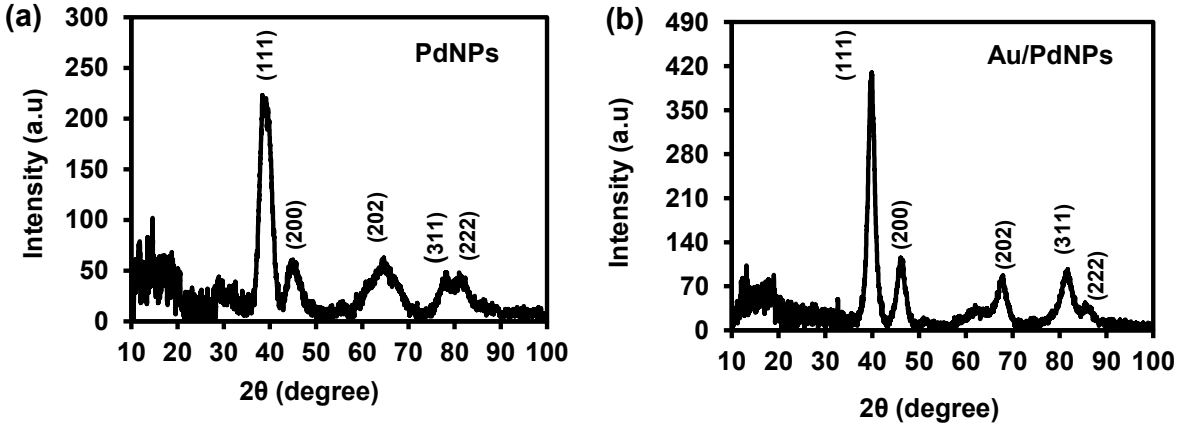

Figure 4.3: X-ray Diffraction (XRD) patterns for (a) PdNPs and (b) Au/PdNPs.

4.3.3. X-ray photoelectron spectroscopy (XPS) characterization of ITO-SiO_2-prS-Au/PdNPs

The composition and oxidation states of Au and Pd on the ITO-SiO_2-prS-Au/PdNPs surface were further investigated using XPS. The survey spectrum in **Figure 4.4(a)** confirmed the presence of Au 4f (0.4%), Pd 3d (3.5%), Si 2p (21.4%), O (34.5%), and C 1s (40.2%) as the elements of interest. The amount of gold was low (0.4%) and this was attributed to the fact that gold was used as seed nanoparticles for the palladium deposition, thus was coated with palladium. This further confirmed the bimetallic formation of Au/PdNPs. **Figure 4.4(b)** shows high-resolution spectrum of Au 4f with Au^0 at 84.0 eV and Au^+ at 85.0 eV oxidation state states with their components also

observed at high binding energies with spin-orbit splitting of 3.62 eV. The components accounted for 59.5% for Au^0 and 35.1% for Au^+. The high-resolution spectrum of Pd in **Figure 4.4(c)** confirmed the Pd^0 component at 335.4 eV which accounted for 35.9% and Pd^{2+} oxidation states at 336.4 eV (19.5%) and at 338.1 eV (44.6%). The spin-orbit coupling of 5.36 eV was observed for Pd components at higher binding energies. Other high-resolution spectra for Si 2p in **Figure 4.4(d)**, O 1s in **Figure 4.4(e)** and C 1s in **Figure 4.4(f)** are from the SiO_2NPs which was used as adsorbent for Au/PdNPs. The component assignments and composition are displayed as an inset. Further characterization was conducted using EDX, as shown in **Figure 4.5**. **Figure 4.5(a)** is similar to the results obtained in **Figure 3.3** and discussed. For ITO-SiO_2-prS-Au/PdNPs in **Figure 4.5(b)**, the presence of both Au (0.8%) and Pd (3.2%) was observed with other elements from ITO-SiO_2NPs. The results confirmed the deposition of gold and palladium NPs.

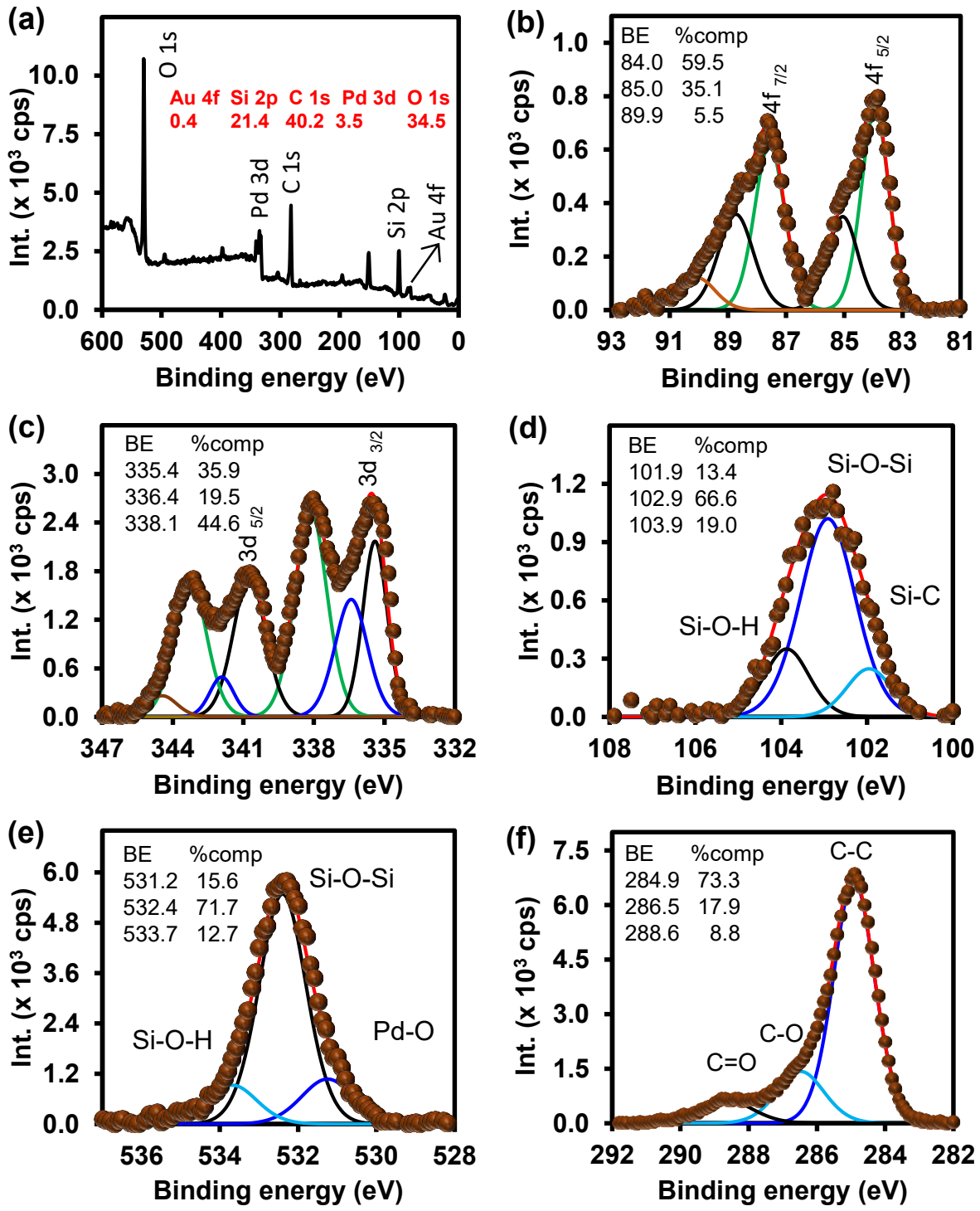

Figure 4.4: (a) Survey spectrum, and high-resolution spectra of (b) Au 4f, (c) Pd 3d, (d) Si 2p, (e) O 1s and (f) C 1s of ITO-SiO_2-prS-Au/PdNPs.

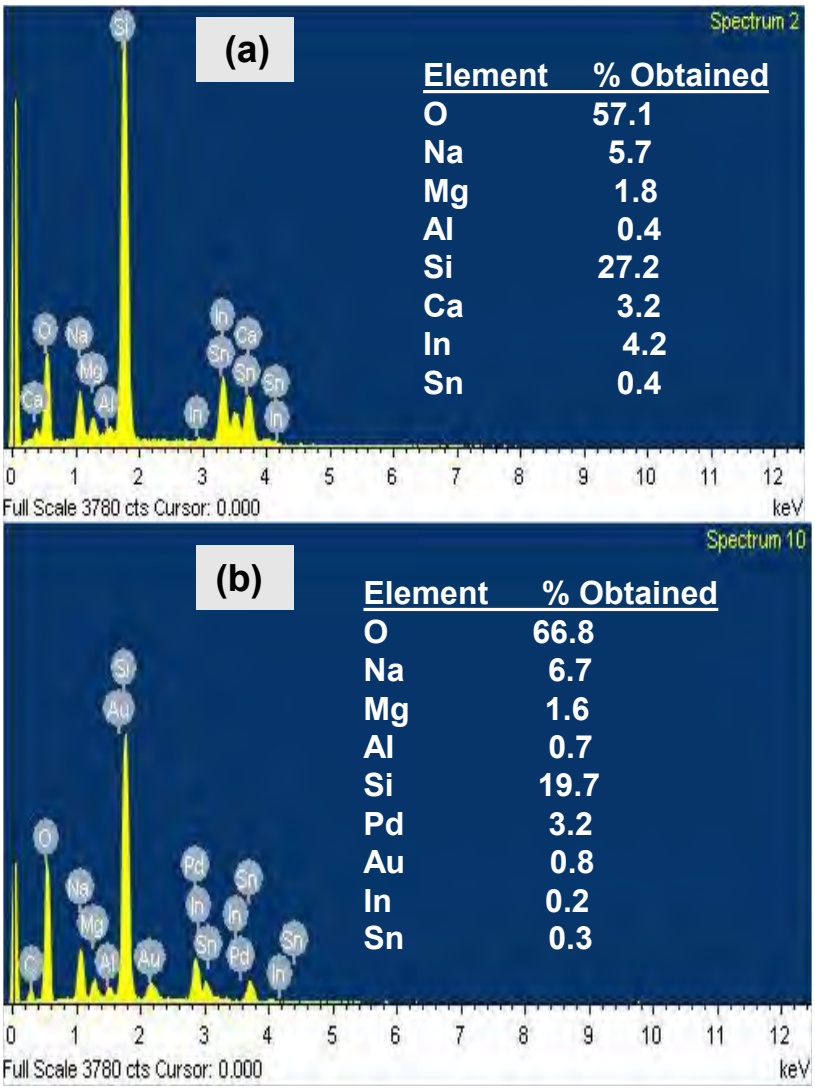

Figure 4.5: Energy Dispersive X-ray spectroscopy (EDX) of (a) bare ITO and (b) ITO-SiO_2-prS-Au/PdNPs.

4.3.4 Peroxidase-like activity of ITO-SiO_2-prS-AuNPs, PdNPs and Au/PdNPs

The peroxidase-like activity of ITO-SiO_2-prS-AuNPs, ITO-SiO_2-prS-PdNPs, and ITO-SiO_2-prS-Au/PdNPs was evaluated in solution containing H_2O_2 and TMB. **Figure 4.6** shows UV-vis spectra of (a)(i) TMB + H_2O_2, (ii) H_2O_2 + ITO-SiO_2-prS-Au/PdNPs, and (iii) TMB + ITO-SiO_2-prS-Au/PdNPs. No significant increase in the absorption was observed when H_2O_2 and TMB were present in solution in **Figure 4.6(a)**. When H_2O_2 and TMB were present in the solution together with ITO-SiO_2-prS-AuNPs in **Figure 4.6b(i)**, ITO-SiO_2-prS-PdNPs in **Figure 4.6b(ii)**, and ITO-SiO_2-prS-Au/PdNPs in **Figure 4.6b(iii)**, the solution color changes from clear to blue as shown in the picture inset in **Figure 4.6(b)**. A blue-color solution was accompanied by an increase in absorbance, in **Figure 4.6(b)**, with intense absorption at 374 nm and 652 nm. No absorption was observed for bare ITO and ITO-SiO_2NPs, the UV-vis spectra were similar to the spectrum reported in **Figure 4.6(a)**, and the solutions remained clear or colourless. The enhanced catalytic activity of ITO-SiO_2-prS-Au/PdNPs was observed in **Figure 4.6(b)(iii)** and was due to the synergistic effect between AuNPs and Pd shell as was reported before [**28**]. The observed UV-vis spectra were similar to the horse-radish peroxidase (HRP) spectrum in solution containing H_2O_2 and TMB [**12**]. The observed peaks in **Figure 4.6(b)** confirm the peroxidase-like activities of the (i) AuNPs, (ii) PdNPs and (iii) Au/PdNPs. The catalytic properties of AuNPs, PdNPs and Au/PdNPs adsorbed as nanozymes on ITO-SiO_2NPs are dependent on the morphology and size of the nanoparticles, and the nature of the catalyst or support used [**35**]. The nanozymes investigated here are spherical NPs, and hence, the morphology has no effect. Therefore, the nature of the catalyst (metallic NPs) and the size were observed to increase from 7.1 ± 1.8 nm for AuNPs and 7.9 ± 1.2 nm for

PdNPs, which increased when Pd was reduced onto AuNPs as nucleation sites to 23.5 ± 3.3 nm for Au/PdNPs (prepared *ex situ* in **Figure 4.2(a)**). The results suggest that both TMB and H_2O_2 are necessary in evaluating the peroxidase-like activity of the NPs adsorbed on ITO-SiO_2NPs. An enhanced peroxidase-like activity of ITO-SiO_2-prS-Au/PdNPs was obtained with intense absorption peaks at 374 nm and 652 nm and was studied further.

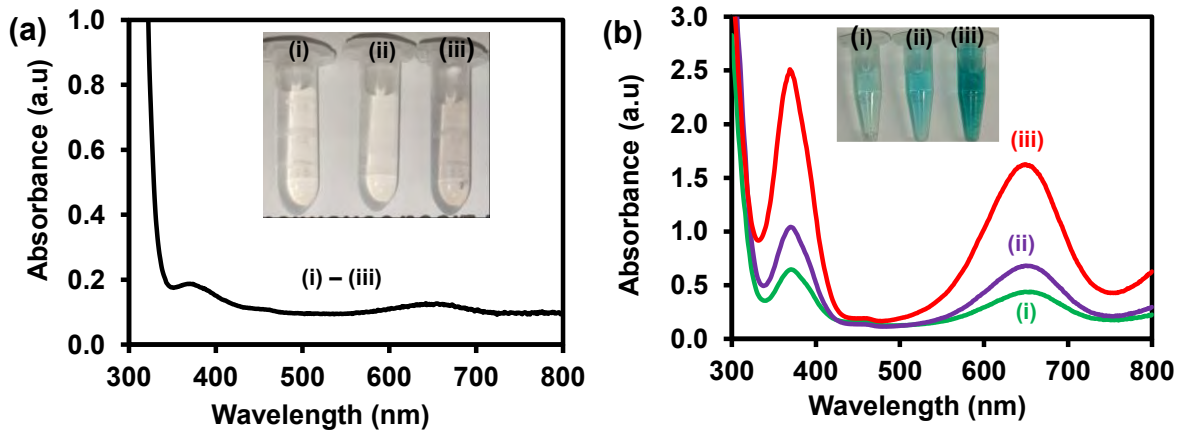

Figure 4.6: UV-vis absorption spectra of (a)(i) H_2O_2 + TMB, (ii) H_2O_2 + ITO-SiO_2-prS-Au/PdNPs, (iii) TMB + ITO-SiO_2-prS-Au/PdNPs. (b) Substrate solution (H_2O_2 + TMB) in the presence of (i) ITO-SiO_2-prS-AuNPs, (ii) ITO-SiO_2-prS-PdNPs, (iii) ITO-SiO_2-prS-Au/PdNPs. Acetate buffer solution (pH 4.0, 0.20 M), with H_2O_2 (0.20 M) and TMB (4.2 mM) was used for all the experiments.

4.3.5 Effect of conditions on peroxidase-like activity of ITO-SiO_2-prS-Au/PdNPs

The peroxidase-like activity of ITO-SiO_2-prS-Au/PdNPs was affected by the reaction and environmental conditions, such as effect of pH, reaction time, concentrations of H_2O_2 and TMB, and effect of temperature. **Figure 4.7** shows the effect of (a) pH (2–6), (b) reaction time (5–50 min), (c) [H_2O_2] (0–16 mM), (d) [TMB] (0.4–1.4 mM), and

temperature (25–90 °C) on ITO-SiO_2-prS-Au/PdNPs. **Figure 4.7(a)** (red) shows that under weak acidic conditions pH 4.0, the highest absorption at 652 nm was observed. A drastic decrease in the activity was observed at pH greater than 4. At lower pH values, nanomaterials break down H_2O_2 to form reactive oxygen radical species (ROS) ($OH^{\bullet-}$, $HO_2^{\bullet-}$ and $O_2^{\bullet-}$ radicals), which oxidize TMB to blue-colored oxidation product (3,3′,5,5′-tetramethylbenzidiimine, TMBDI or oxTMB) [**36**]. Acidic pH conditions were used and preferred to avoid desorption of nanocatalysts (Au/PdNPs) on ITO-SiO_2-prS-Au/PdNPs surface and also not disintegrate the SiO_2NPs which occurs at alkaline pH conditions.

Interestingly, the optimum pH for peroxidase-like activity of the solution Au/PdNPs prepared *ex-situ* (not deposited on ITO-SiO_2NPs) in **Figure 4.7(a)** (black) was pH 5.0, but for ITO-SiO_2-prS-Au/PdNPs was pH 4.0. These results can suggest successful decoration of palladium shell onto to Au core/seed on the ITO-SiO_2-prS-AuNPs to form ITO-SiO_2-prS-Au/PdNPs. In **Figure 4.7(b)**, the oxTMB color intensity increased as reaction time was increased within the studied time from 5 to 50 min. The regression equation for the reaction time for the development of the oxTMB was Abs_{652} = 0.0167x + 0.0297 with R^2 of 0.997. Considering both activity and economy of the catalytic process, 15 min was selected as the optimized condition for further investigations. As shown in **Figure 4.7(c)** and (**d**) increasing the concentration of H_2O_2 and TMB resulted in an increased absorbance at 652 nm. At higher concentrations of H_2O_2 (> 6.0 mM) and TMB (> 0.80 mM), a drastic decrease in absorption was observed for H_2O_2 and for TMB, a plateau was observed. The plateau and decrease in intensity was attributed to the saturation of catalytic sites on the ITO-SiO_2-prS-Au/PdNPs, resulting in the decrease of the catalytic activity. This phenomenon was observed for HRP and some other peroxidase-like nanozymes at high concentrations of H_2O_2 and TMB [**37**–**39**].

The ITO-SiO_2-prS-Au/PdNPs showed optimal concentrations of H_2O_2 and TMB at 6.0 mM and 0.80 mM, respectively. In **Figure 4.7(e)**, the effect of increasing the temperature from 25–90 ºC on the peroxidase-like activity was investigated. The relative activity measured at 652 nm with 100% normalization at 50 °C was >90% and drastically dropped after 70 °C and due to decomposition of H_2O_2 at high temperature. The stability of the ITO-SiO_2-prS-Au/PdNPs signal up to 70 °C was promoted due to absorbing bimetallic Au/PdNPs as catalysts. The stability of the peroxidase-like activity of the ITO-SiO_2-prS-Au/PdNPs was high compared to natural enzymes which has a narrow operation window of activity.

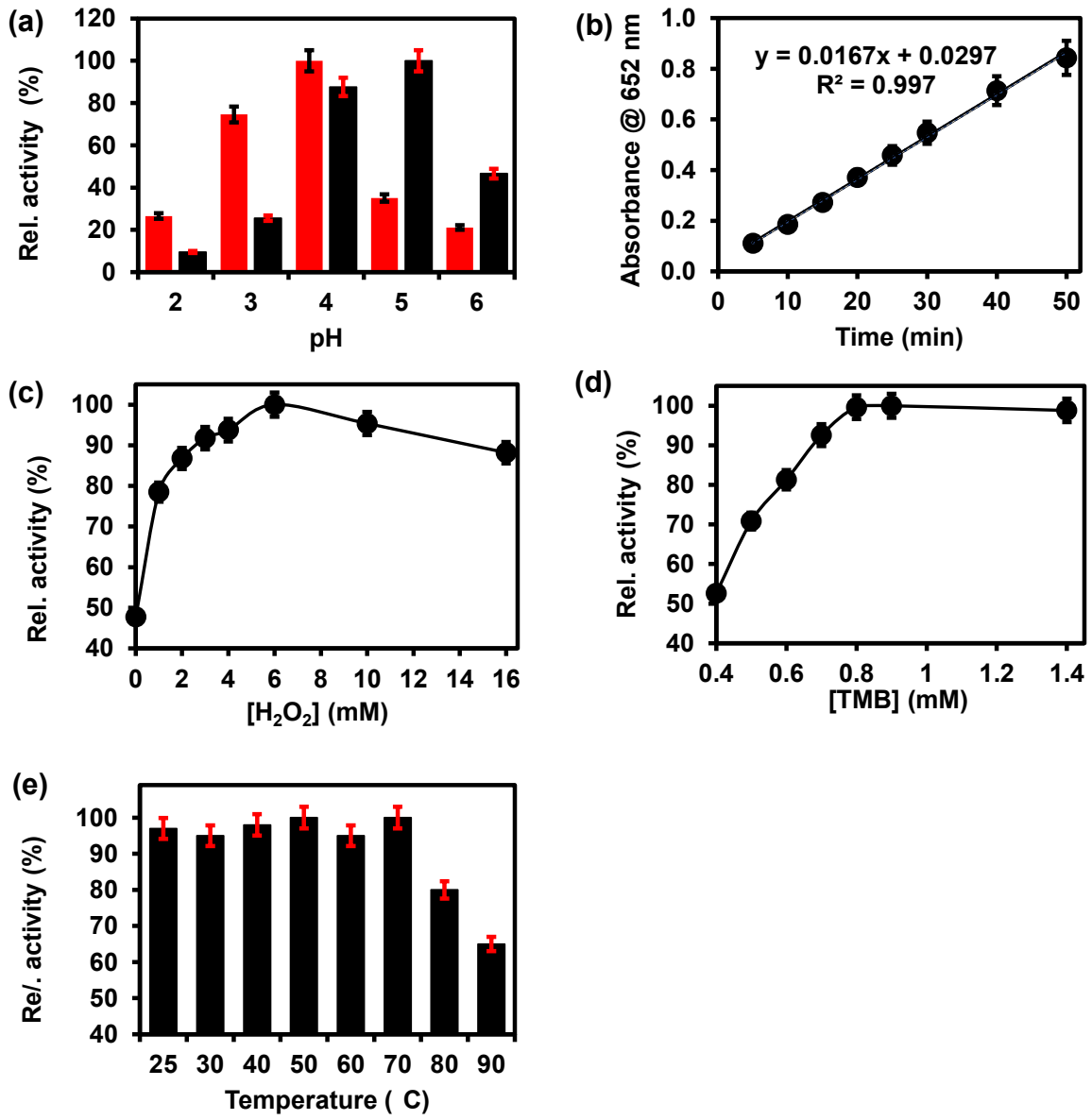

Figure 4.7: Effect of (a) pH (red), (b) time, (c) concentration of H_2O_2, (d) concentration of TMB, and (e) temperature on the peroxidase-like activity of ITO-SiO_2-prS-Au/PdNPs in acetate buffer solution (pH 4.0, 0.20 M), containing H_2O_2 (0.20 M) and TMB (4.2 mM). (Effect of pH (a) (black) on the peroxidase-like activity of Au/PdNPs).

4.3.6 Confirmation of mechanism for enzyme-like properties

The enzyme-like mechanism of ITO-SiO_2-prS-Au/PdNPs was investigated for ROS generation using the oxygen radical (O_2•−) and singlet oxygen ($^1O_2$) quencher (DPBF). The absorption of DPBF at 420 nm in **Figure 4.8(a)** is expected to decrease due to ROS generated. There was no change in the intensity of DPBF for up to 10 min in **Figure 4.8(b)**, confirming that no ROS was generated. A similar study was investigated using TA as a hydroxyl radical trap as described in Section 4.2.7. No fluorescence signal was observed and therefore no ROS of any kind was observed. We then investigated the electron-transfer mechanism by adding H_2O_2 in the pH 4.0 acetate buffer solution using chronoamperometric measurements. **Figure 4.8(c)** shows an increase in the signal due to the addition of H_2O_2 and its oxidation. This results in the reduction of PdNPs, thus further oxidizing TMB to blue-colored products as shown in **Scheme 4.2**.

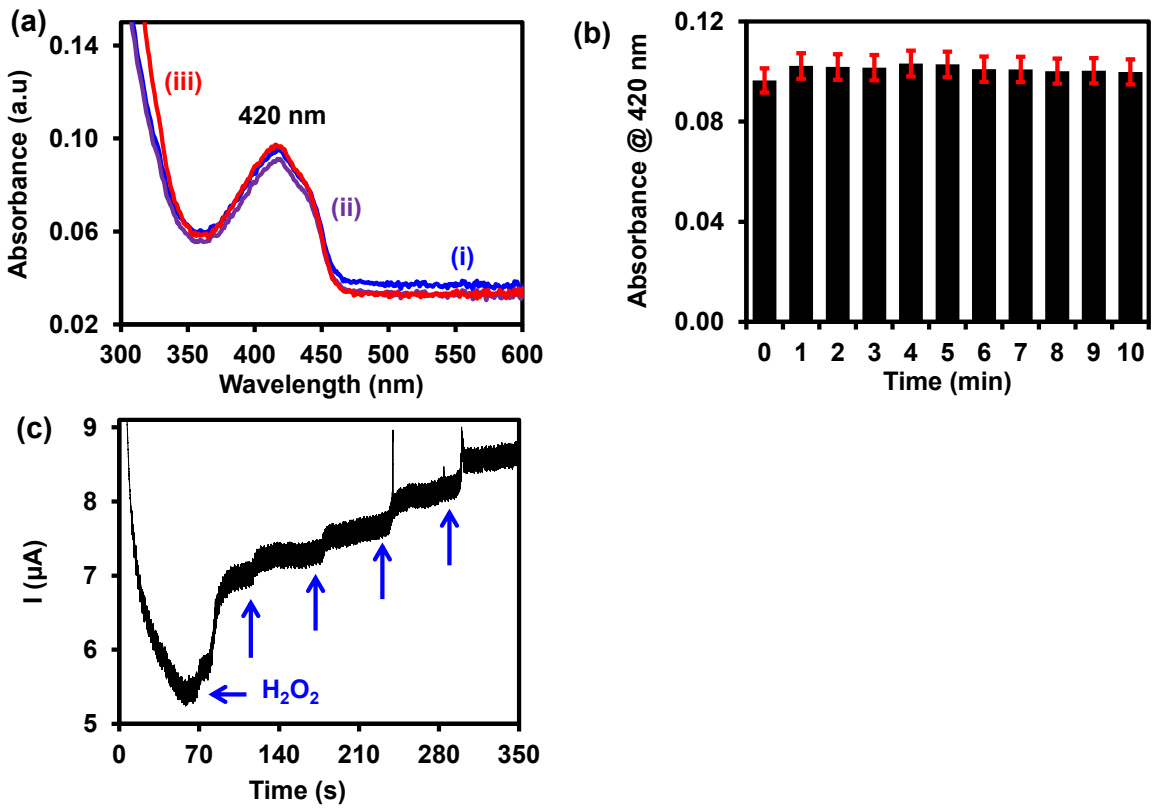

Figure 4.8: UV-vis absorption spectra of (a)(i) DPBF alone (blue), (ii) DPBF + H_2O_2 (purple), (iii) DPBF + H_2O_2 + ITO-SiO_2-prS-Au/PdNPs (red). (b) Absorption of DPBF at 420 nm in the presence of H_2O_2 and ITO-SiO_2-prS-Au/PdNPs at the predetermined time interval of 1 minute up to 10 minutes. (c) Chronoamperomogram of the modified ITO-SiO_2-prS-Au/PdNPs with addition of 10 μL H_2O_2 (1.0 mM) into 10 mL pH 4.0 acetate buffer.

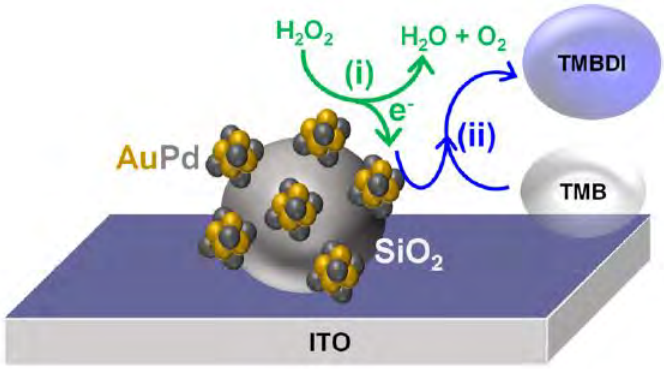

Scheme 4.2: Electron-transfer mechanism for TMB oxidation on the peroxidase-like activity by ITO-SiO_2-prS-Au/PdNPs.

4.3.7 Steady-state kinetics of ITO-SiO_2-prS-Au/PdNPs

The steady-state kinetics using H_2O_2 and TMB as substrates for the peroxidase-like activity of ITO-SiO_2-prS-Au/PdNPs was further investigated by varying the concentration of H_2O_2 at constant TMB and vice versa. A series of initial rates (V_0) of TMB oxidation were obtained from the time-dependent absorption values at 652 nm. The absorbance values were converted to concentration using the molar absorption coefficient (ε) of oxidized TMB at 652 nm using **Equation (4.2):**

$$[ox - TMB] = \frac{A}{\varepsilon L} \qquad \textbf{(4.2)}$$

where A is the absorbance at 652 nm, ε is the molar absorption of oxidized TMB at 652 nm (39, 000 $M^{-1}.cm^{-1}$), and L is the path length (1 cm) [**40**]. In **Figure 4.9(a)**, the plot of initial rates (V_0) against the concentrations of substrate H_2O_2 or TMB (in **Figure 4.9(b)**) was evaluated. The graphs showed an increase in V_0 with increasing concentration of [H_2O_2] in **Figure 4.9(a)** and [TMB] in **Figure 4.9(b)**, and it reached a plateau at high concentrations, 5.0 mM for H_2O_2 and 0.78 mM for TMB. This confirmed

a typical Michaelis−Menten enzyme-like behaviour for the ITO-SiO_2-prS-Au/PdNPs. The double reciprocal plots in **Figure 4.9**(**c**) for H_2O_2 and (**d**) for TMB were used to calculate the K_m from the slope and V_{max} from the y-intercept using **Equation (4.3):**

$$\frac{1}{V_0} = \frac{K_m}{V_{max}} \frac{1}{[S]} + \frac{1}{V_{max}} \qquad \textbf{(4.3)}$$

where V_0 is the initial rate, V_{max} is the maximal reaction rate, [*S*] is the concentration of the substrate (H_2O_2 or TMB), and K_m is the Michaelis−Menten constant. The strength or affinity between the enzyme and the substrate is defined by K_m. High K_m values indicate weak affinity, whereas low K_m values suggest a strong affinity. The calculated kinetic parameters of ITO-SiO_2-prS-Au/PdNPs and the comparison with HRP and other nanozymes are summarized in **Table 4.1**. The K_m value for ITO-SiO_2-prS-Au/PdNPs toward H_2O_2 as the substrate was (0.33 mM) and is lower than that of HRP [**12**] (3.70 mM). Most nanozymes such as Ce/$ZnCo_2O_4$ [**41**] (0.55 mM), Fe_3O_4@SiO_2-NH_2-Au@PdNPs [**42**] (0.35 mM), and CuO-Au nanoalloys [**43**] (4.08 mM), had K_m values higher than ITO-SiO_2-prS-Au@PdNPs. Comparable K_m values were observed for FeNPs [**44**] (0.32 mM), indicating that ITO-SiO_2-prS-Au/PdNPs has greater affinity for H_2O_2. On the other hand, the K_m value for the ITO-SiO_2-prS-Au/PdNPs toward TMB as the substrate was 3.46 mM and much higher than HRP [**12**] (0.43 mM), but comparable to CuO-Au nanoalloys [**43**] (3.54 mM), and lower than Zn/CuO [**45**] (10.0 mM). These results suggest that ITO-SiO_2-prS-Au/PdNPs exhibited intrinsic peroxidase-like activity and had good affinity for H_2O_2 and comparable affinity for TMB with other nanozymes. Thus, ITO-SiO_2-prS-Au/PdNPs can be used as potential nanozymes or artificial enzyme and as substitute for expensive natural enzymes.

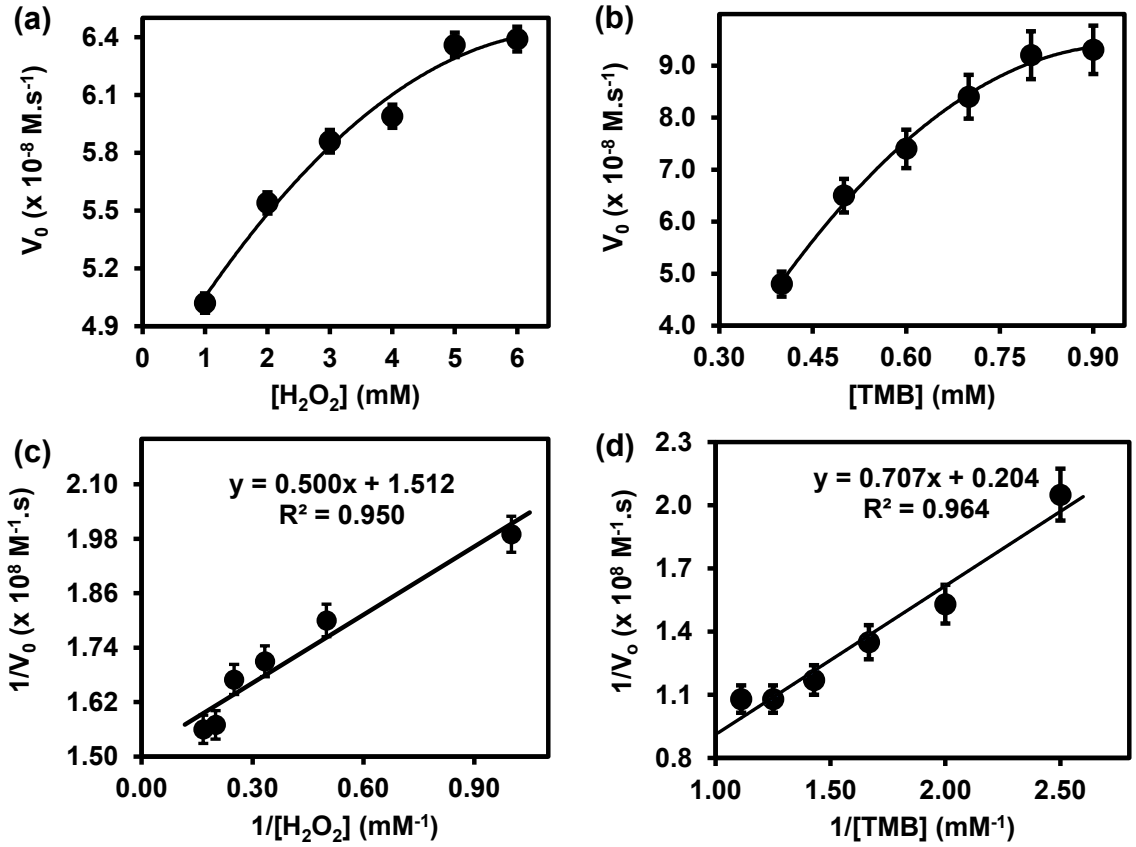

Figure 4.9: The steady-state kinetic plots for the ITO-SiO_2-prS-Au/PdNPs by (a) varying [H_2O_2] at a fixed [TMB], (b) varying [TMB] at a fixed [H_2O_2] and their corresponding double reciprocal plots for [H_2O_2] at a fixed [TMB], and (d) [TMB] at a fixed [H_2O_2]. All measurements were conducted in acetate buffer (pH 4.0, 0.20 M).

Table 4.1: Comparison of the kinetic parameters for the peroxidase-like activity of ITO-SiO_2-prS-Au/PdNPs compared with reported peroxidase-mimetics.

Nanozymes	**K_m (mM)**		**V_{max} (x 10^{-8} M.s^{-1})**	
	H_2O_2	TMB	H_2O_2	TMB
ITO-SiO_2-prS-Au/PdNPs [**TW**]	0.33	3.46	0.66	4.90
HRP [**12**]	3.7	0.43	8.71	10.0
Ce/$ZnCo_2O_4$ [**41**]	0.55	0.0886	2.62	18.80
Fe_3O_4@SiO_2NH-Au@PdNPs [**42**]	0.35	0.009	6.76	11.2
CuO-Au nanoalloys [**43**]	4.08	3.54	0.0105	0.0111
FeNPs [**44**]	0.32	0.38	0.41	0.238
Zn/CuO [**45**]	7.0	10.0	43.4	25.0

TW - This Work

4.3.8 Colorimetric detection of AA using ITO-SiO_2-prS-Au/PdNPs

The peroxidase-like activity exhibited by ITO-SiO_2-prS-Au/PdNPs was evaluated for the potential application towards the detection of ascorbic acid (AA). The AA detection was carried out with H_2O_2 (6.0 mM), TMB (0.80 mM), ITO-SiO_2-prS-Au/PdNPs and varied concentration of AA (0.50–240.0 μM) at room temperature. AA is an oxidant and a mild reducing agent that readily reacts with ROS. In **Figure 4.10(a)**, the oxTMB color changed from deep blue to colourless as the concentration of AA was increased. This is due to the reducing properties of AA in that strong blue TMBDI or oxTMB products are reduced and become colourless TMB solution as the concentration of AA increases. The color intensity of the pictures looked similar to the naked eye, but using UV−vis spectra, there was a clear difference between 0 and 240 μM [AA]. The intensity

values were between 0.12 and 0.36 a.u., as shown in **Figure 4.10(b)**. The UV-vis spectra with the absorption peak of oxTMB at 652 nm gradually decreasing as the concentration of AA was increased from 0.50 to 240.0 μM and due to the reducing properties of AA. The difference value of absorption (∆A) was calculated using **Equation (4.4):**

$$\Delta A = A_0 - A \qquad \textbf{(4.4)}$$

where A_0 and A represent the absorbance at 652 nm in the absence and presence of AA, respectively. When ∆A was plotted against the increasing concentrations of AA, an increase in the ∆A was observed in **Figure 4.10(c)**. The plot of ∆A against the concentration of AA exhibited good linearity from 0.50 to 30.0 μM with a linear regression equation of $\Delta A = 0.00162\ [AA] + 0.258$ with R^2 of 0.98. The LoD and (LoQ) were calculated to be 0.50 μM and 1.65 μM, respectively, by KS_b/slope, where K is equal to 3 (LoD) and 10 (LoQ), S_b is the standard deviation of the blank samples (n = 10) and m is the slope of the linear regression in **Figure 4.10(c)** [**34**]. The LoD of 0.50 μM was taken from the lowest concentration that can be detected and discernible from the blank. The linear range was much lower than 40–120 μM in healthy human serum [**4**]. This was limited by the Au/PdNPs deposition onto ITO-SiO_2-prS-Au/PdNPs. Arrays of ITO-SiO_2-prS-Au/PdNPs will be investigated with an aim of increasing the surface area of our catalytic surfaces and to reach the real sample analysis AA concentrations in human serum. Compared with other detection methods for AA, our proposed colorimetric assay using ITO-SiO_2-prS-Au/PdNPs showed better or comparable detection of limit and linear range than those of the reported nanozymes, nanoparticles for electrochemical and fluorescence AA sensing platforms summarized in **Table 4.2**. The mechanism of colorimetric detection of AA is also summarized in

Scheme 4.3. Briefly, a substrate solution containing (H_2O_2 and TMB) is a clear or colourless. In the presence of ITO-SiO_2-prS-Au/PdNPs, the colour changes to blue due to the electron-transfer mechanism resulting in the catalytic reduction of H_2O_2 and oxidation of TMB to oxTMB (blue-colored compound). In the presence of AA at different concentrations, the oxTMB blue colour intensity decreases and the solution turns from blue to clear or colourless due to the reduction of oxTMB. The colour intensity is related to the concentration of AA, and the linear plot in **Figure 4.10(b)** and **(c)** results.

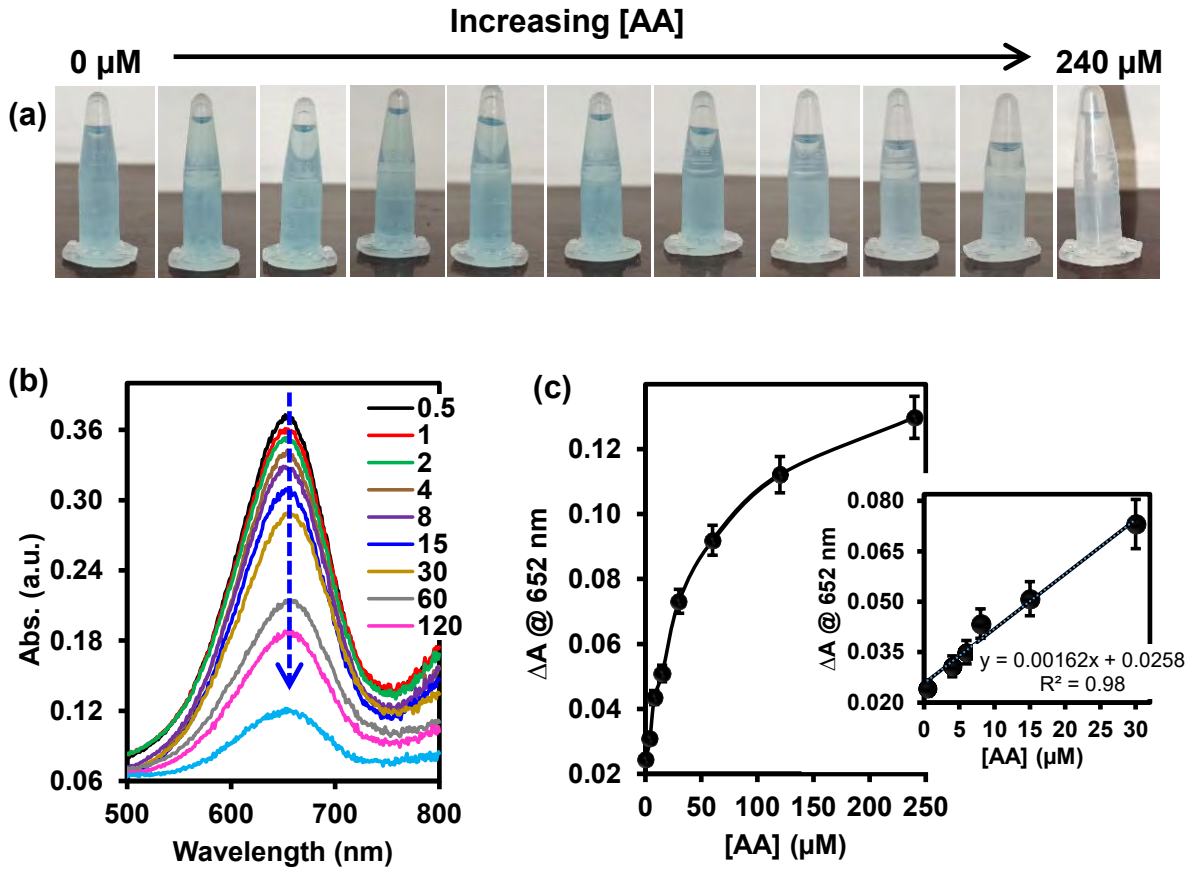

Figure 4.10: (a) Solution images, and (b) UV-vis absorption spectra of H_2O_2 + TMB + ITO-SiO_2-prS-Au/PdNPs in the presence of increasing [AA]. (c) Calibration curve of change in absorbance signal against [AA] and the inset is the linear relationship of ΔA and [AA]. All the measurements were conducted in acetate buffer (pH 4.0, 0.20 M).

Table 4.2: Comparison of different nanozymes or nanomaterial-modified electrode surfaces for colorimetric determination of AA.

Method	Nanozymes	Linear range	LoDs (μM)
Colorimetric	ITO-SiO_2-prS-Au/PdNPs [**TW**]	0.50 – 30.0 μM	0.50
	Co_3O_4NPs [**5**]	10 – 350 μM	3.91
	MIL-53(Fe) [**6**]	30 – 190 μM	15
	MoO_{3-x} nanosheets [**7**]	1.00 – 100 mM	90
	CuNPs@C [**8**]	0.10 – 1.00 mM	141
Electrochemical	CuZEA/RGO/GCE [**9**]	20 – 200 μM	11
	CNT [**10**]	80 – 140 μM	20
	Fe_3O_4/GO sheets [**11**]	0.16 – 7.20 mM	20
	Gr flowers modified CF [**12**]	50 – 1.49 mM	24.7
	ZnO@SiO_2 nanospheres [**13**]	0.10 – 1.50 mM	64.5
	Ni–Pt alloys [**14**]	0.57 – 5.68 mM	570
Fluorescence	CdTe QDs [**15**]	20 – 240 μM	433

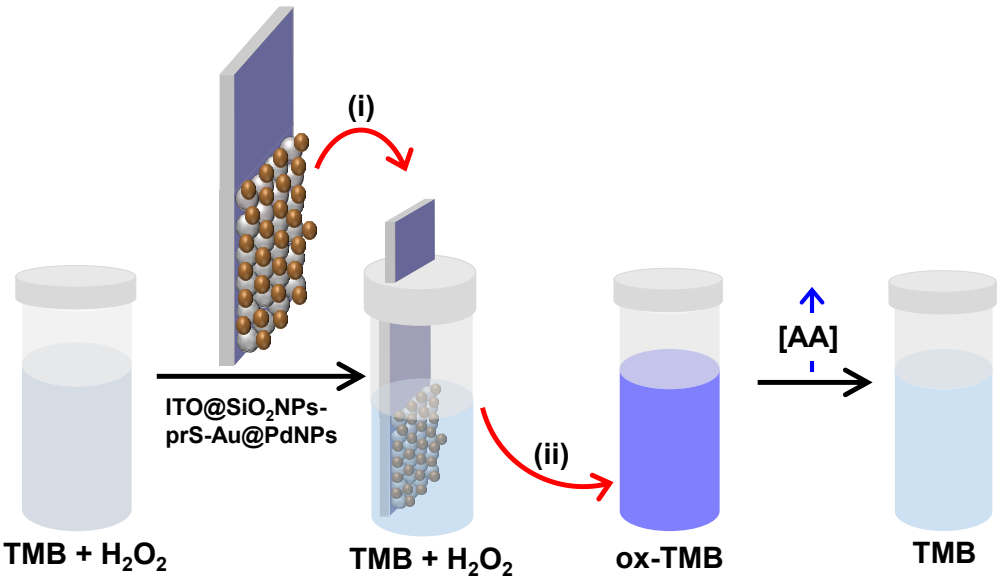

Scheme 4.3: Schematic illustration for the colorimetric determination of AA using ITO-SiO_2-prS-Au/PdNPs in the substrate solution (H_2O_2 and TMB).

4.3.9 Selectivity studies

UV-vis absorption at 652 nm were recorded for ITO-SiO_2-prS-Au/PdNPs in the presence of several possible interfering species such as glucose (Glu), sucrose (Suc), Urea, Glycine (Gly), Cytosine (Cyt), Adenine (Ade), Guanine (Gua), NaCl, KCl, $CaCl_2$, $MgSO_4$, all measured against 240.0 µM AA. **Figure 4.11(a)** shows that the various species do not affect the determination of AA exhibited intense signal absorption at 652 nm. The inset in **Figure 4.11(a)** shows the solution of each of the interfering species. The selected species were found in various samples with AA and are grouped as metabolic carbohydrates, amino acids, and inorganic salts. The blank solution in **Figure 4.11(a)** resulted in colour change to blue and due to the reaction of H_2O_2 + TMB + ITO-SiO_2-prS-Au/PdNPs. In the presence of AA, the absorption peak intensity at 652 nm dramatically decreased and no obvious blue colour was observed compared to the control experiment. The addition of other interfering substances alone resulted in blue coloured products which were almost similar to the control experiment. This indicated that there were no obvious inhibiting effects caused by the interfering substances. Although the addition of glucose and some inorganic salts ($CaCl_2$) caused a minor absorbance change, this was far less compared to that of AA. The intensity values are even lower in **Figure 4.11(a)** from 0.06 to 0.16 a.u, and using UV-vis spectra, there discernible differences in intensity values. UV-vis spectroscopy is the sensitive equipment to monitor the small intensity differences. The results were conducted in triplicates in the same concentration, and there no observable changes to the signal.

4.3.10 Colorimetric detection of AA in new-born calf serum (NCS) samples

To investigate the feasibility of our proposed AA colorimetric sensor (ITO-SiO_2-prS-Au/PdNPs) in real samples, 10% new-born calf serum (NCS) in acetate buffer (pH 4.0, 0.20 M) was spiked with known concentrations of AA. The concentration of AA to be spiked was within the linear calibration curve in inset **Figure 4.10(c)**, and this was used to correlate the observed absorption to the concentration detected. As listed in **Table 4.3**, the percentage recovery of AA in real samples were between 98.7 and 110%, and the percentage relative standard deviations (%RSD) were between 1.13 and 2.08%. In the blank sample (10% NCS acetate buffer), there was no change in solution and no absorption of the UV-vis spectrum. The results showed feasible and reliability of the proposed ITO-SiO_2-prS-Au/PdNPs for detecting AA in real samples.

Table 4.3: Detection of AA in real samples (n = 3) using recovery method in spiked 10% NCS in acetate buffer (pH 4.0, 0.20 M).

Added [AA] (μM)	Detected [AA] (μM	% Recovery	% RSD
4.5	4.6	102.2	1.19
6.0	6.6	110.0	1.50
7.5	7.4	98.7	1.13
15.0	16.0	106.7	2.08

4.3.11 Reusable and reproducible ITO-SiO_2-prS-Au/PdNPs for AA detection

The reproducibility of ITO-SiO_2-prS-Au/PdNPs for AA detection was investigated by applying the same experimental condition for eight successive cycles. After each measurement, the ITO-SiO_2-prS-Au/PdNPs was removed from the H_2O_2/TMB reaction solution and washed several times with ethanol, methanol and distilled water. The recovered ITO-SiO_2-prS-Au/PdNPs was reused for AA detection as shown in **Figure 4.11(b)**. The %RSD value for the activity of ITO-SiO_2-prS-Au/PdNPs for each of the eight successive cycles was 3.1%. About 92.8% of the signal could be regenerated after eight successive catalytic cycles of usage. Five batches of ITO-SiO_2-prS-Au/PdNPs were prepared fresh following the same procedure and used to detect AA. There was a slight decrease in batch number 2, but the four other batches were reproducible and reusable for the detection of AA. The %RSD value for the activity of each batch of ITO-SiO_2-prS-Au/PdNPs was 5.9%, as shown in **Figure 4.11(c)**. The work investigated shows the successful fabrication of ITO-SiO_2-prS-Au/PdNPs with excellent peroxidase-like activity and for colorimetric AA detection

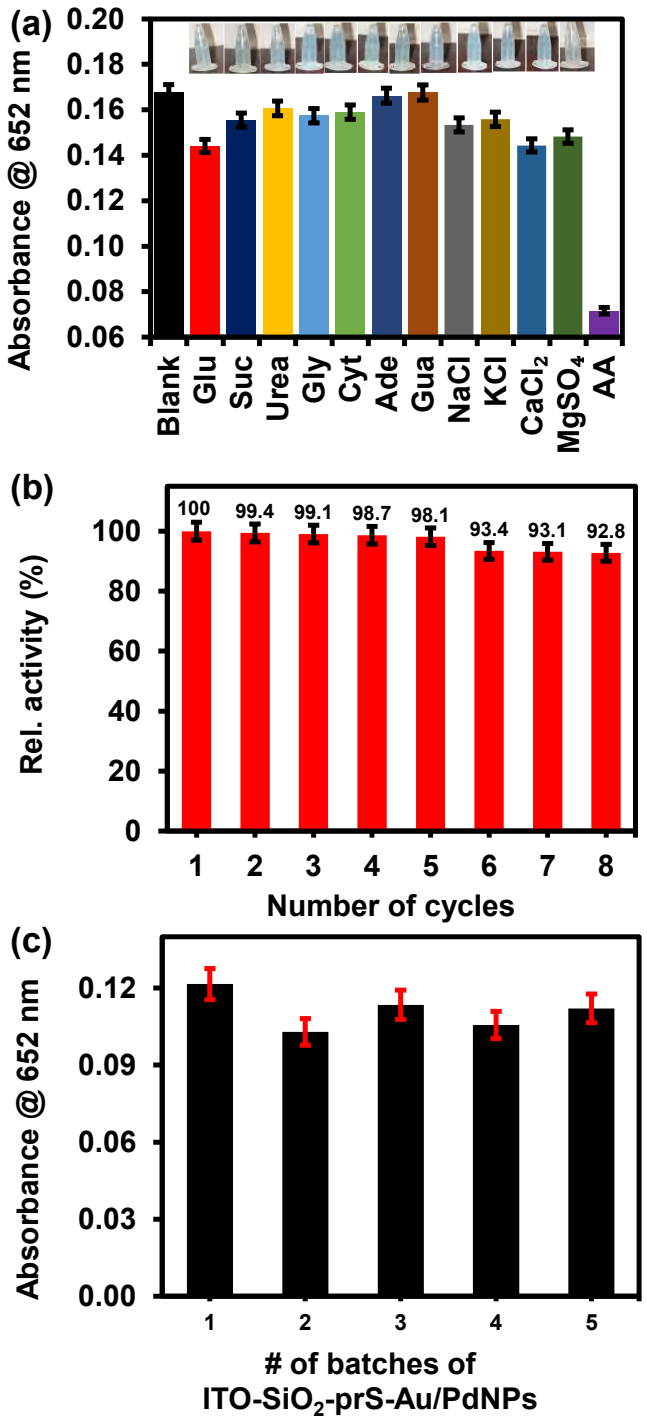

Figure 4.11: (a) Selectivity of colorimetric assay for AA detection and other interfering substances for ITO-SiO_2-prS-Au/PdNPs AA (inset: the corresponding images of the reaction solutions), (b) colorimetric detection signal towards AA reproducibility and (c) reproducible method of ITO-SiO_2-prS-Au/PdNPs (batches).

4.4 Conclusions

In this work, the fabricated ITO-SiO_2-prS-Au/PdNPs surface exhibited enhanced peroxidase-like activity, better than ITO-SiO_2-prS-AuNPs and ITO-SiO_2-prS-PdNPs. The enhanced catalytic activity shown by ITO-SiO_2-prS-Au/PdNPs was attributed to the synergistic interaction between AuNPs as core and Pd as a shell. The following parameters were optimized: pH, time, [H_2O_2], [TMB], and temperature. A typical Michaelis−Menten enzyme-like behaviour was observed for the ITO-SiO_2-prS-Au/PdNPs under steady-state kinetic analysis. The ITO-SiO_2-prS-Au/PdNPs showed good affinity for both H_2O_2 (K_m, 0.33 mM) and TMB (K_m, 3.46 mM) compared to HRP and other previously reported peroxidase-mimetics. A simple colorimetric assay with high sensitivity and selectivity toward AA detection was established using H_2O_2 + TMB + ITO-SiO_2-prS-Au/PdNPs reaction system. The designed AA colorimetric sensor exhibited good linear concentration range from 0.50 to 30.0 μM, with LoD of 0.50 μM and LoQ of 1.65 μM. The high stability, reusablility and reproducibility of ITO-SiO_2-prS-Au/PdNPs could be used to detect AA in real samples (NCS).

4.5 References

(1) Eipper, B. A.; Stoffres, D. A.; Mains, R. E. The Biosynthesis of Neuropeptides: Peptide Alpha-Amidation. *Annu. Rev. Neurosci*. **1992**, 15, 57−85. https://doi.org/10.1146/annurev.ne.15.030192.000421

(2) Nishikimi, M.; Fukuyama, R.; Minoshima, S.; Shimizu, N.; Yagi, K. Cloning and Chromosomal Mapping of the Human Nonfunctional Gene for L-gulono-γ-lactone Oxidase, the Enzyme for L-ascorbic Acid Biosynthesis Missing in Man. *J. Biol. Chem*. **1994**, 269, 13685−13688. https://doi.org/10.1016/s0021-9258(17)36884-9

(3) Ausman, L. M.; Mayer, J. Critical and Recommendations for Vitamic C Intake. *Brief Critical Reviews* **1999**, 57, 222–224.

https://doi.org/10.1111/j.1753-4887.1999.tb06946.x

(4) Harding, A. H.; Wareham, N. J.; Bingham, S. A.; Khaw, K.; Luben, R.; Welch, A.; Forouhi, N. G. Plasma Vitamin C Level, Fruit and Vegetable Consumption, and the Risk of New-Onset Type 2 Diabetes Mellitus. *Arch. Interm. Med*. **2008**, 168, 1493−1499. https://doi.org/10.1001/archinte.168.14.1493

(5) Alexandrescu, D. T.; Dasanu, C. TA.; Kauffman, C. L. Acute Scurvy During Treatment with Interleukin-2. *Clin. Exp. Dermatol*. **2009**, 34, 811−814.

https://doi.org/10.1111/j.1365-2230.2008.03052.x

(6) Padayatty, S. J.; Katz, A.; Wang, Y.;Eck, P.; Kwon, O.; Lee, J. H.; Chen, S.; Corpe, C.; Dutta, A.; Dutta, S. K.; Levine, M. Vitamin C as an Antioxidant: Evaluation of its Role in Disease Prevention. *J. Amer. College Nutrition* **2003**, 22, 18−35. https://doi.org/10.1080/07315724.2003.10719272

(7) Moretti, M.; Budni, J.; Freitas, A. E.; Rosa, P. B.; Rodrigues, A. L. S. Antidepressant-like Effect of Ascorbic Acid is Associated with the Modulation of Mammalian Target of Rapamycin Pathway. *J. Psychiatr. Res*. **2014**, 48, 16−24. http://dx.doi.org/10.1016/j.jpsychires.2013.10.014

(8) Malashikhina, N.; Pavlov, V. DNA-Decorated Nanoparticles as Nanosensors for Rapid Detection of Ascorbic Acid. *Biosens. Bioelectron*. **2012**, 33, 241−246. https://doi.org/10.1016/j.bios.2012.01.011

(9) Ma, Y.; Zhou, M.; Jin, X.; Zhang, B.; Chen, H.; Guo, N. Flow-Injection Chemiluminescence Determination of Ascorbic Acid by Use of the Cerium (IV)-Rhodium B System. *Anal. Chim. Acta* **2002**, 464, 289−293.

https://doi.org/10.1016/S0003-2670(02)00483-X

(10) A. M. Pisoschi, A. M.; Pop, A.; Serban, A. I.; Fafaneata, C. Electrochemical Methods for Ascorbic Acid Determination. *Electrochim. Acta* **2014**, 121, 443−460.

https://doi.org/10.1016/j.electacta.2013.12.127

(11) Lin, Y.; Ren, J.; Qu, X. Catalytically Active Nanomaterials: A Promising Candidate for Artificial Enzymes. *Acc. Chem. Res*. **2014**, 47, 1097−1105.

https://dx.doi.org/10.1021/ar400250z

(12) Gao, L.; Zhuang, J.; Nie, L.; Zhang, J.; Zhang, Y.; Gu, N.; Wang, T.; Feng, J.; Yang, D.; Perret, S.; X. Yan. Intrinsic Peroxidase-like Activity of Ferromagnetic Nanoparticles. *Nat. Nanotech*. **2007**, 2, 577−583.

https://doi.org/10.1038/nnano.2007.260

(13) Liu, X.; Han, Q.; Zhang, Y.; Wang, X.; Cai, S.; Wang, C.; Yang, R.Green and Facile Synthesis of Rh/GO Nanocomposites for High Catalytic Performance. *Appl. Surf. Sci*. **2019**, 471, 929−934. https://doi.org/10.1016/j.apsusc.2018.12.065

(14) Gao, Y.; Wang, W.; Chang, S.; Huang, W. Morphology Effect of CeO_2 Support in the Preparation, Metal-Support Interaction, and Catalytic Performance of Pt/CeO_2 Catalysts. C*hemCatChem*. **2013**, 5, 3610−3620.

https://doi.org/10.1002/cctc.201300709

(15) Song, J.; Pandain, V.; Mauki, M. G.; Bau, H. H.; Cherry, S.; Tisi, L. C.; Liu, C. Smartphone-Based Mobile Detection Platform for Molecular Diagnostics and Spatiotemporal Disease Mapping. *Anal. Chem*. **2018**, 90, 4823−4831.

https://doi.org/10.1021/acs.analchem.8b00283

(16) S. Wang, S.; Deng, W.; Yang, L.; Tan, Y.; Xie, Q.; Yao, S. Copper-Based Metal-Organic Framework Nanoparticles with Peroxidase-Like Activity for Sensitive Colorimetric Detection of Staphylococcus aureus. *ACS Appl. Mater. Interf.* **2017**, 9, 24440–24445. https://doi.org/10.1021/acsami.7b07307

(17) Othman, A.; Karimi, A.; Andreescu, S. Functional Nanostructures for Enzyme Based Biosensors: Properties, Fabrication and Applications. *J. Mater. Chem. B*. **2016**, 4, 7178–7203. https://doi.org/10.1039/C6TB02009G

(18) Shanmugaraj, K.; Ilanchelian, M. Colorimetric Determination of Sulfide Using Chitosan-Capped Silver Nanopartilces. *Microchim. Acta* **2016**, 183, 1721−1728. https://doi.org/10.1007/s00604-016-1802-y

(19) Drozd, M.; Pietrzak, M.; Parzuchowski, P. G.; Malinowska, E. Pitfalls and Capabilities of Various Hydrogen Donors in Evaluation of Peroxidase-Like Activity of Gold Nanoparticles. *Anal. Bioanal. Chem*. **2016**, 408, 8505−8513.

https://doi.org/10.1007/s00216-016-9976-z

(20) Shi, W.; Fan, H.; Ali, S.; Zhu, L. Honeycomb-Like Nitrogen-Doped Porous Carbon Supporting Pt Nanoparticles as Enzyme Mimic for Colorimetric Detection of Cholesterol. *Sens. Act. B. Chem*. **2015**, 221, 1515−1522.

https://doi.org/10.1016/j.snb.2015.06.157

(21) Zhou, N.; Zou, S.; Zou, L.; Shen, R.; Zhou, Y.; Ling, L. Peroxidase-like Activity of Palladium Nanoparticles on Hydrogen-Bond Supramolecular Structures Over a Broader pH Range and Application in Glucose Sensing. *Can. J. Chem*. **2019**, 97, 317−323. https://doi.org.10.1139/cjc-2018-0302

(22) Wang, Z.; Yang, X.; Yang, J.; Jiang, Y.; He, N. Peroxidase-Like Activity of Mesoporous Silica Encapsulated Pt Nanoparticles and Its Application in Colorimetric Immunoassay. *Anal. Chim. Acta* **2015**, 862, 53−63.

https://doi.org/10.1016/j.aca.2014.12.046

(23) He, W.; Lui, Y.; Yuan, J.; Yin, J. J.; Wu, X.; Hu, X.; Zhang, K.; Liu, J.; Chen, C.; Ji, Y.; Guo, Y. Au@Pt Nanostructures as Oxidase and Peroxidase Mimetics for Use in Immunoassays. *Biomat*. **2011**, 32, 1139−1147.

https://doi.org/10.1016/j.biomaterials.2010.09.040

(24) Mu, J.; Wang, Y.; Zhao, M.; Zhang, L. Intrinsic Peroxidase-Like Activity and Catalase-like Activity of Co_3O_4 nanoparticles. *Chem. Commun*. **2012**, 48, 2540–2542.

https://doi.org/10.1039/c2cc17013b

(25) Bhagat, S.; Srikanth, N. V.; Vallabani, V.; Shutthanandan, M.; Bowden, A.; Karakoti, S. Gold Core/Ceria Shell-Based Redox Active Nanozyme Mimicking the Biological Multienzyme Complex Phenomenon. *J. Colloid Int. Sci*. **2018**, 513, 831–842. https://doi.org/10.1016/j.jcis.2017.11.064

(26) Ma, T.; Liang, F.; Chen, R.; Liu, S.; Zhang, H. Synthesis of Au-Pd Bimetallic Nanoflowers for Catalytic Reduction of 4-Nitrophenol. *Nanomat.* **2017**, 7, 239. https://doi.org/10.3390/nano7090239

(27) He, H.; Xu, X.; Wu H.; Jin, Y. Enzymatic Plasmonic Engineering of Ag/Au Bimetallic Nanoshells and Their Use for Sensitive Optical Glucose Sensing. *Adv. Mater*. **2012**, 24, 1736−1740. https://doi.org/10.1002/adma.201104678

(28) Li, Z.; Kurouski, D. Probing the Redox Selectivity on Au@Pd and Au@Pt Bimetallic Nanoplates by Tip-Enhanced Raman Spectroscopy. *ACS Photonics* **2021**, *8*, 2112–2119. https://doi.org/10.1021/acsphotonics.1c00561

(29) Xu, D.; Qi, S.; Chen, Y.; Yin, M.; Zhang, L.; Ge, K.; Wei, X.; Tian, X.; Wang, P.; Li, M.; Wei, J.; Wang, Z.; Qiu, J. Hierarchical Mesoporous Hollow Ce-MOF Nanosphere as Oxidase Mimic for Highly Sensitive Colorimetric Detection of Ascorbic Acid. *Chem. Phys. Lett*. **2021**, *777*, 138749.

https://doi.org/10.1016/j.cplett.2021.138749

(30) Han, Y.; Luo, L.; Zhang, L.; Kang, Y.; Sun, H.; Dan, J.; Sun, J.; Zhang, W.; Yue, T.; Wang, J. Oxidase-like Fe–Mn Bimetallic Nanozymes for Colorimetric Detection of Ascorbic Acid in Kiwi fruit. *LWT–Food Sci. Technol*. **2022**, *154*, 112821.

https://doi.org/10.1016/j.lwt.2021.112821

(31) Shah, M.; Shah, J.; Arya, H.; Vyas, A.; Vijapura, A.; Gajipara, A.; Shamal, A.; Bakshi, M.; Thakore, P.; Shah, R.; Saxena, V.; Varade, D.; Singh, S. Biological Oxidase Enzyme Mimetic Cu-Pt Nanoalloys: A Multifunctional Nanozyme for Colorimetric Detection of Ascorbic Acid and Identification of Mammalian Cells. *ChemistrySelect*. **2019**, *4*, 6537–6546. https://doi.org/10.1002/slct.201900681

(32) Sun, H.; Liu, X.; Wang, X.; Han, Q.; Qi, C.; Li, Y.; Wang, C.; Chen, Y.; Yang, R. Colorimetric Determination of Ascorbic Acid using a Polyallylamine-Stabilized IrO_2/Graphene Oxide Nanozyme as a Peroxidase Mimic. *Microchimi. Acta* **2020**, *187*, 1-9. https://doi.org/10.1007/s00604-019-3897-4

(33) Iqbal, M.; Usanase, G.; Oulmi, K.; Aberkane, F.; Bendaikha, T.; Fessi, H.; Zine, N.; Agusti, G.; Errachid.; Elaissari. Preparation of Gold Nanoparticles and Determination of Their Particles Size via Different Methods. *Mater. Res. Bull*. **2016**, 79, 97−104. https://doi.org/10.1016/j.materresbull.2015.12.026

(34) Pati, P.; McGinnis, S.; Vikesland, P. J. Life Cycle Assessment of 'green' Nanopartilces Synthesis Methods. *Environ. Eng. Sci*. **2014**, 31, 410−420. htttps://doi.org/10.1089/ees.2013.0444

(35) Chen, M.; Sun, L.; Ding, Y.; Shi, Z.; Liu, Q. N,N ′-Di-carboxymethyl Perylene Diimide Functionalized Magnetic Nanocomposites with Enhanced Peroxidase-Like Activity for Colorimetric Sensing of H_2O_2 and Glucose. *New J. Chem*. **2007**, 41, 5853–5862. https://doi.org/10.1039/C7NJ00292K

(36) Wu, J.; Wang, X.; Wang, Q.; Lou, Z.; Li, S.; Zhu, Y.; Qin, L.; Wei, H. Nanomaterials with Enzyme-like Characteristics (Nanozymes): Next-Generation Artificial Enzymes (II). *Chem. Soc. Rev*. **2019**, 48, 1004–1076. https://doi.org/10.1039/C8CS00457A

(37) Chen, L.; Li, X.; Zhang, J.; Fang, J.; Huang, Y.; Wang, P.; Ma, J. Production of Hydroxyl Radical via the Activation of Hydrogen Peroxide by Hydroxylamine. *Environ. Sci. Technol*. **2015**, 49, 10373–10379. http://dx.doi.org/10.1021/acs.est.5b00483

(38) Yang, Y.; Shen, D.; Long, Y.; Xie, Z.; Zheng, H. Intrinsic Peroxidase-Like Activity of Ficin. *Sci. Rep*. **2017**, 7, 1–8. https://doi.org/10.1038/srep43141

(39) Nicell, J. A.; Wright, H. A Model of Peroxidase Activity with Inhibition by Hydrogen Peroxide. *Enz. Microb. Technol*. **1997**, 21, 302–310. https://doi.org/10.1016/S0141-0229(97)00001-X

(40) Liu, Y.; Zhu, G.; Yang, J.; Yuan, A.; Shen, X. Peroxidase-Like Catalytic Activity of Ag_3PO_4 Nanocrystals Prepared by a Colloidal Route. *PLoS One*. **2014**, 9, 1−7. https://doi.org/10.1371/journal.pone.0109158

(41) Yin, D.; Yang, H.; Wang, S.; Yang, Z.; Liu, Q.; Zhang, X. Ce-doped Zn/Co_2O_4 Nanospheres: Synthesis, Enzyme-like Performances, Catalytic Mechanism and Fast Colorimetric Determination for Glutathione. *Coll. Surf. A* **2020**, 607, 125466. https://doi.org/10.1016/j.colsurfa.2020.125466

(42) Adeniyi, O.; Sicwetsha, S.; Mashazi, P. Nanomagnet-Silica Nanoparticles Decorated with Au@Pd for Enhanced Peroxidase-Like Activity and Colorimetric Gucose Sensing. *ACS Appl. Mater. Interf*. **2020**, 12, 1973–1987. https://doi.org/10.1021/acsami.9b15123

(43) Mvango, S.; Mashazi, P. Synthesis, Characterization of Copper Oxide-Gold Nanoalloys and Their Peroxidase-Like Activity towards Colorimetric Detection of Hydrogen Peroxide and Glucose. *Mater. Sci. Eng. C*. **2019**, 96, 814–823. https://doi.org/10.1016/j.msec.2018.12.010

(44) Wu, H.; Wang, E. Nanomaterials with Enzyme-ike Characteristics (Nanozymes): Next-Generation Artificial Enzymes, *Chem. Soc. Rev*. **2013**, 42, 6060–6093. https://doi.org/10.1039/C3CS35486E

(45) Chen, Y.; Cao, H.; Shi, W.; Liu, H.; Huang, Y. Fe-Co Bimetallic Alloy Nanoparticles as a Highly Active Peroxidase Mimetic and its Application in Biosensing. *Chem. Commun*. **2013**, 49, 5013–5015. https://doi.org/10.1039/C3CC41569D

CHAPTER 5

5 Conclusions and future perspectives

5.1 Conclusions

In this thesis, we reported a method of fabricating nanomaterials of gold, palladium, gold/palladium as thin nanoparticle films on catalytically inert surfaces, while allowing for their recovery and reuse. The successful deposition of AuNPs, PdNPs, and Au/PdNPs on ITO-SiO_2-prSH to form ITO-SiO_2-prS-AuNPs, ITO-SiO_2-prS-PdNPs, and ITO-SiO_2-prS-Au/PdNPs was confirmed by EDX and XPS. The fabricated films were evaluated for the enzyme-like catalytic activity. The fabricated thin film with bimetallic NPs, ITO-SiO_2-prS-Au/PdNPs, exhibited excellent peroxidase-like activity for the oxidation of TMB with H_2O_2 when compared with monometallic thin nanoparticle films, ITO-SiO_2-prS-AuNPs and ITO-SiO_2-prS-PdNPs. The enhanced catalytic activity of ITO-SiO_2-prS-Au/PdNPs was attributed due to the synergistic effect between AuNPs and Pd shell. Further confirmation of the formation of the Pd shell was confirmed by XRD.

The modified surfaces of ITO-SiO_2-prS-PdNPs and ITO-SiO_2-prS-Au/PdNPs were successfully used for the colorimetric detection of glucose and AA, respectively. Glucose detection was accomplished using ITO-SiO_2-prS-PdNPs with linear concentration range up to 30 μM. The LoD and LoQ were calculated and found to be 1.84 μM and 6.14 μM, respectively. The detection of AA was accomplished using ITO-SiO_2-prS-Au/PdNPs. Instead of monitoring the increase in absorbance, a decrease in intensity was observed with increase in AA concentrations. The blue oxTMB with an

absorbance at 652 nm became colorless as the concentration of AA was increased. This was due to the antioxidant or mild reducing properties of AA. The plot of ΔA against the concentration of AA exhibited good linearity from 0.50 to 30.0 µM. The LoD and LoQ were calculated and found to be 0.50 µM and 1.65 µM, respectively, with R^2 of 0.98. For both surfaces, ITO-SiO_2-prS-PdNPs and ITO-SiO_2-prS-Au/PdNPs, the peroxidase-like activity was determined to proceed via the electron-transfer mechanism. The use of fabricated ITO-SiO_2-prS-PdNPs and ITO-SiO_2-prS-Au/PdNPs surfaces for detection of glucose and AA, respectively, was a great achievement in this thesis. The NP-modified surfaces were reusable after rinsing, thus affording a low-cost fabrication of the novel ITO-SiO_2-prS-PdNPs and ITO-SiO_2-prS-Au/PdNPs. The ITO-SiO_2-prS-PdNPs and ITO-SiO_2-prS-Au/PdNPs were successfully used to detect glucose and AA in the real and complex sample matrix respectively, i.e. new-born calf serum (10% NCS).

5.2 Future Perspectives

Colorimetric detection sensors based on nanozymes designed in this thesis for glucose and AA still requires the use of arrays of ITO-SiO_2-prS-PdNPs and ITO-SiO_2-prS-Au/PdNPs with an aim of increasing the surface area of our catalytic surfaces and to reach the real sample analysis glucose and AA concentrations in human serum.

- For glucose, the detection of glucose in various human skin compartments such as epidermis, dermins, and adipose tissues will be investigated and the use of computational models will assist in understanding glucose transport processes for glucose sensor development.

- For AA, the detection of reducing agents similar to AA such as cysteine and glutathione is ongoing.

Both of these studies are subject of our continued investigation towards the development of a low-cost detection of glucose and ascorbic acid (AA) sensors based on nanomaterials.